

POLITECNICO DI TORINO

Corso di Laurea Magistrale in Ingegneria Biomedica

Tesi di Laurea Magistrale



Engineered design of mesoporous silica-based nanoparticles functionalised by layer-by-layer technique as multifunctional nanotheranostic agents for cancer treatment

Supervisors

Prof. Gianluca Ciardelli

Dr. Piergiorgio Gentile

Prof. Chiara Tonda Turo

Dr. Irene Carmagnola

Candidate

Andrea Mele

S267391

A. Y. 2019/2020

Declaration of work

I declare that this thesis is based on my own work and has not been submitted in any form for another degree at any University or any other tertiary education. Information derived from published and unpublished work of others have been acknowledged in the text and in the list of references given in the bibliography.

ABSTRACT

Cancer is the second leading cause of death globally and it is responsible for an estimated 9.6 million deaths in 2018, with 13.2 million deaths are expected in 2030 for global population. Due to the limits of conventional cancer treatments currently in use, an emerging field of treatments, known as nanotheranostics, has been studied for the past years, demonstrating a great potential thanks to the use of nano sized platforms with the dual capability of therapeutics and diagnostics. Researchers have focused on developing innovative systems in order to improve drug delivery at the specific target sites, kinetic drug release, biodistribution, and multimodal therapy through the combination of different therapeutic methods such as chemotherapy and phototherapy. In this work, starting from state-of-the-art about nanotheranostic efficient systems, we have investigated the design of an innovative theranostic nanoparticle built through a bottom-up strategy, and characterised by a mesoporous silica-based nanoparticle (MSN) as internal core. According to the literature, MSNs have been widely applied in theranostic field as drug delivery carriers thanks to their high surface area, controllable pore size and morphology, and chemically modifiable surface. Particularly, synthesized MSN with an expected diameter of 50 nm, loaded with tirapazamine (TPZ), can be then functionalized with 3-aminopropyltriethoxysilane (APTES) to obtain a positively charged MSN-NH₂. Layer-by-layer self-assembly strategy has been proposed to coat MSN-NH₂ with specific biomaterials in order to provide a multifunctional shell structure, incorporating another drug as Doxorubicin for a dual drug effect. Two charged bilayers of hyaluronic acid and poly(L-lysine) can be alternating deposited on the MSN-NH₂ to obtain a pH-responsive structure able to control the kinetics release. For providing a combination of different therapies, the first bilayer is composed by two hyaluronic acid layers stabilised through incorporation of a porphyrin-based photosensitizers (PSs) by using of β -cyclodextrins. In fact, PSs are key factors for photodynamic therapy (PDT). Additionally, according to the literature, PSs have demonstrated efficiency in NIR fluorescence, contributing to imaging-guided tumour targeted therapy. Moreover, PSs, generating deleterious reactive oxygen species (ROS) to irreversible damage tumour cells, TPZ, a drug that is only cytotoxic to hypoxic cells, strongly cooperate with PDT. Finally, the external layer can be functionalised with the hydrophilic chain polymer polyethylene glycol (PEG) linked with folic acid (FA) to avoid the effect of immune system, improve biostability and

increase circulation time in the blood environment, and to promote active targeting to the tumour mass. The active targeting of the PEG-linked molecule is modifiable grafting specific biomolecules like antibodies depending on the treated tumour. The whole platform has been designed to satisfy the biocompatibility standard requirements set by Food and Drug Administration (FDA). In conclusion, a brief discussion on a MATLAB computational study is proposed as a possible future way to analyse and predict kinetics release from a multilayer platforms in a biological medium in order to efficiently select materials and biomolecules doses to insert in the systems, reducing time consumption and costs for experimental tests.

TABLE OF CONTENTS

Abstract.....	II
List of Figures	VII
List of Tables	X
1 Introduction.....	1
1.1 Overview of Cancer	1
1.2 Cancer Statistics.....	4
1.3 Conventional Cancer Treatments.....	5
1.3.1 Surgery	5
1.3.2 Radiation Therapy	6
1.3.3 Chemotherapy.....	6
1.3.4 Targeted Therapy.....	6
1.3.5 Immunotherapy.....	8
1.4 Cancer Diagnostics and Monitoring	9
2 Nanotheranostics: an emerging strategy.....	12
2.1 Introduction.....	12
2.2 Nanomaterials For Nanotheranostic	15
2.2.1 Gold-based Nanomaterials	16
2.2.2 Magnetic Nanomaterials.....	18
2.2.3 Polymeric Nanomaterials	20
2.2.4 Silica-Based Nanomaterials.....	23
2.2.5 Carbon Nanomaterials	25
2.2.6 Other Nanomaterials.....	25
3 Design of Engineered Nanoparticle.....	27
3.1 Aim and Objectives	27
3.2 Deep Analysis of Key Elements	31
3.2.1 Core of Nanoparticles	31
3.2.2 Multilayer coating of nanoparticles	41
3.2.3 External Surface Functionalization	53
3.2.4 Drugs for Cancer Treatment.....	59
3.2.5 Materials and Methods: manufacturing process proposal	62

4	Brief Computational Approach.....	64
4.1	Basic MATLAB Study on Drug Kinetics Release from Multilayer Capsules	64
4.2	LigandScout Molecular Dynamic Simulations.....	67
5	Conclusion and Future Perspectives	69
	Appendix.....	71

List of Figures

Figure 1.1: The biological hallmarks of the cancer.....	2
Figure 1.2: Heterogeneity of tumour microenvironment	3
Figure 1.3: Estimated age-standardized incidence rates in 2018, both sexes, all ages....	4
Figure 1.4: Incidence - ASR(W) vs Human Development Index, all cancers, in 2018, both sexes, all ages.	5
Figure 1.5: CAR (Chimeric Antigen Receptor)-T Cell Therapy.....	8
Figure 2.1: Worm-like NP with block copolymer PCL-PEG and Taxol	13
Figure 2.2: Representative scheme for the synthesis of gold-iron oxide functionalized NPs.	14
Figure 2.3: Summary of therapeutic methods, diagnostic strategies, and corresponding nanomaterials.....	15
Figure 2.4: Development of theranostic AuNPs in the treatment of cancer.....	16
Figure 2.5: Schematic representation of MMP-AuNR for simultaneous imaging and PTT on top. Temperature increase of MMP-AuNR as a function of laser irradiation time on bottom.....	17
Figure 2.6: Schematic illustration of a multifunctional magnetic nanoparticle structure with different types of coatings, target ligands and imaging agents	20
Figure 2.7: Schematic illustration of the design and proposed mechanism of the multifunctional MMSN for tumour-targeted MRI and precise therapy.....	24
Figure 3.1: Schematic representation of nanotheranostic platform.....	30
Figure 3.2: Mesoporous silica nanoparticles as versatile drug delivery systems for a variety of therapeutic agents including pharmaceutical drugs, therapeutic genes, and therapeutic proteins and peptide	35
Figure 3.3: Transmission electron microscopy images of different MSNs with different size, morphology, composition, and mesostructured	37
Figure 3.4: On the left, TEM images of mesoporous silica with different average sizes: a) 280 nm, b) 170, c) 110, d) 50, e) 30 nm. f) High-resolution TEM image of a single particle in (c). On the right, DLS measurements of MSNs synthesized with decreasing pH values from 11.52 to 10.86.....	38
Figure 3.5: On the left, CLSM images of HeLa cells after incubation for 5 h at 37°C with fluorescent MSNs (100 µg mL ⁻¹ , green) of size a) 170, b) 110, c) 50 and d) 30 nm. On the right, cell uptake of fluorescent MSNs.....	39
Figure 3.6: A) Properties of four different-sized MSNs. B) TEM images of (i) MSNs, (ii) MSNs-NH ₂ , in different diameters: (a) 25 nm, (b) 50 nm, (c) 67 nm, (d) 105 nm. C) Pore size distribution of different-sized MSNs.....	40

Figure 3.7: Schematic of common LbL approaches and common interactions exploited in LbL assembly.	41
Figure 3.8: Schematic illustration of immersive assembly on particulate substrates using centrifugation in between washing steps.	43
Figure 3.9: A) Schematic illustration of immersive LbL assembly on a planar substrate using oppositely charged polymers and the charge characteristics of the films after each deposition step. B) Schematic illustration of expedited immersive assembly on a planar substrate using a magnetic stirrer bar in the polymer solutions..	43
Figure 3.10: On the top, schematic illustration of conventional spin coating. On the bottom, schematic illustration of spin assembly using an automatic injection system. .	44
Figure 3.11: Schematic illustration of manual spray assembly using polymer solutions.	45
Figure 3.12: Schematic illustration of different characterization techniques applicable to characterize films on particulate substrates	47
Figure 3.13: A) Polyanion and B) polycation components of the LbL nanoparticle.. ..	48
Figure 3.14: Formation of host-guest inclusion complex between the Porphyrin TPPS4 and the β CD.....	49
Figure 3.15: Schematic illustration of the first bilayer, with a focus on the HA-CD-TPPS4 complex.	50
Figure 3.16: On the top, fluorescence images of SCC-7 tumour-bearing nude mice at pre-set time and ex vivo tissue imaging after 24 h post-injection. On the bottom, corresponding MFI of tumour, spleen, kidney, liver, heart, and lung at 24 h post-injection.	50
Figure 3.17: Real-time CLSM observation of intracellular photoactivity of MSNs. AO staining assay of detecting acid organelles disruption in COS7, MCF-7, and SCC-7 cells under laser irradiation (660 nm, 1 W cm^{-2}) over time.	51
Figure 3.18: Schematic illustration of normal and cancerous vasculature.....	53
Figure 3.19: Schematic illustration of 2D chemical structure and ball-and-sticks model of folic acid.....	57
Figure 3.20: Schematic illustration of endocytotic pathway of nanoparticle conjugated to folate..	58
Figure 3.21: Tirapazamine mechanism of action.	61
Figure 4.1: Schematic illustration of multilayer model of nanocapsule.....	65
Figure 4.2: Representation of drug concentration variation in time for core and each layer.	66
Figure 4.3: Illustration of pharmacophore based on the best ligand for CD44 receptor (A) and $\alpha v \beta 3$ integrin (B)	68

Figure 4.4: Representation of binding affinity in receptor pocket site..... 68

List of Tables

Table 3.1: Summary table (INSERIRE NEL TESTO) of the theranostic and design of the nanoplatform.....	29
Table 3.2: Theranostic polymeric and metal-based nanoplatforms under study for clinical applications in different cancers (according to clinicaltrials.gov and clinicaltrialsregister.eu). Readapted from Silva et al., 2019.....	32
Table 3.3: Summary of the different-tailored mesopore structure of MSNs, and the possible effects on the loading and release of drug molecules.....	34
Table 3.4: Drug-delivery systems stabilized with PEG that have received regulatory approval in the USA and/or the EU.....	54
Table 3.5: PEGylated anticancer nanocarriers in preclinical and clinical trials or approved for clinical use.	55
Table 3.6: Nanomedicines currently approved and in clinical trials phase	59

1 INTRODUCTION

1.1 OVERVIEW OF CANCER

The word “*Cancer*” is referred to a group of diseases where some of the body’s cells begin to divide without stopping and spread into surrounding tissue. Cancer cells differ from normal cells because they can grow out of control and continue to divide without stopping; in fact, cancer cells do not mature into distinct cell types, but they remain undifferentiated. Cancer is caused by changes to genes controlling the cells behaviour and principally, genetic changes are inherited. However, other causes are the exposition to several environments and to lifestyle related risk factors, i.e. tobacco, alcohol, poor diet, lack of physical activity and being overweight (Meijers & De Boer, 2019). It has been demonstrated that the principally involved genes in the tumour progression are proto-oncogenes, tumour suppressor genes and DNA repair genes. At first, the proto-oncogenes, normal genes coding for protein that help to regulate the cell growth and differentiation; upon acquiring an activating mutation, they become tumour-inducing agents, i.e. oncogenes. The tumour suppressor genes that slow down cell division and repair DNA mistakes; when these genes mutate to cause a loss or reduction in their function, the cells can progress to cancer. Finally, the DNA repair genes, involved in fixing damaged DNA; cells with mutations in these genes tend to develop additional mutations in other genes and together, these mutations may cause the cells to become cancerous (Yokota, 2000). Moreover, each person’s cancer has a unique combination of genetic changes, but Hanahan and Weinberg have provided a common group of eight capabilities and two key facilitators to acquire them for the tumour progression (Hanahan & Weinberg, 2017). They called them “hallmarks of cancer” and are showed in the [Figure 1.1](#). Each capability provides a specific functional role in supporting the development, progression and persistence of tumours. The first hallmark capability regards a group of inductive signals that causes the cell growth and division to generate daughter cells. The principal mechanism of sustaining proliferative signalling involves the mutational modification of some genes in the cancer cells that transform them into drivers of cell proliferation. These genes are called oncogenes. In normal cells, tumour suppressor genes (TSGs) encode specific proteins, such as the retinoblastoma protein (pRb), in order to break the proliferative mechanism. Nevertheless, most tumours can evade growth suppressors by mutational alterations in TSGs, resulting in their loss of function.

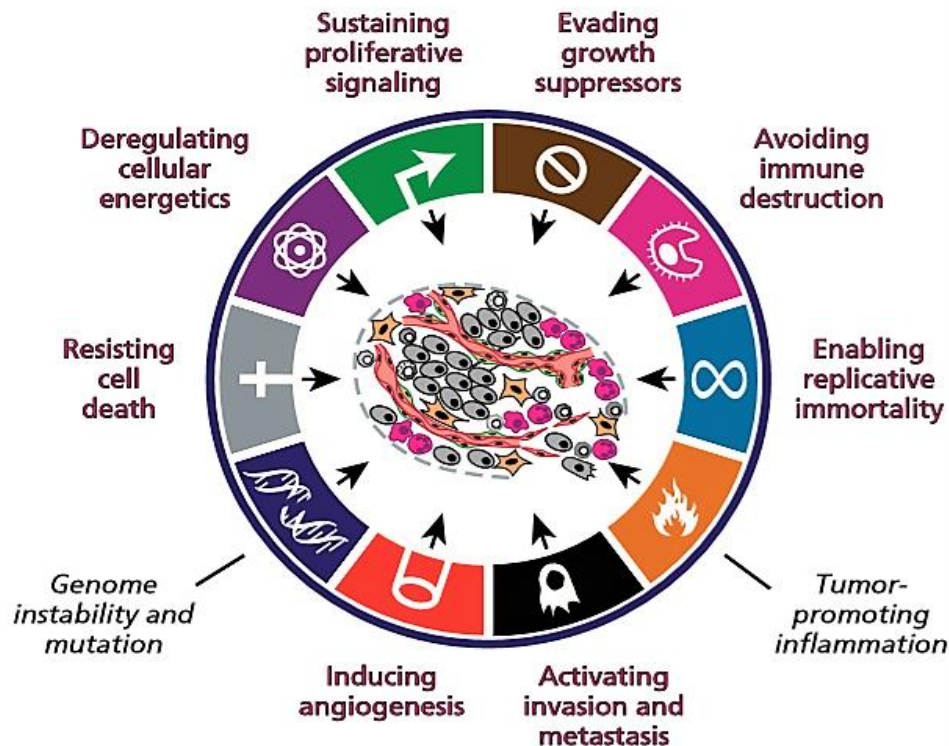


Figure 1.1 **The biological hallmarks of the cancer.** Hallmarks and key facilitators (in black italics) of the cancer. These hallmark traits may be acquired at different stages in the multistep development of cancer, via distinctive mechanisms in different forms of human cancer (D. Hanahan and R. Weinberg, 2017).

Moreover, cancer cells tend to resist cell death, bypassing the three mechanism for triggering cell death, i.e. apoptosis, necroptosis and autophagy. Cancer cells are also able to involve various stress-response systems, of which the most important is the secretion of growth factors useful for angiogenesis. Consequently, new tumour blood vessels provide oxygen and nutrients to the tumour cells. Finally, the most critical event is the activation in epithelial cancer cells of a developmental program termed epithelial-mesenchymal transition (EMT). During this latter, cells acquire a mesenchymal phenotype and intravasate into the blood vessels and the lymphatic system in order to create a new tumour mass in a distant site of the body. This represent the core of the metastatic process and increase exponentially the mortality rate in cancer patients. The acquisition of this hallmark capability can occur at various points along the tumour progression (in an early stage as well as in a late stage) (Hanahan & Weinberg, 2017). The development of these different features leads to create and sustain an ideal environment for the cancer cells, the tumour microenvironment (TME) ([Figure 1.2](#)). This latter consists not only of a heterogeneous population of cancer cells but also a variety of

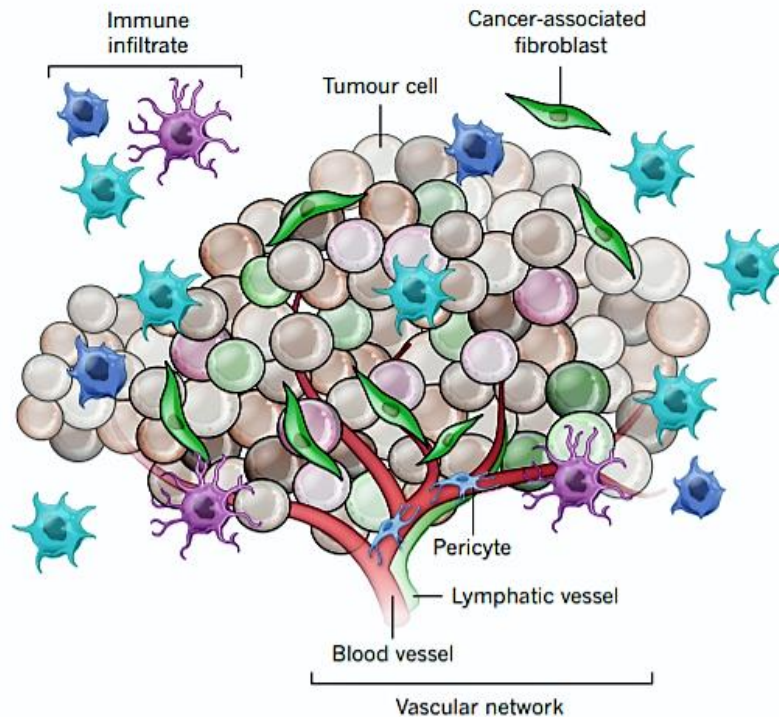


Figure 1.2 **Heterogeneity of tumour microenvironment** (Melissa R. Junttila & Frederic J. de Sauvage, 2013).

resident and infiltrating host cells, secreted factors and the extracellular matrix (ECM) proteins. Tumour progression is profoundly influenced by interactions of cancer cells with their environment that ultimately determine whether the primary tumour is eradicated, metastasizes or establishes dormant micrometastasis and moreover, TME can also shape therapeutic responses and resistance.

Normal fibroblasts responding to a damage typically suppress tumour formation, but cancer-associated fibroblasts (CAFs) can promote tumour genesis because they have a high level of proliferation and increase the ECM production and the release of cytokines. This fibroblasts behaviour causes a huge tissue remodelling and the creation of a new vascular network. The tumour vasculature provides nutrient and other factors in order to allow cancer cells proliferation and division, but it's disorganized and many researchers have studied how attach tumour cells exploiting tumour vasculature. Moreover, it has been demonstrated that cancer cells have the ability to evade the immune system and even to use it to stay alive and grow, thanks to the presence of tumour-associated macrophages (TAM) that play an important role in cell development, survival and growth (Brian F. Zamarron and WanJun Chen, 2011).

1.2 CANCER STATISTICS

Cancer is the second leading cause of death globally, and, based on the data from *World Health Organization* (WHO), it is responsible for an estimated 9.6 million deaths in 2018. Globally, about 1 out of 6 deaths is due to cancer. Furthermore, there were about 18 million new cases in 2018 worldwide, most of them were in more developed countries, as shown in the [Figure 1.3](#) and [Figure 1.4](#) (Globocan, 2019).

In particular, there are around 367,000 new cancer cases in UK every year and around 167,000 cancer deaths during the same years (from data between 2015 and 2017) (*Cancer Research UK*, 2020).

In Italy, in 2019, 371,000 new diagnosis are estimated (196,000 men and 175,000 women) and 179,502 deaths were counted in 2016 (*salute.gov.it*, 2020).

Lung, prostate, colorectal, stomach and liver cancer are the most common types of cancer in men, while breast, colorectal, lung, cervix and thyroid cancer are the most common among women (Globocan, 2019).

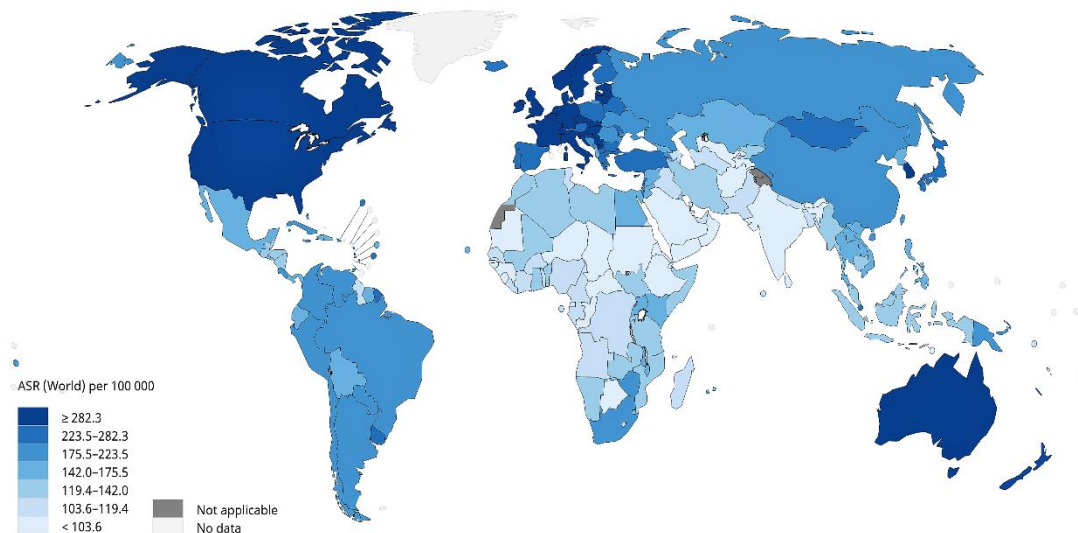


Figure 1.3 Estimated age-standardized incidence rates in 2018, both sexes, all ages. The age-standardised rate (ASR) is a summary measure of the rate that a population would have if it had a standard age structure. It is necessary when comparing several populations that differ with respect to age because age has a powerful influence on the risk of dying from cancer (World Health Organization).

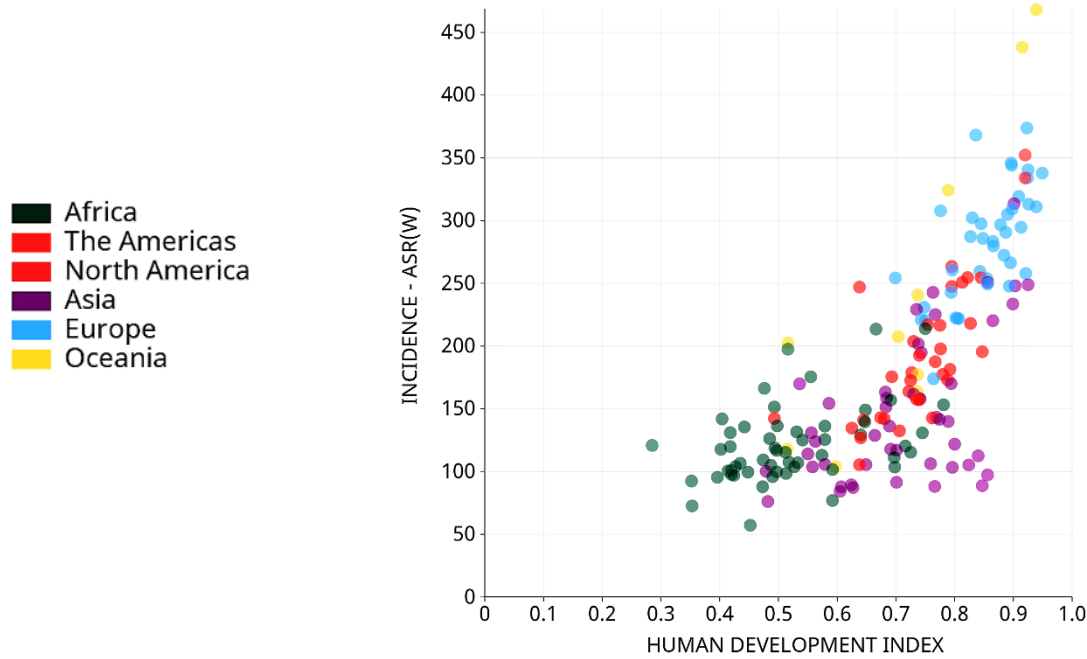


Figure 1.4 *Incidence - ASR(W) vs Human Development Index, all cancers, in 2018, both sexes, all ages (World Health Organization).*

1.3 CONVENTIONAL CANCER TREATMENTS

The goal of any cancer treatment is to kill as many cancer cells as possible and minimize the death of normal cells. Cancer treatment depends on the type of cancer and how advanced it is, and it is possible to supply patients only one treatment or a combination of treatments (National Cancer Institute, 2020). For local cancer, a cure is possible for several cancer types, but once it is metastasized, the treatments are often palliative. Before the 21st century, surgery, radiation and chemotherapy were the most used types of treatment, but in the last two decades, novel treatment options have been shown promising, such as molecularly targeted therapies, immunotherapies and gene therapies (Prabhakar et al., 2019). A brief overview of the current treatment approaches is proposed in the following sections.

1.3.1 Surgery

Practiced as early as the 1700s, surgery is a procedure in which surgeon removes as much as possible of solid tumours from patient's body. The conventional procedures are the open surgery and the laparoscopic surgery, but there are other ways of performing this treatment such as cryosurgery, using extreme cold produced by liquid nitrogen or argon

gas to destroy abnormal tissue, laser treatment with powerful beams of light to cut through tissue for precise surgery, and hyperthermia, using high temperatures to damage and kill cancer cells. Surgery is often not able to remove or kill microscopic disease around the edges of the tumour, leaving tumour cells in the patient after treatment. In order to overcome this issue, it is beneficial to combine surgery with another type of treatment, for instance radiotherapy or chemotherapy, improving efficacy and outcomes of the treatment (Prabhakar et al., 2019).

1.3.2 Radiation Therapy

Radiotherapy uses high doses of high energy radiation to kill cancer cells and shrink tumours, damaging cancer cells DNA over time. It is possible to have an external beam radiation therapy or an internal radiation therapy (systemic therapy) (Dawson & Sharpe, 2006). Unfortunately, radiation damages more quickly actively dividing cells, such as cancer cells and fast-dividing normal cells, like skin and bone marrow. Moreover, radiotherapy is inefficient to kill cancer cells in areas that do not have a good supply of oxygen. In order to reduce side effects, involved doses are fractionated and this treatment may last for many weeks (Prabhakar et al., 2019).

1.3.3 Chemotherapy

In the chemotherapeutic treatment, small drug-like molecules disrupt the normal functioning of a cell by interfering with DNA synthesis, replication and cell division, resulting in cell death; most effective drugs available are Paclitaxel, Doxorubicin and Docetaxel, in fact they induce a great degree of cytotoxicity against cancer cells (Moorthi et al., 2011). As the radiotherapy, target cells are represented by the fast-dividing cells and, in this case, side effects are principally alopecia, nausea, bone marrow depression and emesis. In recent years, novel drug delivery approaches have been developed in order to maximize treatment benefit and overcome multidrug resistance (MDR) (Prabhakar et al., 2019).

1.3.4 Targeted Therapy

In the TME, cancer cells and the surrounding tissues overexpress genes encoding for specific protein or altered signaling pathways that ensure uncontrolled cells growth and cells survival. Targeted therapy consists in a set of small drug-like molecules or

monoclonal antibodies (mAbs) that are administered orally or intravenously in order to inhibit these proteins or signalling pathways. For example, it has been demonstrated that tyrosine kinase inhibitors (TKIs) can improve treatment efficacy of some advanced non-small cell lung cancer inhibiting certain tyrosine kinases secreted by the epidermal growth factor receptor (EGFR) tyrosine kinases. In general, targeted therapies are less toxic than chemotherapies or radiotherapies. In particular, toxicity depend on the presence of the target proteins on healthy cells. In [Table 1.1](#) some examples of targeted therapies and respective drugs are presented (Prabhakar et al., 2019).

Table 1.1 Readapted from Prabhakar et al. (2019).

TYPE OF INHIBITORS	CANCER TARGET	EXAMPLE DRUGS (BRAND NAMES): CANCER INDICATIONS
Signal Transduction Inhibitors	ErbB1 (EGFR)	<i>Cetuximab (Erbix®)</i> : CRC, HNSCC
	ErbB2 (HER2)	<i>Trastuzumab (Herceptin®)</i> : breast and stomach cancer
	TKs (EGFR)	<i>Gefitinib (Iressa®)</i> : NSCLC
	TKs (BCR-ABL, KIT, PDGFR)	<i>Erlotinib (Tarceva®)</i> : NSCLC, renal, pancreatic cancer
	Kinases (B-raf, VEGFR2, EGFR, PDGFR)	<i>Imatinib mesylate (Gleevec®)</i> : GIST, CML
	BTK	<i>Sorafenib (Nexavar®)</i> : kidney and liver cancer <i>Sunitinib (Sutent®)</i> : GIST and kidney cancer
	P13K	<i>Ibrutinib (Imbruvica®)</i> : CLL <i>Idealisib (Zydelig®)</i> : CLL
Apoptosis Inhibitors	20s proteasome	<i>Bortezomib (Velcade®)</i> and <i>Carfilzomib (Krypolis®)</i> : multiple myeloma
Angiogenesis Inhibitors	VEGF	<i>Bevacizumab (Avastin®)</i> : CRC, GBM, ovarian, cervical and kidney cancer
Immune Cell Targeted	CD20	<i>Rituximab (Rituxan®)</i> : B-cell lymphoma
	CD19, CD3	<i>Blinatumomab (Blincyto®)</i> : ALL
Immune Checkpoint Inhibitors	PDI, PD-L1	<i>Nivolumab (Opdivo®)</i> : NSCLC, kidney cancer <i>Pembrolizumab (Keytruda®)</i> : NSCLC, melanoma
	CTLA4	<i>Atezolizumab (Tecentriq®)</i> : NSCLC <i>Ipilimumab (Yervoy®)</i> : melanoma

1.3.5 Immunotherapy

Immunotherapy is a promising way to treat cancer. Cancer cells are able to develop alternative pathways or mechanism to suppress or avoid the attacks of the innate immune system in order to continue growing. Immunotherapy utilizes different ways to stimulate immune activation pathways or to block the immune system suppression. For example, immune checkpoint inhibitors are drugs that block immune checkpoints, normal part of the immune system that keep immune responses from being too strong. Another way is to create a vaccine designed to work against cancer by boosting the immune system's response to cancer cells. A recent promising type of immunotherapy is the CAR (Chimeric Antigen Receptor)-T Cell Therapy ([Figure 1.5](#)), in which T cells are taken from the patient's immune system, genetically modified *ex vivo* to express receptors to recognize selected antigens. Viral or non-viral vectors are used to insert genetic material into the cells in order to express receptors. After this, T cells are expanded *in vitro* and put back into the patient's body in order to strongly attack cancer cells. This therapy has led to complete remission in acute lymphocytic leukemia (ALL) in 90% of patients (Maude et al., 2015). Cytokine release syndrome is the most severe side effect caused by this therapy and it need to be better investigated. Nevertheless, in 2017, Novartis

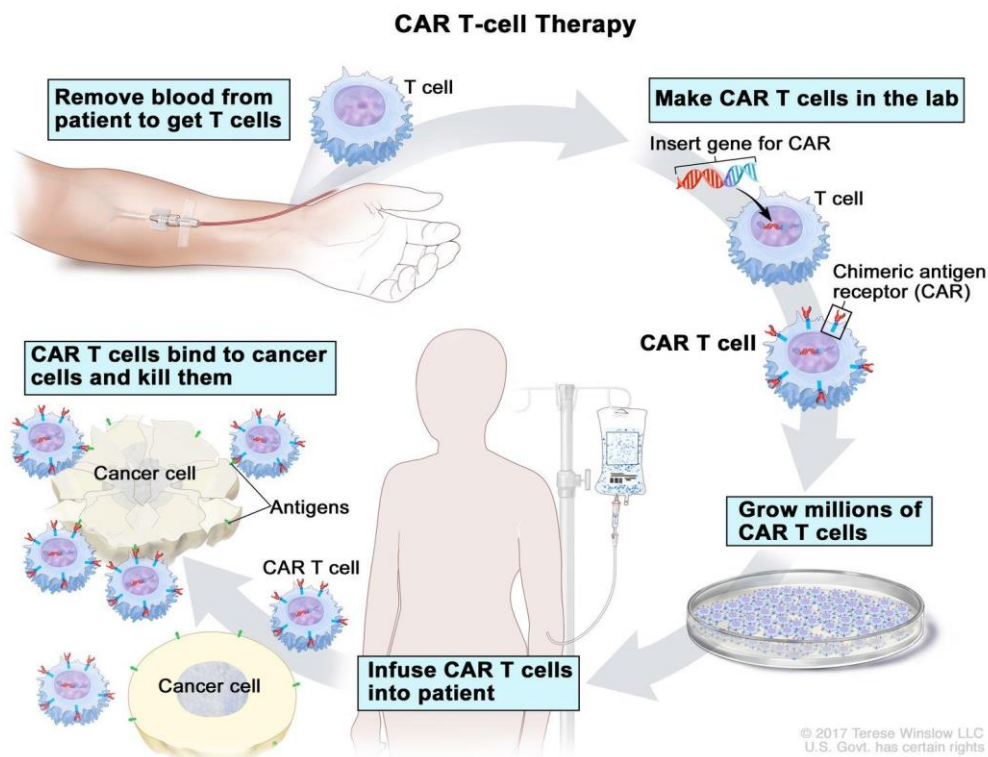


Figure 1.5 CAR (Chimeric Antigen Receptor)-T Cell Therapy (www.cancer.gov).

announced that FDA has approved Kymriah™, the first CAR-T Cell Therapy for the treatment of patients with ALL¹. (National Cancer Institute, 2020).

1.4 CANCER DIAGNOSTICS AND MONITORING

An efficient early detection of tumour is essential in order to develop a successful workflow with the right combination of treatments. Medical imaging processes are used for diagnostic, computer tomography (CT), positron emission tomography (PET), magnetic resonance imaging (MRI), X-ray, ultrasound and endoscopy. However, the evaluation of tumour biomarkers is useful to estimate risk of disease and screen primary cancers, reducing invasive procedures and unsafe exposures to radiations. In fact, biomarkers are present in samples such as sputum, urine, whole blood, serum or plasma. Before utilizing a biomarker for tumour detection, it must be validated with test for sensitivity and specificity, accuracy and reproducibility, and the benefit-to-harm ratio must be assessed. Nowadays, 20 biomarkers have been approved for cancer prediction (Table 1.2) (Prabhakar et al., 2019).

Tabel 1.2 Readapted from Prabhakar et al. (2019).

BIOMARKER	CLINICAL USE	CANCER TYPE	SPECIMEN
Pro2PSA (truncated form of prostate-specific antigen, PSA)	Discriminating cancer from benign disease	Prostate	Serum
ROMA (HE4 + CA-125) (Risk of Ovarian Malignancy Algorithm)	Prediction of malignancy	Ovarian	Serum
OVA1 (panel of multiple proteins)	Prediction of malignancy	Ovarian	Serum
HE4 (human epididymis protein)	Monitoring recurrence or progression of disease	Ovarian	Serum
Fibrin/fibrinogen degradation product (DR-70)	Monitoring progression of disease	Colorectal	Serum
AFP-L3% (alpha-fetoprotein protein isoform)	Risk assessment for development of disease	Hepatocellular	Serum
Circulating tumor cells (EpCAM (epithelial cell adhesion molecule), CD45, cytokeratins 8, 8+, 19+)	Prediction of cancer progression and survival	Breast	Whole Blood

¹ <https://www.novartis.com/news/media-releases/novartis-receives-first-ever-fda-approval-car-t-cell-therapy-kymriah-ctl019-children-and-young-adults-b-cell-all-refractory-or-has-relapsed-least-twice>

p63 protein	Aid in differential diagnosis	Prostate	FFPE tissue
c-Kit	Detection of tumors, aid in selection of patients	Gastrointestinal stromal tumors	FFPE tissue
CA19-9 (cancer antigen 19-9)	Monitoring disease status	Pancreatic	Serum, plasma
Estrogen receptor (ER)	Prognosis, response to therapy	Breast	FFPE tissue
Progesterone receptor (PR)	Prognosis, response to therapy	Breast	FFPE tissue
Her-2/neu	Assessment for therapy	Breast	FFPE tissue
CA-125	Monitoring disease progression, response to therapy	Ovarian	Serum, plasma
CA15-3	Monitoring disease response to therapy	Breast	Serum, plasma
CA27.29	Monitoring disease response to therapy	Breast	Serum
Free PSA	Discriminating cancer from benign tissue	Prostate	Serum
Thyroglobulin	Aid in monitoring	Thyroid	Serum, plasma
Nuclear mitotic apparatus protein (NuMA, NMP22)	Diagnosis and monitoring of disease (professional and home use)	Bladder	Urine
Alpha-fetoprotein (AFP)	Management of cancer	Testicular	Serum, plasma, amniotic fluid
Total PSA	Diagnosis and monitoring of disease	Prostate	Serum
Carcinoembryonic antigen	Aid in management and prognosis	Not specified	Serum, plasma
Human hemoglobin (fecal occult blood)	Detection of fecal occult blood (home use)	Colorectal	Feces

Regarding cancer monitoring, the same approaches are currently utilized for imaging in vivo of the tumour progress in order to obtain an optimal follow-up for patients. It is essential to assess the state of tumour and to plan new treatment cycles. The most used modalities are the imaging processes because they are non-invasive and easy to use, but, in several cases, their detection sensitivity and specificity are highly variable and often low for early detection of recurrences (Meads et al., 2013).

In recent years, nanotheranostics is emerging as a promising strategy for treatment and imaging of tumours. By combining therapeutic and diagnostic capability into one single agent, it seems to provide more specific and efficient systems for curing and evaluate tumour progress. Many researchers have made great efforts in order to develop novel

nanoplatfroms and more efficient contrast agents for obtaining a standard of care suitable for most tumours. Emerging nanotechnology is offering great opportunities to design and generate such agents, wherein the detection modality is extensively allowed to run not only before or after but also through the treatment regimen (L. S. Wang et al., 2012).

2 NANOTHERANOSTICS: AN EMERGING STRATEGY

2.1 INTRODUCTION

The term “theranostics” results from the merging of the words “therapeutics” and “diagnostics”. It was used for the first time in 1998 by John Funkhouser in a press release by the company PharmaNetics to describe diagnostics that influence the physicians’ therapy decisions in patients’ treatment (Wiesing, 2019). In a broad definition, theranostics involves a more specific connection between diagnostic and therapy: the purpose is to use diagnostic process on the molecular or nano-level in order to choose a specific therapy for an individual patient. According to this definition, diagnostics and therapy take place at different times because therapy is the result of diagnostics. However, this definition has led to very controversial opinions; several doctors and scientists have strongly criticised it because it adds nothing new to the relation between diagnostics and therapy. The only innovative aspect is the nano-level investigation, but it does not explain the introduction of a new term. On the other side, in a narrow definition, theranostics can be used for simultaneous targeted drug delivery and release and diagnosis including monitoring disease progression and response to therapy. A combined diagnostic-therapeutic intervention does not avoid prior diagnostic procedures, instead it focuses on providing additional and more accurate diagnostic information useful for monitoring diseases in order to modulate the therapeutic interventions. This latter definition demonstrates the importance of the nanotheranostics field (Wiesing, 2019).

A theranostic platform consists of a one system composed by a therapeutic drug, a carrier of the therapeutic payload, targeting ligands and signal emitters for imaging (Roy Chowdhury et al., 2016).

The progress of nanotechnology research has allowed the development of materials suitable for nanoplateforms for nanotheranostic applications. Carriers most frequently used are nanoparticles (NPs) made by polymeric, metallic, silica-based or composite materials because of their distinctive properties, such as high surface-area-to-volume ratio to give loading capacity to imaging probe and targeting ligands, specific small size to increase the chances of adsorption from tumour blood vessels into tumour tissues (Penet et al., 2014). The physiochemical characteristics as size, shape, charge and surface

functionalisation of nanoparticles are significant for the therapy because small nanoparticles (<20 nm) have fast body distribution but also a rapid renal clearance, larger ones (>200 nm) are cleared by phagocytic system and accumulate in body organs (Zhang et al., 2009). Moreover, the pore size of tight endothelial junction in normal blood vessels is <10 nm whereas the size of tight junction in tumour microenvironment is >200 nm and, in addition, NPs cannot escape the tumour thanks to the enhanced permeability and retention (EPR) effect. According to Banerjee et al. (2016), the NPs size must range from 50 to 200 nm in order to have effective transport and absorption. NPs can be easily modified using different bioconjugation techniques to increase the functionalities. For example, in a study by Loverde et al. (2011) the researchers demonstrate that the conjugation of a PCL-PEG spacer to a worm-like NPs with chemotherapy agent Taxol improve the stability of the system *in vivo* and provide a more controlled release kinetics ([Figure 2.1](#)) (Loverde et al., 2011).

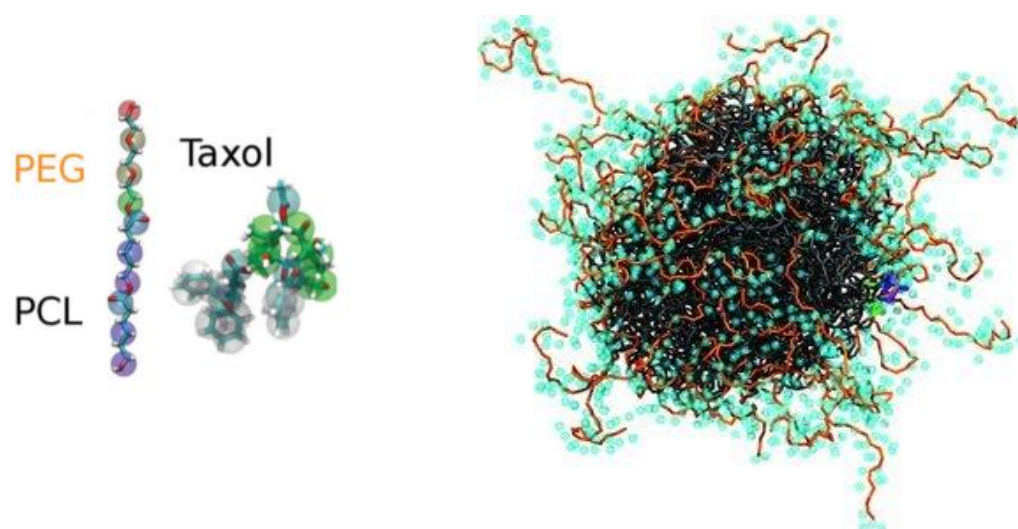


Figure 2.1 Worm-like NP with block copolymer PCL-PEG and Taxol. Readapted from Loverde et al. (2011).

Besides, surface functionalisation consents an active targeting to cancer cells and combination of light-based modalities, such as photothermal therapy (PTT) and photodynamic therapy (PDT) (Dykman & Khlebtsov, 2016). For instance, Kostevsek et al. (2016) developed a one-step synthesis of gold-iron oxide nanoparticles functionalised with a biocompatible chitosan matrix, which combined photothermal heating properties and photoacoustic imaging (PAI). The researchers have taken advantage of the magnetic properties of iron oxide for magnetic-guided delivery towards the target organ. The

systems are expected to exhibit surface plasmon resonance properties due to the incorporation of gold: this allows for both imaging (PAI) and therapy (PTT). A variation of NPs surface with particularly chitosan chains was carried out in order to create a highly biocompatible shell able to protect and deliver the NPs within the body (Figure 2.2) (Kostevsek et al., 2016).

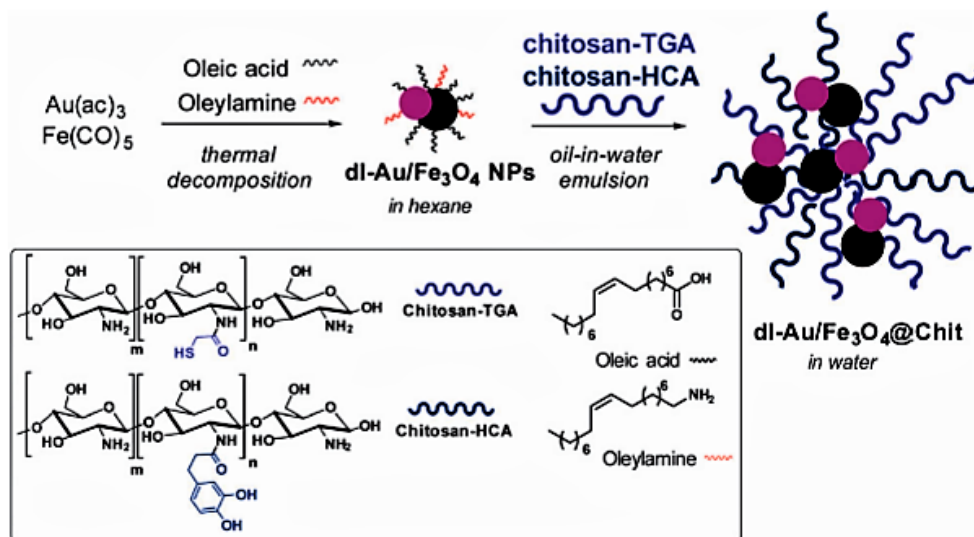
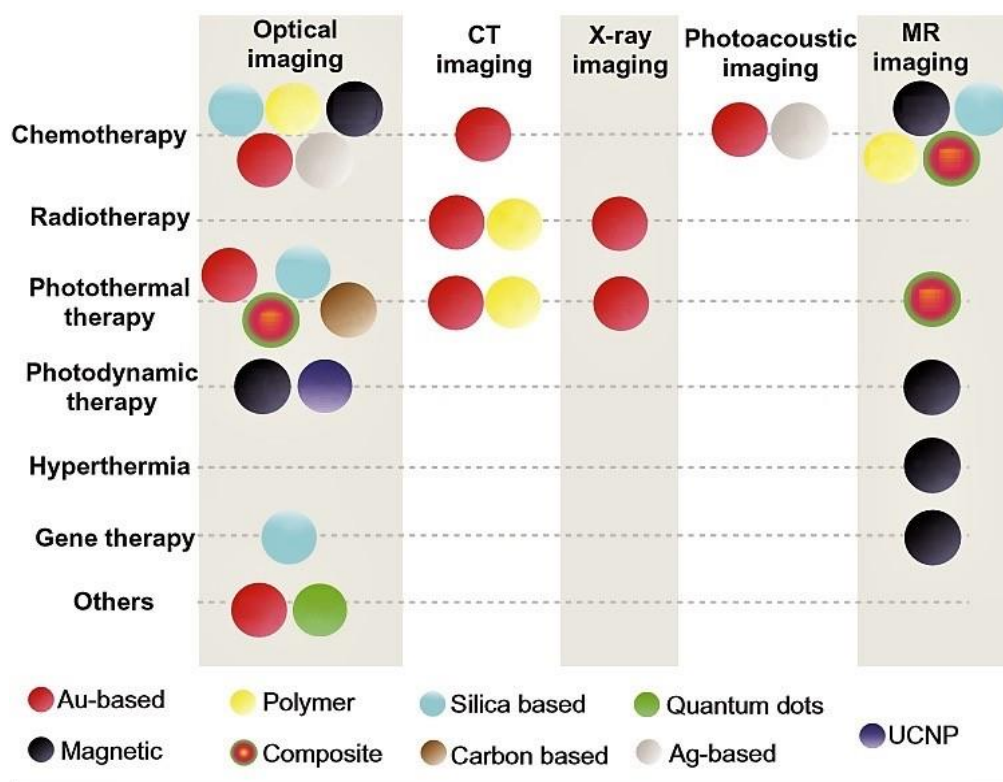


Figure 2.2 Representative scheme for the synthesis of gold-iron oxide functionalized NPs (Kostevsek et al., 2016).

As summarized in the figure 2.3, optical and MRI are the preferable modalities performed for imaging functionality, through use of near-infrared (NIR) emission and magnetic agents, respectively. These two imaging strategies are mostly integrated with either PTT to produce multiple functions that have been demonstrated by employing different core nanomaterials (L. S. Wang et al., 2012).

The human body has multitiered physical, physiological, chemical, and biological barriers to safeguard it against external substances. Example of the barriers that nanomaterials might encounter in biological systems are the skin, air-blood barrier in the lungs, reproductive system, circulation, and blood-brain barrier (BBB). Nanomaterials must be accurately engineered to overcome these biological obstacles and perform nanotherapeutics at the disease site (Meng et al., 2018; Nabil et al., 2019).



Abbreviations: CT, computed tomography; MR, magnetic resonance; UCNP, up-conversion nanoparticle.

Figure 2.3 Summary of therapeutic methods, diagnostic strategies, and corresponding nanomaterials. Readapted from L.S. Wang et al. (2012).

2.2 NANOMATERIALS FOR NANOTHERANOSTIC

Nanocarriers, or nanoplatforms, are the crucial components of theranostic nanosystems. They are used to integrate the therapeutic and imaging agents in one entity and realize their functionalities simultaneously. The physical properties of the systems must allow for simple biological examining, continuing stable under physiological situations when being delivered (Kelkar & Reineke, 2011). The agent must have no significant toxic side effects and be able to penetrate through biological barrier in order to reach the target organ or tissue (Sahoo et al., 2014). Nanoplatforms for nanotheranostic applications are made by several materials capable of detecting and treating disease in one single procedure. The developing nanotechnology is offering great opportunities to design and generate several shapes of them according to the features of target sites (L. S. Wang et al., 2012). Different studies have properties and characteristics of polymeric micelles, magnetic nanoparticles, gold-based nanoparticles, metallic nanorods, carbon nanotubes,

dendrimers, lipid-based nanocarriers, nanodiamonds and others. Typical and widely used nanomaterials used for construction of them are listed up below.

2.2.1 Gold-based Nanomaterials

Gold nanomaterials have been investigated for nanotheranostic applications thanks to their high degree of biocompatibility and efficient strategies for surface modifications such as gold-thiol bonding. The optical and photothermal characteristics of gold nanoparticles allow for engineering them as sensing modalities as well as therapeutic agents (L. S. Wang et al., 2012). The localised surface plasmon resonance (LSPR) can be controlled by tuning size, shape, structure, and surface chemistry of nanoplatforms in order to apply them as imaging agent (Cobley et al., 2011). In this regard, Jain et al. (2006) have demonstrated that the increase in gold nanosphere size from 20 to 80 nm improve the magnitude of excitation and absorption cross section compared to conventional absorbing iodine based agents in CT imaging, making gold nanoparticles as an efficient candidate for cancer monitoring and imaging. In addition, different forms of gold nanoformulations with different sizes and shapes can be used as multifunctional agents in cancer treatments ([Figure 2.4](#)) (Guo et al., 2017).

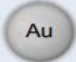



AuNPs	Theranostic applications
 Nanosphere (2–100 nm)	<ul style="list-style-type: none"> • Cell imaging (visible lights) • PTT (visible lights) • Delivery of therapeutic cargos (ie, photosensitizers)
 Nanorod (10–100 nm)	<ul style="list-style-type: none"> • Tumour imaging (enhanced radiative property; NIR) • PTT (enhanced nonradiative property; NIR) • Delivery of therapeutic cargos (ie, photosensitizers)
 Nanoshell (100 nm)	<ul style="list-style-type: none"> • Tumour imaging (enhanced radiative property; NIR) • PTT (enhanced nonradiative property; NIR) • PDT (unique shape and structure) • Delivery of therapeutic cargos (ie, photosensitizers)
 Nanocage (40–50 nm)	<ul style="list-style-type: none"> • Tumour imaging (enhanced radiative property; NIR) • PTT (enhanced nonradiative property; NIR) • PDT (unique shape and structure) • Delivery of therapeutic cargos (ie, photosensitizers)

Figure 2.4 Development of theranostic AuNPs in the treatment of cancer. Commonly used AuNPs can be categorized depending on the particle shape, including Au nanospheres, nanorods, nanoshells, and nanocages.. Readapted from Guo et al. (2017).

Gold nanomaterials are not only good CT imaging contrast agents but also great radiotherapy sensitizer thanks to their high X-ray absorption coefficient (L. S. Wang et al., 2012). The main challenge for radiation therapy is to reach the highest probability of efficient treatment without substantial side effects. According to the literature, targeted delivery of radiotherapy sensitizer to the tumour site seems to be useful to deliver more targeted doses while reducing the impact on surrounding tissues, improving the accuracy of radiation treatment. In their study, Huang et al. (2011) synthesised a folic acid-conjugated silica-modified gold nanorod (GNR-SiO₂-FA) and demonstrated that such multifunctional nanoprobe was created to improve functions in tumour targeting, imaging, and selective therapy, testing the enhanced RT and PTT effects on gastric cancer cells.

In a further work, a group of researchers designed and developed a matrix metalloprotease (MMP)-sensitive gold nanorod (MMP-AuNR) as a probe for cancer diagnosis and therapy (Yi et al., 2010). MMP is a family of zinc-dependent proteins, and its production is related with cancer metabolism. The imaging of MMP could provide valuable information about cancer diagnosis (Egeblad & Werb, 2002). Yi et al. created a fluorescent probe for detecting MMP, used to analyse the progress of cancer by monitoring the fluorescence recovery of quenched Cy5.5, by conjugating Cy5.5 with a peptide that can be degraded by MMP, and then putting modified Cy5.5-peptide complex on the surface of AuNR. Moreover, the photothermal effect was induced by MMP-AuNR by absorption of NIR laser raising the surrounding environment temperature to 60°C, causing the damage of tumour tissue ([Figure 2.5](#)) (Yi et al., 2010).

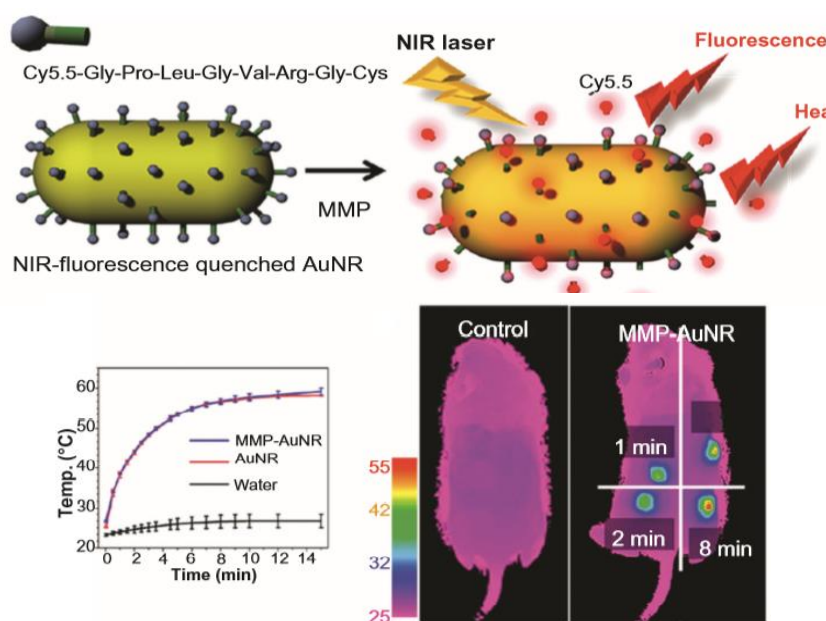


Figure 2.5 Schematic representation of MMP-AuNR for simultaneous imaging and PTT on top. Temperature increase of MMP-AuNR as a function of laser irradiation time on bottom. Readapted from Yi et al. (2010).

2.2.2 Magnetic Nanomaterials

Magnetic NPs-based theranostics are the major category of NPs in nanotheranostic research thanks to their intrinsic biocompatibility, cost-effectiveness, and magnetic property as nanostructured contrast probes for MRI (L. S. Wang et al., 2012). MNPs are used as agents for MRI because of their superparamagnetic properties, allowing them to be magnetized under an externally applied magnetic field, and to lose this magnetization once the field is removed (Laurent et al., 2007). This is important when MNPs are introduced into living systems because the disappearance of magnetization in the absence of an external magnetic field could avoid the agglomeration in target drug delivery (Belyanina et al., 2017). General characteristics of magnetic NPs such as nanometric dimensions, enhanced permeability retention, high surface area for molecular therapeutic binding and functionalization with cancer ligands make them interesting in nanotheranostic field, in particular regarding cancer diagnosis and treatment (Greish, 2007).

Hydrophilic polymers are added to passivate the nanocrystal surface protecting particles from aggregation in order to provide colloidal suspendibility to the MNPs. Furthermore, specific polymers are used to coat MNPs to facilitate drug encapsulation (L. S. Wang et al., 2012). For instance, in their work Santra et al. (2009) coated iron oxide nanoparticles (IONPs) with poly (acrylic acid) (PAA). Then they reported the co-encapsulation of a lipophilic near infrared (NIR) dye and an anticancer drug within hydrophobic pockets in the polymeric matrix of PAA in order to provide combined optical imaging, MRI detection. In addition, folate was conjugated onto PAA-IONPs for targeted cancer therapy (Santra et al., 2009). IONPs have gained attention for personalized medicine thanks to their magnetic properties. In particular, superparamagnetic IONPs (SPIONs) have become the common and principal candidate for biomedical applications. They have attracted great interest as MRI T_2 contrast agents and they have also been recognized as mediators for hyperthermia treatment because SPIONs generate heat under alternating magnetic fields. This magnetic hyperthermia enables selective ablation of tumour tissue with minimal collateral damage to normal tissue (Kobayashi, 2011). For example, folic acid (FA)-functionalized PEGylated SPION nanoclusters have been developed for combining MRI with hyperthermia (Hayashi et al., 2013). Allyl-functionalized SPIONs of 7 – 9 nm diameter were PEGylated via Thiol-End Click (TEC) chemistry using bifunctional thiol-PEG-FA. FA-PEG-SPION NCs showed much higher relativity

compared to the commercial MRI agent, Resovist, at equivalent iron concentrations. Following intravenous administration, FA-PEG-SPON NCs efficiently accumulated in tumour tissues and produced strong MRI signal intensity. Moreover, by applying an alternating magnetic field the tumour tissue could be heated by 6 °C within 20 minutes, which resulted in significant inhibition of tumour growth with no hepatotoxicity or nephrotoxicity observed (Hayashi et al., 2013).

Additionally, anticancer drugs can be loaded in SPIONs for combining MRI and chemotherapy. For instance, Yu et al. (2008) developed DOX-loaded SPIONs; they prepared an antibiofouling polymer-coated SPIONs using a thermal crosslinking method (TCL-SPIONs). Positively charged DOX molecules were incorporated into the negatively charged polymer shells of TCL-SPIONs by electrostatic interactions. MRI confirmed that DOX-loaded TCL-SPIONs having a hydrodynamic diameter of 21 nm significantly accumulated in tumour xenografts following intravenous injection due to the EPR effect. When delivered by TCL-SPIONs, a larger amount of DOX was delivered to tumour than free DOX. Selective accumulation of nanoparticles enhanced therapeutic efficacy with minimal systemic toxicity (M. K. Yu et al., 2008).

In addition to polymers, silica coating on MNPs is common due to simplicity of synthesis and its stability in aqueous condition (L. H. Reddy et al., 2012). MNPs modification by phospholipid layer is also a typical method. The liposomes structure is similar to biological membranes and determines their biocompatibility and efficacy in the targeted delivery systems (Lee et al., 2015). Recently, more attention has been given to the preparation of magnetic nanoparticles with carbon coatings, in the light of their advantages over polymers or silica, such as a much higher chemical and thermal stability (A. H. Lu et al., 2007). After the nanoparticle is covered with a appropriate coating, its surface is further modified with various functional groups, e.g. azido, amino, carboxyl, sulfhydryl, hydroxyl, imide, thiol, and others that consent the nanoparticles to bind to target biomolecules or therapeutic agents ([Figure 2.6](#)) (Belyanina et al., 2017).

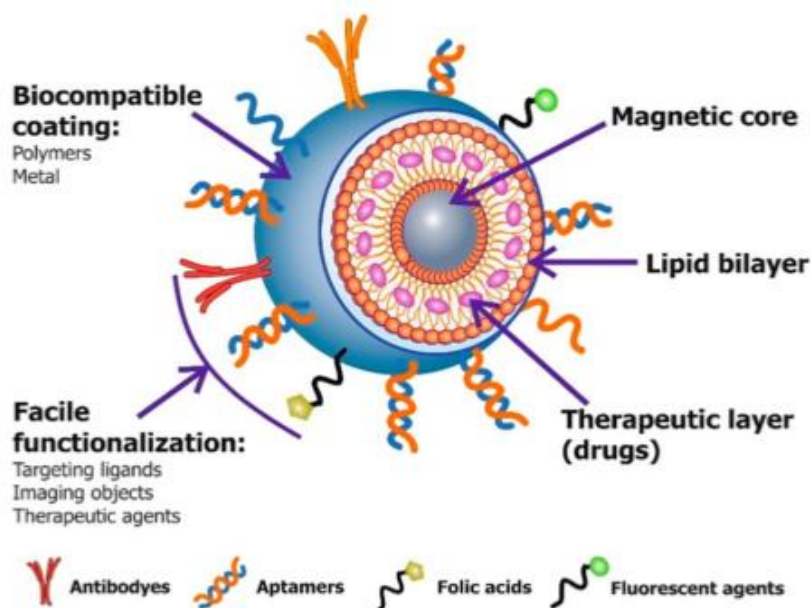


Figure 2.6 Schematic illustration of a multifunctional magnetic nanoparticle structure with different types of coatings, target ligands and imaging agents. Readapted from Belyanina et al. (2017).

2.2.3 Polymeric Nanomaterials

Polymeric micelles/conjugates have been emerging as a highly integrated theranostic nanoplatform for cancer diagnosis and therapy (L. S. Wang et al., 2012). These NPs can be formulated by integrating various functional units to soluble macromolecules via self-assembly of copolymers. Polymeric formulations can be loaded with different types of therapeutic and imaging agents (Peer et al., 2007). However, polymeric NPs require successful strategies to minimize the immunogenicity and antigenicity as well as to enhance the residence time and stability inside the biological system. Among numerous materials, the most successful strategy has been to modify nanocarriers with PEG, which leads to decreases in immunogenicity and antigenicity as well as increases in body-residence and stability. Moreover, PEG can shield the core of nanocarriers from degradation by steric issues, reducing kidney clearance thanks to an increased hydrodynamic size of PEG-carrier conjugate, and, as a result of its hydrophilicity, increasing the nanocarriers' solubility (L. S. Wang et al., 2012).

Conventional natural polymers including chitosan, gelatin, albumin, sodium alginate, and synthetic polymers such as polylactic acid (PLA), poly (lactic-co-glycolic acid) (PLGA), poly-glutamic acid, poly aspartic acid, and hyaluronic acid (HA) are widely used in the synthesis of polymeric NPs (Rai & Jamil, 2019). The polymeric nanoparticles thus

formulated can be obtained as nanocapsules, nanospheres, polymeric micelles, drug-polymer conjugates, dendrimers, polymerosomes, and polyplexes (Prabhu et al., 2015). Moreover, the physiochemical properties, e.g. crystallinity, molecular weight, hydrophobicity, and polydispersity index, regulate the dissolution and drug delivery kinetics of the polymeric NPs (Sonali et al., 2018).

In the literature, the most common nanoparticle size referred to is ranging between 100-500 nm, in order to avoid fast clearance upon intravenous administration, extend circulation half-life, and, at the same time, increase the probability of crossing various biologic barriers and preventing accumulation in capillaries and other organs (Deng et al., 2020).

2.2.3.1. Polymeric Shell

Various polymers have been employed for the formulation of nanocapsules shell, to satisfy the different application requirements.

Polysaccharides have been broadly used as drug carriers thanks to their biocompatibility; they are rich in deprotonated amino groups or carboxylic acid groups, resulting in cationic or anionic charges, thereby to form polymeric shells by electrostatic attractive interactions (Hayashi et al., 2013; Li et al., 2008). Alginate is one of the anionic natural polysaccharides which has been developed as drug carrier, taking advantages of its biocompatibility, low immunogenicity and mild gelation conditions (Sarmiento et al., 2006; T. Wang et al., 2007). In addition, alginate is also a pH-responsive polymer, allowing for protection for payloads at acidic pH conditions, while achieving drug release at alkaline pH (J. Yang et al., 2013).

Protein-based polymers have been also processed as polymeric shell for nanocapsules, due to their biocompatibility and tuneable properties (De Frates et al., 2018). Albumin is a water soluble and biodegradable protein and it has served as shell for nanocapsules; beside controlling drug permeation rate, albumin corona can reduce the nanoparticles' immunogenicity and thus assist them to escape from the reorganization of reticuloendothelial system (RES). Due to its biogenic properties, albumin can also serve as targeting ligand for albumin receptors which are overexpressed on endothelial cells of tumour blood vessels, providing an excellent drug targeting system (Gaber et al., 2019). Additionally, protein can be engineered into a hollow caged nanostructure by self-assemble of a defined number of subunits. For example, an HspG41C mutant protein-

based nanocapsule formed through self-assembly of 24 individual monomeric proteins was developed as drug carrier for anti-cancer drug doxorubicin, showing a good biocompatibility and successfully delivering doxorubicin to various cancer cell lines (Toita et al., 2013).

Synthesized materials were indicated advantages over natural materials since they have reproducible quality and purity. In addition, they can be tuned with different chemical ionic, mechanical, solubility and degradability properties, according to the applications (Deng et al., 2020). Aliphatic polyesters and relative copolymers are very common synthetic polymers and have been deeply studied and developed as drug delivery systems, due to their biocompatibility and biodegradability. Concerning polymeric shell, the most common are PLA, PLGA, poly(ϵ -caprolactone) (PCL) (Deng et al., 2020).

2.2.3.2. Liquid/Solid/Hollow Core

The core of nanocapsules can be hollow or consists in a liquid or solid phase, thus making it able to carry different drugs (Deng et al., 2020). Nanocapsules can present an oleic core highly suitable for the encapsulation of lipophilic molecules (De Matteis et al., 2018). In this regard, Venturini et al. (2015) used copaiba oil as oily core of a PCL nanocapsule in order to increase the solubility of imiquimod which is a hydrophobic anti-cancer drug (Venturini et al., 2015).

Polymeric nanocapsules can also be manufactured with aqueous core to act as promoting platform for sustained delivery of hydrophilic molecules (Abulateefeh et al., 2019). Hydrophilic anti-cancer drugs, such as gemcitabine hydrochloride and doxorubicin, have been successfully encapsulated into polymeric nanocapsules with aqueous core (Cosco et al., 2015; Vrignaud et al., 2013). Moreover, nanocapsules can also be characterized by a hollow internal structure (Gil et al., 2008). In general, nanocapsules with a hollow core are fabricated by first preparing a solid sphere that is subsequently sacrificed after polymeric shell formation. The use of solid sphere as sacrificial template can specifically provide a strong spherical framework for the assembly of nanocapsules, consisting in multiple polymer shells (Deng et al., 2020). The materials considered as the template core should be easily removed by mild conditions in order to avoid shell damage. Metallic materials such as iron oxide (Yunessnia lehi et al., 2019) and gold spheres were used as template core and can be removed by hydrochloric acid or potassium cyanide solution after that polysaccharide shell is formed. Calcium carbonate as an inorganic candidate

template core of nanocapsules can be removed by adding ethylene diamine tetra acetic (EDTA) acid into a nanocapsule water dispersion at pH 7 (Elbaz et al., 2020). Silica is another inorganic material used as template core and removable by complete dissolution in hydrofluoric acid (Ménard et al., 2019).

2.2.4 Silica-Based Nanomaterials

Unlike many other nanomaterials, of which size-dependent properties are commonly observed as their size approaches the nanoscale and as the percentage of atoms at the surface of a material becomes significant, silica-based nanoparticles (SiNPs) have constant physical properties similar to those of bulk material, except the total surface area increases as the size decreases. In addition to the higher surface area, what really makes SiO₂ NPs prevail in nanomedicine is their tuneable nanostructures and well-established siloxane chemistry, which allow us to fabricate effectively the desired functionalized surface for diagnostic and therapeutic applications (L. S. Wang et al., 2012).

He et al. (2009) described the development of a bifunctional NP-based carrier for simultaneous *in vivo* imaging and PDT by encapsulating methylene blue (MB) in the phosphonate-terminated silica matrix (PSiNPs). The photosensitizer was encapsulated inside the PSiNPs. An appropriate dose of irradiation to the MB-encapsulated PSiNPs under a light of 635 nm resulted in the production of single oxygen that led to photodynamic damage to a cell line derived from cervical cancer (X. He et al., 2009).

Mesoporous silica nanoparticles (MSNs) are promising candidates for well-developed theranostic NPs. The high surface area provides a larger amount of space to be functionalized with desired ligands. In a study by Zhang et al. (2009), a multifunctional SiNP containing a nonporous dye-doped silica core and a mesoporous silica shell enclosing photosensitizer molecules, called hematoporphyrin, was designed and synthesized. The mesoporous silica nanoplateform acted as not only a carrier for the photosensitizer but also a nanoreactor to facilitate the photo-oxidation reaction (Zhang et al., 2009).

Chen et al. (2016) developed a multifunctional theranostic magnetic mesoporous silica nanoparticle (MMSN) with magnetic core for magnetic-enhanced tumour-targeted MR imaging and precise therapy ([Figure 2.7](#)). The gatekeeper β -cyclodextrin (β -CD) was immobilized on the surface of mesoporous silica shell via platinum (IV) prodrug linking for reduction-triggered intracellular drug release. Then Arg-Gly-Asp (RGD) peptide ligand was introduced onto the gatekeeper β -CD via host-guest interaction for cancer

targeting purpose. After active-targeting endocytosis by cancer cells, platinum(IV) prodrug in MMSNs would be restored to active platinum(II) drug in response to the reducing microenvironment in cancer cells, resulting in the detachment of β -CD gatekeeper and thus simultaneously triggering the *in situ* release of anticancer drug doxorubicin (DOX) entrapped in the MMSNs to kill cancer cells. It was found that drug loaded MMSNs showed high contrast in MR imaging *in vivo*, with the aid of an external magnetic field, and exhibited magnetically enhanced accumulation in the cancer site, leading to significant inhibition of cancer growth with minimal side effects. This multifunctional MMSN will find great potential as a theranostic nanoplatform for cancer treatment (W. H. Chen et al., 2016).

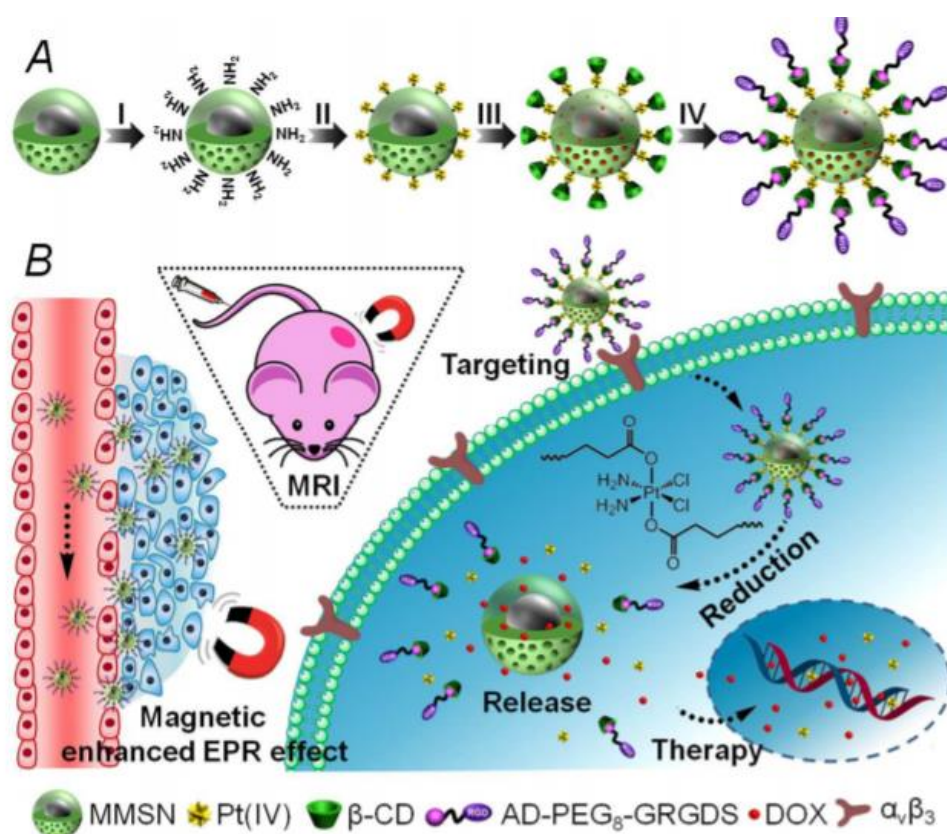


Figure 2.7 Schematic illustration of the design and proposed mechanism of the multifunctional MMSNs for tumour-targeted MRI and precise therapy. (A) The functionalization protocol of the MMSN. (B) The precise treatment strategy by using multifunctional MMSNs. Readapted from Chen et al. (2016).

2.2.5 Carbon Nanomaterials

Carbon nanomaterials can be classified into zero-dimensional fullerene, carbon dot, nanodiamond, one-dimensional carbon nanotube, and two-dimensional graphene, each of them possessing exceptional physical and chemical properties. For example, carbon dot and nanodiamond can display natural fluorescence emission, thanks to their optoelectronic properties. On the other hand, graphene and carbon nanotube exhibit unique mechanical, electrical, thermal, and biological properties for a variety of applications, including nanomedicine (L. S. Wang et al., 2012). Robinson et al. (2010) were the first that demonstrated dual application in NIR imaging and PTT using PEGylated phospholipid functionalized single-walled carbon nanotube (SWNT) (Robinson et al., 2010). SWNT is promising as a theranostic agents thanks to its strong optical absorbance in the NIR region, which can not only emit photoluminescence in the 1.0-1.4 μm region for *in vivo* tumour imaging but also act as an efficient NIR absorber and heater for photothermal ablation of tumours with low injected dose (Moon et al., 2009). Graphene has also been demonstrated as a photothermal transducer due to its higher optical absorbance in the NIR region. According to a study by K. Yang et al. (2010), an high tumour uptake of nanographene sheet (NGS) was found in several xenograft tumour-bearing mouse models. Such PEGylated NGS was used for *in vivo* PTT, revealing that an ultra-efficient tumour ablation after intravenous administration of NGS and low-power NIR laser irradiation on the tumour could be reached (K. Yang et al., 2010).

2.2.6 Other Nanomaterials

In addition to the conventional nanomaterials, there has been increasing attention in employing upper-conversion nanoparticles (UCNPs) for theranostic applications. UCNPs are lanthanide-doped nanocrystals that emit higher light energy (visible) upon excitation by lower light energy (978 nm) via an up-conversion process (L. S. Wang et al., 2012). Electromagnetic waves in the NIR region are known to be relatively transparent in biological tissues. The limit of PDT is that photosensitizer itself can only be excited by visible light that shows poor penetration ability in biological tissue. Combining UCNPs with photosensitizer may settle the problem for PDT: by encapsulating photosensitizer in the polymer modified on UCNP, PDT can be executed under NIR irradiation, in which

biological tissue may have minimal light absorption (Shan et al., 2011; C. Wang et al., 2011).

Quantum dots (QDs) are semiconductor nanocrystals that exhibit stable and bright fluorescence. By tuning particle size and composition, their optical properties can be adjusted. CdSe, CdTe, InAs, and ZnSe have been utilized to synthesize QDs in varied sizes, resulting in the production of semiconductor nanoparticles that span the full visible and NIR spectrum. However, QD-based theranostic carrier has been relatively less examined, principally owing to innate toxicity and instability (L. S. Wang et al., 2012).

3 DESIGN OF ENGINEERED NANOPARTICLE

3.1 AIM AND OBJECTIVES

Aim: the main purpose of this work is to propose and theoretically validate an innovative nanotheranostic platform for cancer treatment and imaging. The nanosystem is engineered to have an internal mesoporous silica-based core covered by polyelectrolytes deposited through Layer-by-Layer (LbL) self-assembly process. LbL technique allows to incorporate drugs and photosensitizers (PSs) to provide a multimodal therapy, chemotherapy and photodynamic therapy, able to overcome lacking responses of tumours to monotherapy approach in many clinical cases. Moreover, PSs are useful tools for an NIR fluorescence imaging-guided tumour targeting therapy. An external biomolecules-linked polyethylene glycol (PEG) functionalisation is elaborated in order to avoid immune system activation, increase circulation time in blood environment, and to promote active targeting on tumour cells. Nature of external biomolecules depends on treated types of tumour, representing a modifiable parameter of the nanoplatform. In [table 3.1](#) all the specifics of our designed nanoplatform are summarised.

Objective 1: to review and analyse literature for acquiring competence on cancer characteristics and weaknesses pf conventional therapy and on theranostic field. State-of-the-art about nanotheranostic is of fundamental importance to understand major problems of actual trialled products and to propose a platform trying to overcome them.

Objective 2: discussion of therapeutic requirements, FDA required biocompatibility standards, technical engineering specifications of nanotheranostic system and reliability of manufacturing processes. Core component needs to be biocompatible, stable in biological conditions and externally charged to allow LbL electrostatic deposition. Polyelectrolytes must be biocompatible, promote active and passive targeting, respect dimensions for intra-tumoral accumulation, and to be stimuli sensitive in order to control kinetics drug release. Drugs must operate in the tumour therapeutic window. Finally, an efficient imaging process needs to be provided for an imaging-guided tumour targeting therapy. Therapeutic efficacy is assessed through proper biological characterisation in order to evaluate the *in vitro* and *in vivo* biological performance of the designed and manufactured nanotheranostics.

Objective 3: deep analysis of the single key elements for investigating different approaches to their synthesis and corporation in the proposed nanotheranostic system. We start studying various components for the nanoplatform, evaluating strengths and weaknesses of them, and successively we select the elements best suitable for our purpose. For instance, core size and pore dimension must be able to incorporate selected drugs, particle Zeta potential and external layer charge have a fundamental role on absorption of non-specific biomolecules during circulation in blood environment and on location of the platform in the tumour cells, natural and synthetic polyelectrolytes present different characteristics and have strongly effects on the stability of the nanostructure and active and passive targeting. Moreover, we develop a manufacturing plan for an experimental realisation of the nanoparticles, respecting FDA requirements and process reliability.

Objective 4: brief presentation of innovative computational *in silico* approaches that could be implemented in order to have useful tools for a high throughput screening of materials and biomolecules to build nanotheranostic platforms, reducing costs and time consumption. A MATLAB study is proposed for controlling kinetics drug release from a multilayer architecture in a biological medium and molecular dynamic simulations are conducted to analyse the strength of interactions between different biomolecules and receptors overexpressed on cancer cells through the computer software LigandScout.

Table 3.1 Summary table of the theranostic specifics and design of the nanoplatform.

	CHALLENGES	SPECIFICATIONS	VALUE/ DETAILS
CORE	Biocompatibility, Size, Pores dimension	Mesoporous silica-based nanoparticle with NH ₂ (MSN-NH ₂)	Size: ~ 50 nm Pores: ~ 2.9 nm Surface charge: 32.2 mv
LAYER-BY-LAYER	Biocompatibility, pH-responsive, passive targeting and EPR effect, drug release, size	Polyelectrolytes (polyanion/polycation): TPPS ₄ /PLL (first bilayer) HA/PLL (second bilayer)	pH operativity: acidic conditions particle size: ~ 100-120 nm drug efficiency loading: > 60% drug release kinetics: controlled up to 50 hours
DRUGS AND BIOMOLECULES	Biocompatibility, load efficiency	Doxorubicin (DOX) Tirapazamine (TPZ)	DOX: 10 ml DOX water solution (2.5 mg mL ⁻¹) TPZ: 2.9 wt%
EXTERNAL COATING	Biocompatibility, Immune system stealth strategy, Increase circulation time	Hydrophilic polymer grafting: polyethylene glycol (PEG)	PEG: 40 mg Avoided immune system activation Increase circulation time Improve colloidal stability
EXTERNAL SURFACE FUNCTIONALIZATION	External probes, active targeting, tumor specificity, bioactivity	Folic Acid (FA) (HER-2 antibody, EGFR, Transferrin, etc.)	Active targeting on cancer cells
IMAGING	Imaging-guided tumor targeting therapy	NRI fluorescence imaging and MRI	Confirmed superior tumor accumulation capacity after 24 h administration
THERAPEUTIC MODE	Multimodal therapy	Chemotherapy and PDT	Very low cell viability after 1.5 min laser irradiation

[Figure 3.1](#) schematically present the nanotheranostic layer-by-layer functionalised mesoporous silica-based nanoparticles, focusing on the selected materials and molecules, chosen to satisfy the requirements mentioned above. We adopted a bottom-up strategy starting from the core and all key elements and possible alternatives well be deeply analysed in the following sections.

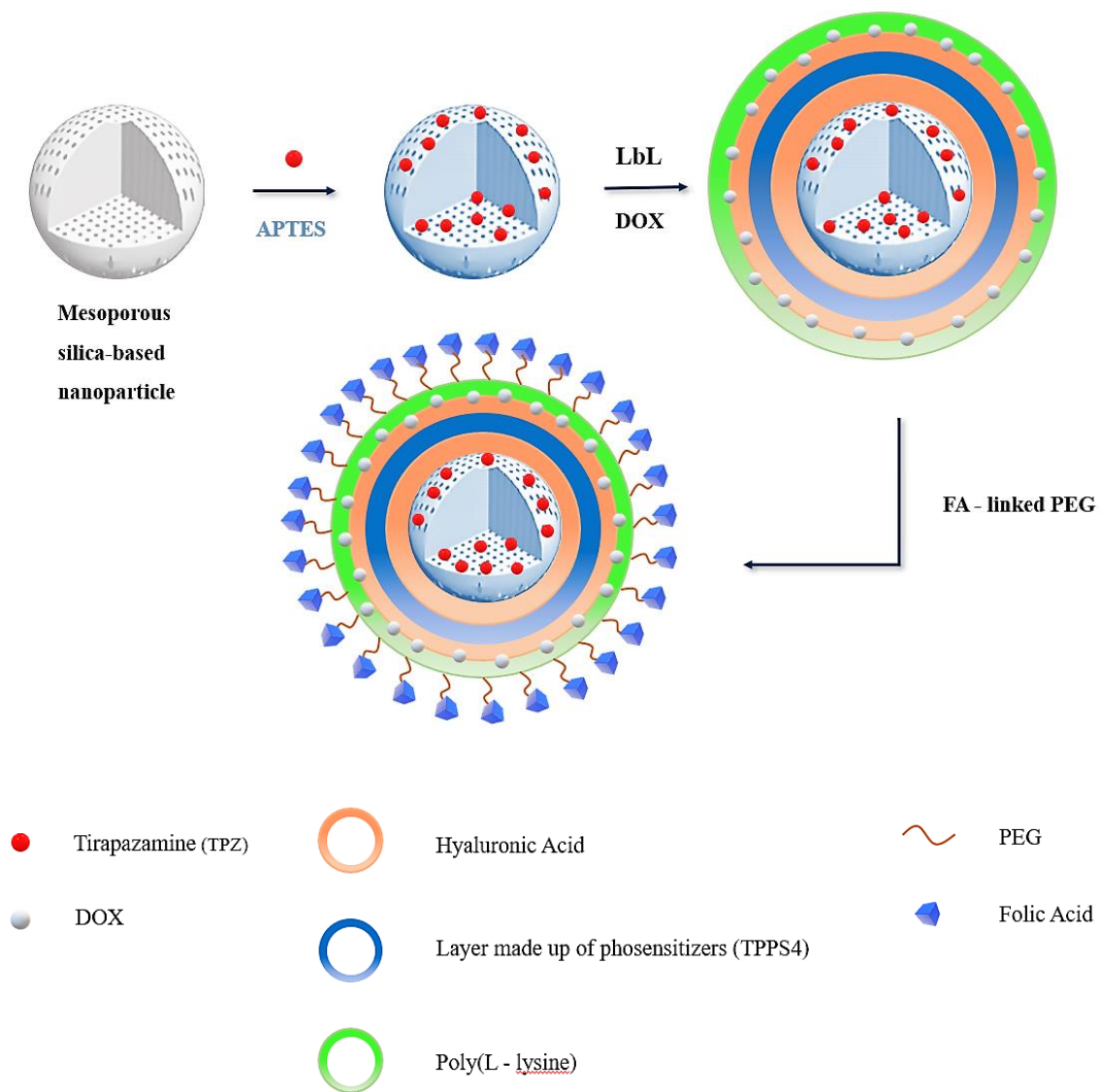


Figure 3.1 Schematic representation of nanotheranostic platform.

3.2 DEEP ANALYSIS OF KEY ELEMENTS

3.2.1 Core of Nanoparticles

In the last decades, according to the literature, nanomedicine formulations for nanotheranostic applications have been widely investigated and they are emerging to provide an efficient alternative to conventional cancer management. In a bottom-up strategy to produce theranostic nanoparticles, first step involves preparation of the internal core, fundamental in terms of dimension, biological environment stability, biocompatibility, and capacity of receive external functionalisation. Several studies have been conducted on the realization of polymeric nanoparticles as drug carrier systems, demonstrating high drug-loading efficiency and rapid intracellular delivery of the drug (Haley & Frenkel, 2008). For instance, Mattu et al., proposed the creation of five different polymeric NPs through a modified single emulsion solvent evaporation method utilizing PCL, PLA, PLGA and two biodegradable polyesterurethanes (PURs) based on PCL, functionalised with absorption of Herceptin monoclonal antibody (HER) on the surface through hydrophilic/hydrophobic interactions to provide active targeting (Mattu et al., 2013). In recent years, polymeric nanocapsules with a solid/oil core have generated a great interest in drug delivery and theranostic applications thanks to their core-shell microstructure, useful to increase drug-loading efficiency and to reduce polymeric matrix content of NPs (Deng et al., 2020). Focusing on biodegradability and biocompatibility, natural and synthetic polymers have been studied for obtain performing formulations. Metallic NPs are also widely studied for bio-imaging and drug administration thanks to their unique properties. In particular, well established protocols are available to synthesize metallic nanosystems with tuneable size and morphology, and they themselves can act as therapeutic and imaging agent, so they can be easily functionalised for more sophisticated theranostic approaches (Ma et al., 2016). M. Chen et al., developed an uniform plasminic Pd-Au core-shell bimetallic nanoplates, modified with SH-PEG on the surface to provide good biocompatibility, prolonged blood circulation and high tumour accumulation, demonstrating their application for PA imaging, CT imaging, and PTT (M. Chen et al., 2014). In another paper, W. Yang et al., synthesized a biocompatible gadolinium integrated CuS nanotheranostic agent with ultrasmall size of about 9 nm exhibiting high photothermal conversion efficiency, photostability under NIR laser irradiation, and demonstrating prominent tumour-contrasted imaging performance both on photoacoustic and magnetic resonance imaging modalities (W. Yang et al., 2016).

According to the literature, the main nanotheranostic polymeric and metal-based formulations currently under clinical assessment are summarized in [Table 3.2](#) (Silva et al., 2019).

Table 3.2 Theranostic polymeric and metal-based nanoplatforms under study for clinical applications in different cancers (according to clinicaltrials.gov and clinicaltrialsregister.eu). Readapted from Silva et al., 2019.

PRODUCT	COMPANY	CLINICAL PHASE	THERAPEUTIC MODALITY	DIAGNOSTIC MODALITY	PROPOSED INDICATION	CT IDENTIFIER
CriPec® docetaxel	Cristal Therapeutics	Phase I	Docetaxel	PET (Zirconium-89)	Solid tumours	NCT03712423
AGuIX®	NHTherAguix	Phase I	Radiation therapy	MRI (gadolinium- chelates)	Brain metastases	NCT02820454
AGuIX®	NHTherAguix	Phase I	Radiation therapy or brachytherapy or chemotherapy (cisplatin)	MRI (gadolinium- chelates)	Gynecologic cancer	NCT03308604
Iron oxide nanoparticles (SPIONs)	M.D. Anderson Cancer Center	Early Phase I	-	Ferumoxytol- based MRI	HNSCC	NCT01895829
NBTXR3®	Nanobiotix	Phase I/II	Hafnium oxide nanoparticles (50 nm)	Radiation- stimulated technology (NanoX-Ray) via electron production	Multiple solid cancers, including head and neck cancer, rectal cancer, prostate cancer and breast cancer	NCT02805894 NCT03589339 NCT02901483 NCT02901483 NCT02465593 (Total of 5 active clinical trials)

Among various nanoparticles, superparamagnetic iron oxide nanoparticles (SPIONs) particularly magnetite (Fe_3O_4) and maghemite ($\gamma\text{-Fe}_3\text{O}_2$) nanoparticles are used primarily in cancer theranostic applications such as magnetic resonance imaging (MRI) and magnetic hyperthermia due to their significant magnetic properties (Kandasamy & Maity, 2015).

CaCO_3 nanoparticles have been exploited as intelligent carriers thanks to their biocompatibility, biodegradability and sensitivity to pH. Volodkin et al., proposed a new approach to fabricate polyelectrolyte microcapsules based on porous inorganic

microparticles of calcium carbonate (Volodkin et al., 2004). Starting from this paper, Trushina et al., tried to set up a process to reduce the dimensions of CaCO_3 NPs, finding that it is possible to synthesize nanosized particles using vaterite, an anhydrous polymorph phase of CaCO_3 precipitated in aqueous solution (Trushina et al., 2016). In a recent work, Xing et al., proposed the synthesis of polymer assembled mesoporous CaCO_3 NPs for molecular targeting and pH-responsive controlled drug release for cancer treatment, by exploiting CaCO_3 as sacrificial template in order to create nanocapsules with Doxorubicin in the core (Xing et al., 2020).

After a deep analysis of recent advances in nanotheranostic formulations reported in literature, it was decided to use a mesoporous silica-based nanoparticle (MSN) as core for the engineered design of our nanotheranostic platform, exploiting its unique characteristics including large surface area and volume, tuneable pore size, functionalizable surface, and high level of biological safety and the well-established capacity to load and delivery drugs (Rajendra K. Singh et al., 2017).

3.2.1.1 Mesoporous Silica-Based Nanoparticles (MSNs)

The rationale on the use of MSNs as platform for theranostic applications is due to their high surface area, capability for uniform particle morphology and facile surface modifications, and mesoporous nature (N. Knežević & Kaluderović, 2017; Rajendra K. Singh et al., 2017). Differently from other silicon-based materials, synthesis of MSNs involves the use of a bottom-up approach, by hydrolysis and condensation of alkoxysilane precursors in basic aqueous environment, ensuring uniform mesoporous structure thanks to the presence of pore-templating surfactants during the synthesis. After removal of surfactants, the resultant MSNs present a bulk Si-O-Si composition and exhibit Si-OH moieties on the surface, useful for functionalization (N. Knežević & Kaluderović, 2017). Pore morphology and diameter can be modified by the choice of different surfactants and employing co-surfactants and pore expanding additives (N. Ž. Knežević & Durand, 2015). Mesoporous characteristic, with pore size ranging from a few to tens of nanometers, is of fundamental importance because it determines the loading capacity of drug, and provide a controlled and sustained delivery of drug and consequently satisfactory therapeutic actions (Rajendra K. Singh et al., 2017). In the [table 3.3](#) are summarized the most analysed mesopore structure of MSNs with different size and

morphology, and the resultant properties and effects on the loading and release of drug (Rajendra K. Singh et al., 2017).

Table 3.3 Summary of the different-tailored mesopore structure of MSNs, and the possible effects on the loading and release of drug molecules. Readapted from Rajendra K. Singh et al., 2017).

PARAMETER	TAILORED PROPERTIES	POSSIBLE EFFECTS
PORE SIZE	3-40 nm	Drug type, loading amount, release pattern
PORE SHAPE	Cubic, hexagonal, laminar	Loading amount
PORE ALIGNMENT	Oriented, random, wormhole	Release pattern
SURFACE AREA	200-1215 m ² /g	Loading amount
PORE VOLUME	0.45-1.5 cm ³ /g	Loading amount

Biocompatibility of MSNs is another fundamental aspect to analyse. It was demonstrated that unmodified amorphous silica NPs cause haemolysis with red blood cells (RBC), reporting issues in drug delivery applications such as intravenous administration and transport (Rajendra Kumar Singh et al., 2015). However, controlled morphology and surface functionalization can provide tissue compatibility and bio-distribution in vivo (N.-T. Chen et al., 2013; Shang et al., 2014). PEGylation is the most used strategy to allow for the escape from capture by liver, spleen, and lung tissues extend the in vivo biodistribution, and to enhance the blood circulating capacity of MSNs (Q. He et al., 2011; Y.-S. Lin et al., 2011). Moreover, it has been demonstrated that biocompatibility *in vitro* is concentration and cell-type dependent and has been studied in different cell lines (Vivero-Escoto et al., 2010). For instance, Lin and co-workers have proved that MSNs are biocompatible toward Chinese Hamster Ovary (CHO) and HeLa cells at concentrations below 100 µg mL⁻¹ and increasing the concentration above 200 µg mL⁻¹ resulted in cell damage (Lai et al., 2003; Slowing et al., 2006). Nature degradation under physiological conditions is another aspect to consider in the biocompatibility of MSNs. It is ideal that the NPs degrade upon accomplishing their mission, generating non-toxic biodegradable products (Manzano & Vallet-Regí, 2020). The main element of MSNs is a SiO₂ matrix susceptible to nucleophilic attack by hydroxyl groups from water in aqueous media, causing a hydrolytic break-down of the network and generating orthosilicic acid as product. This latter is biocompatible and excreted through the urine. Accordingly to this, degradability of MSNs is governed by dissolution mechanism of silica particles into silicic acid in biological media (Croissant et al., 2017). As a consequence, dissolution rate

depends on the particle characteristics and on the degradation medium characteristics, but it has been proved that the incorporation of different inorganic or organic molecules such as photosensitizer and anticancer drugs can modify the dissolution rate of MSNs (Zhao et al., 2015; Zhou et al., 2015).

In the past few years, shape of MSNs has generated great interest and research have mainly focused on *in vitro* shape-dependent cellular uptake (F. Tang et al., 2012). Trewyn et al., proposed an analysis on the uptake of spherical and rod-like shaped MSNs by CHO cells and human fibroblast cells and they demonstrated that for CHO cells, the endocytosis rates for both MSNs were similar and rapid, whereas endocytic rate of sphere particles was significantly faster than that of rod-like ones by fibroblast cells (Trewyn et al., 2008).

Thanks to the versatile and tuneable structures, it is possible not only to functionalise the particle surface but also to load a variety of guest molecules including pharmaceutical drugs, therapeutic peptides and proteins and genes (F. Tang et al., 2012). In the [figure 3.2](#) are summarized a collection of biomolecules useful for a bulk functionalization of both nanosphere and hollow/rattle mesoporous nanoparticles.

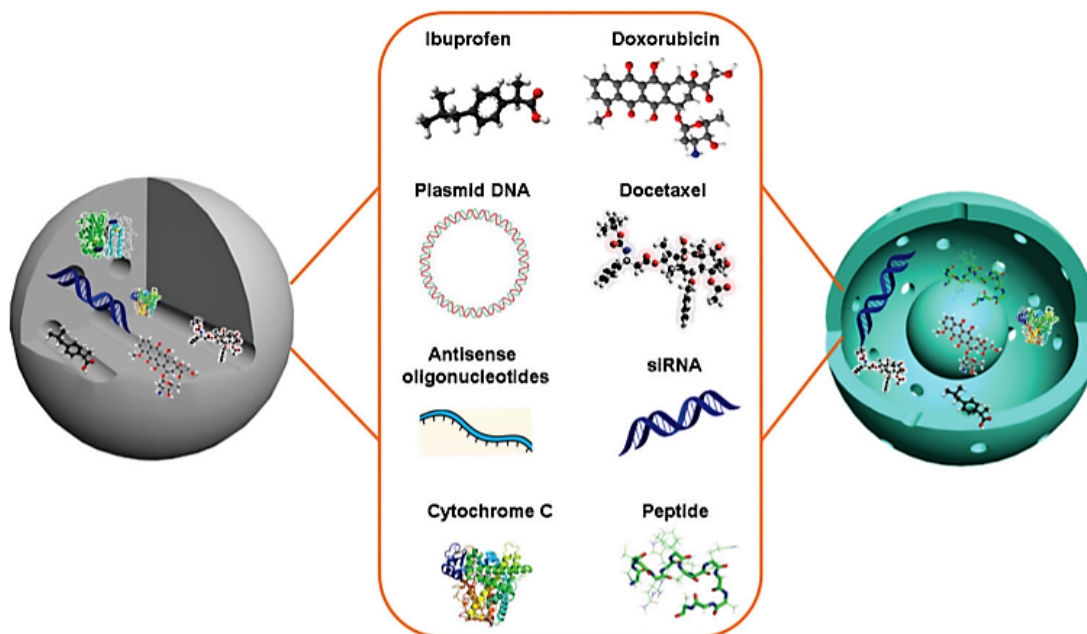


Figure 3.2 Mesoporous silica nanoparticles as versatile drug delivery systems for a variety of therapeutic agents including pharmaceutical drugs, therapeutic genes, and therapeutic proteins and peptide. Readapted from Tang et al. (2012).

Silica nanoparticles are composed of colloidal amorphous metal oxide that can be produced via the *sol-gel* method and present diameters between 50 and 300 nm (Manzano & Vallet-Regí, 2020). There is a variety of methods that can be used to create MSNs but, for all of them, the general process to synthesize silica particles is composed by three steps: the *sol-gel* process for producing silica, the use of surfactants as structure directing agents for producing mesoporous materials, and a modification of the Stöber method under dilute conditions to yield spherical nanoparticles (Q. Cai et al., 2001; Fowler et al., 2001; Nooney et al., 2002). Silica nanoparticles are conventionally obtained through the hydrolytic *sol-gel* process that involves hydrolysis and condensation of silicon alkoxide precursors under acidic or basic catalysis. Surfactant molecules act as a template of the structure during the polycondensation, the precursors form an oxide network leading to a colloidal solution (*sol*) that gradually evolves until the formation of a *gel* or discrete particles depending on the conditions (Zha & Roggendorf, 1991). It has been demonstrated that the use of more dilute conditions allows obtaining monodispersed spherical silica particles (Stöber et al., 1968). The type and concentration of surfactants strongly influence the self-assembling process and, therefore, it has relevant effects on the final mesostructure of the material. Then, the silica precursor is added dropwise providing dilute concentration of the silica precursors. After *sol-gel* process takes place, the droplets gradually transform into nanoparticles. The surfactant template is removed through solvent extraction leading to mesoporous nanoparticles made of pure silica (Manzano & Vallet-Regí, 2020). In [figure 3.3](#) are showed TEM images of MSNs with different particle diameters, pore diameters, porosity with parallel channels or radial pores.

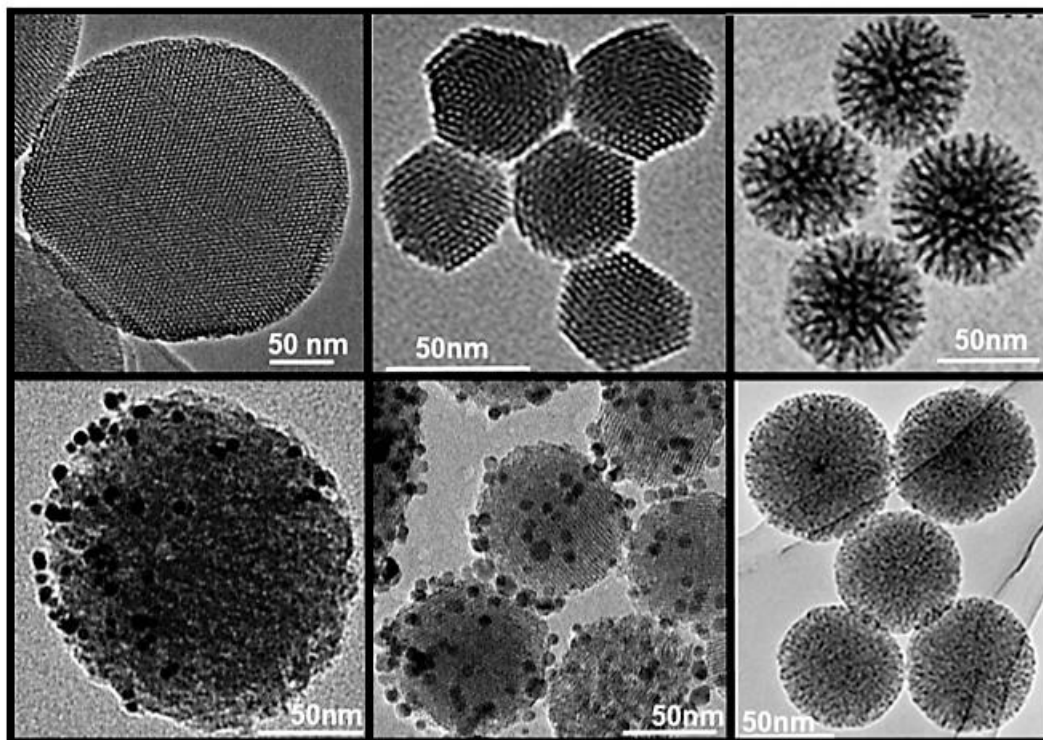


Figure 3.3 Transmission electron microscopy images of different MSNs with different size, morphology, composition, and mesostructured. First row: longitudinal or 2D hexagonal MSNs with different particle diameter (150 and 50 nm), MSNs with centre radial porosity. Second row: MSNs nanoparticles coated with gold nanoparticles, MSNs coated with magnetite nanoparticles and magnetite nanoparticles as core of MSNs. Readapted from Manzano & Vallet-Regí (2020).

In the field of nanomedicine, several studies proved that particle size has a fundamental impact on the NPs mechanism and rate of cell uptake and its ability to permeate through tissue in biomedicine applications (Smith et al., 2008; Tallury et al., 2008). As example, F. Lu et al. (F. Lu et al., 2009) reported a simple method to modify the size of dispersed MSNs by adjusting the pH of the reaction medium, obtaining a series of MSNs with uniform size ranging from 30 to 280 nm. After NPs production, they studied the particle size effect on the cell uptake efficiency with human cervical cancer cells (HeLa cells). In [figure 3.4](#) are shown the TEM images of the resulting MSNs and the DLS measurements of particles size. A fluorescent dye was added to the particles for analysing NPs cellular uptake with confocal laser scanning microscopy (CLSM). As a result, they found that cellular uptake was higher in the 50 nm nanoparticles, specifically it was approximately 2.5 times that of 30 nm particles, 4 times that of 110 nm particles, 20 times that of 170 particles, and 11 times that of 280 nm particles. In [figure 3.5](#) we can observe the confocal images of the fluorescent MSNs in the HeLa cells and the mass of silicon in the different

size particles. Most recent studies confirm the value of 50 nm as optimum size for a nanomedicine platform. For instance, L. Tang et al., investigated the size-dependent biodistribution, tumour tissue penetration and clearance of monodisperse drug-silica nanoconjugates (camptothecin-NCs) with a size of 20 nm, 50 nm, and 200 nm that represent the upper size limit of systemic anticancer nanomedicines to extravasate leaky tumour vasculature (Hobbs et al., 1998). 200 nm NPs showed a limited tissue penetration and 20 nm NPs were characterized by a fast clearance from tumours. On the other hand, 50 nm nanoparticles showed the optimal balance of deep tissue penetration and high retention in tumours, ensuring not only the efficient distribution in tumour tissue, but also the prolonged availability of drug-containing NPs to the tumour tissue, resulting in a superior anticancer efficacy (L. Tang et al., 2014). The optimum size of 50 nm was reported from other several studies in the literature (Chithrani et al., 2006; Jiang et al., 2008; Osaki et al., 2004).

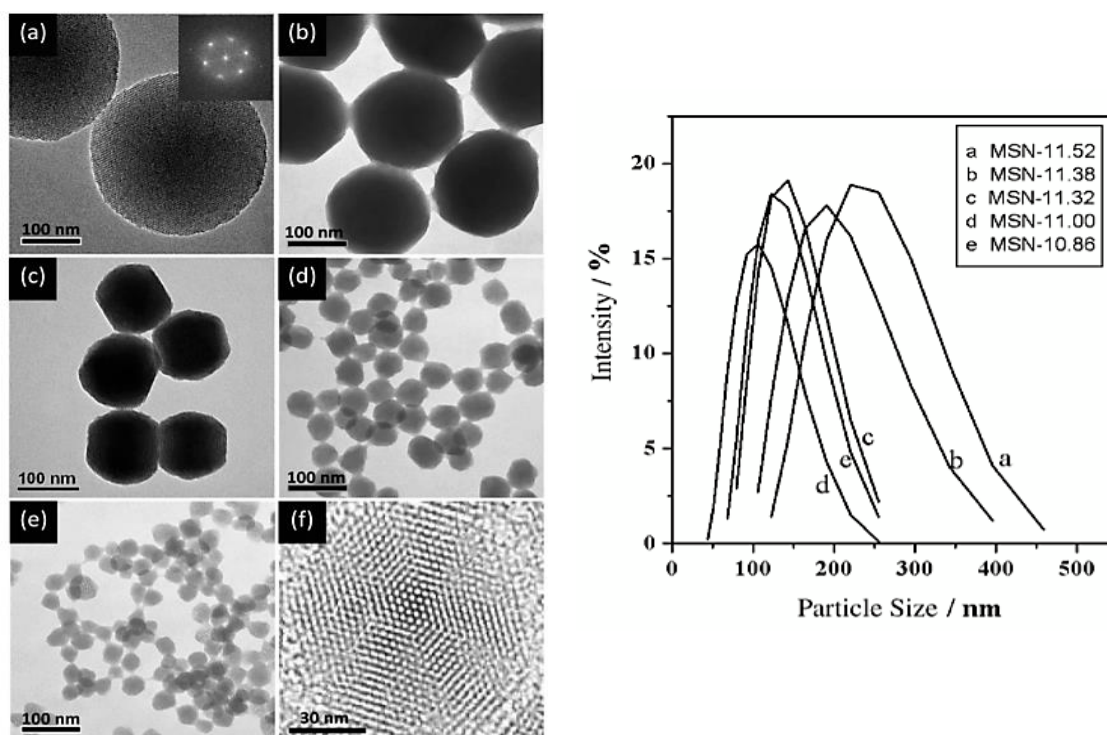


Figure 3.4 On the left, TEM images of mesoporous silica with different average sizes: a) 280 nm, b) 170, c) 110, d) 50, e) 30 nm. f) High-resolution TEM image of a single particle in (c). On the right, DLS measurements of MSNs synthesized with decreasing pH values from 11.52 to 10.86. Readapted from F. Lu et al. (2009).

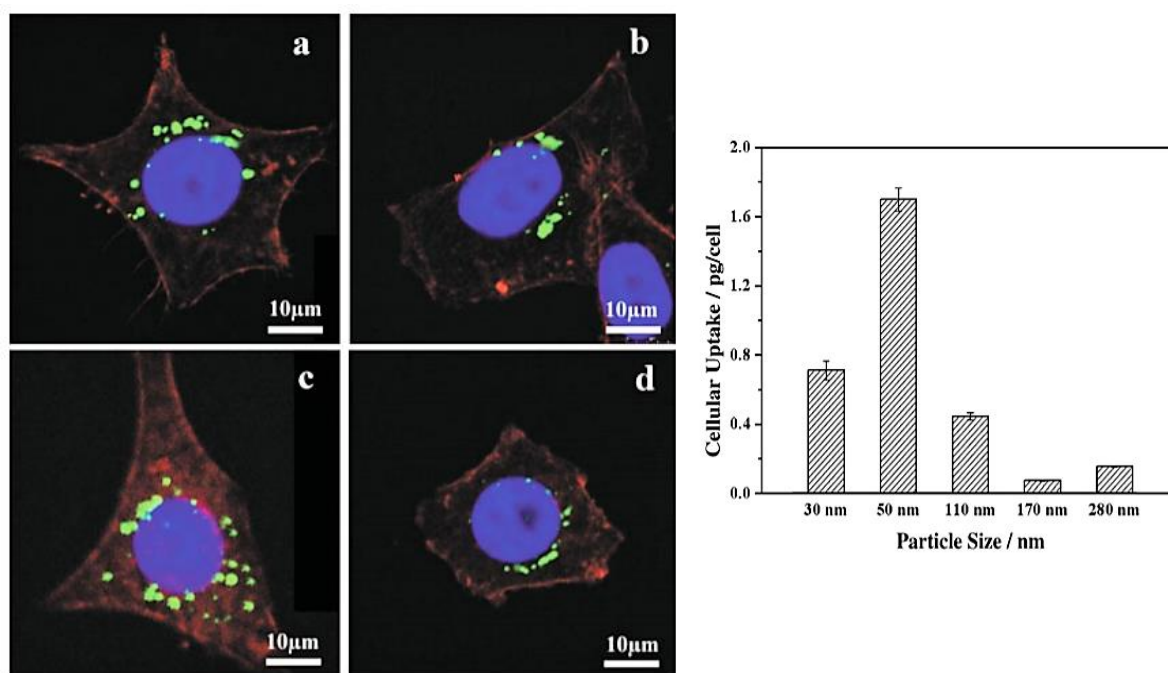


Figure 3.5 On the left, CLSM images of HeLa cells after incubation for 5 h at 37°C with fluorescent MSNs ($100 \mu\text{g mL}^{-1}$, green) of size a) 170, b) 110, c) 50 and d) 30 nm. The cell skeleton was stained with rhodamine phalloidin (red), and the cell nucleus with 4',6-diamidino-2-phenylindole (DAPI; blue). On the right, cell uptake of fluorescent MSNs. The graph shows the mass of silicon per cell versus size of MSNs. Readapted from F. Lu et al. (2009).

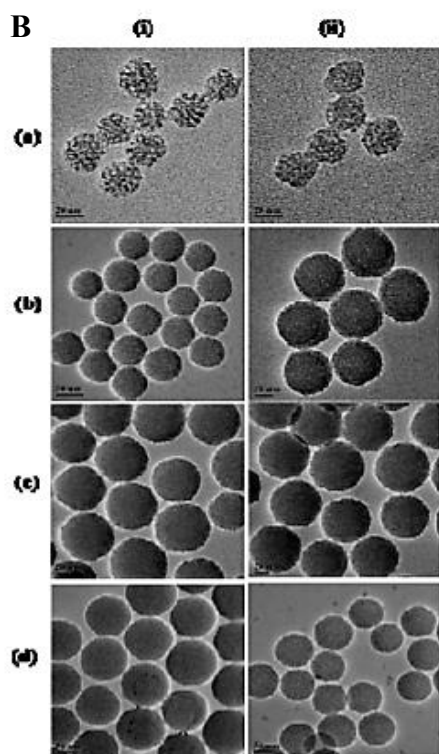
For the design of our nanoplatform, we propose the creation of monodispersed colloidal MSN following a previously reported method via co-condensation of silicates with the treatment of triethanolamine (TEA) (Pan et al., 2012; Silica et al., 2008). Pan et al., by controlling the concentration of TEA, provide a method to synthesize different size MSNs as shown in the [figure 3.6 A, B](#). We chose 50 nm particles for an optimal cellular uptake and efficient *in vivo* performance as mentioned above. NPs are reported to have pore diameter of 2.8 nm in the mesoporous structure ([figure 3.6 C](#)), ensuring efficient encapsulation of drug molecules. Then, a 3-aminopropyltriethoxysilane (APTES) functionalization was led in order to obtain MSN-NH₂ for acquiring a subsequent multilayer coating, resulting in a change of surface charge from -41.8 mV to $+25.3 \text{ mV}$ (W. H. Chen et al., 2017; Pan et al., 2012).

Aminated MSNs was loaded with tirapazamine (TPZ), a bioreductive drug that is only cytotoxic to hypoxic cells (TPZ application will be further explain in the following section) (Brown, 2000; Y. Liu et al., 2015).

A

Sample	TE A [g]	Surface area [m ² g ⁻¹]	Pore volume (V _p) [mL g ⁻¹]	Pore diameter [nm]	TEM average diameter r [nm]	DLS average diameter [nm]	PDI	Number of nanoparticles per gram sample [a]	Zeta potential [mV]
MSNs-25	0.08	561.0	1.41081	2.5	25	58.26	0.146	5.5*10 ¹⁶	-42.3
MSNs-50	0.06	537.9	1.097343	2.8	50	72.36	0.216	7*10 ¹⁵	-41.8
MSNs-67	0.04	478.9	0.904125	2.8	67	91.95	0.139	2.8*10 ¹⁵	-43.2
MSNs-105	0.02	389.5	0.895371	2.7	105	136.2	0.180	7.5*10 ¹⁴	-42.5

B



C

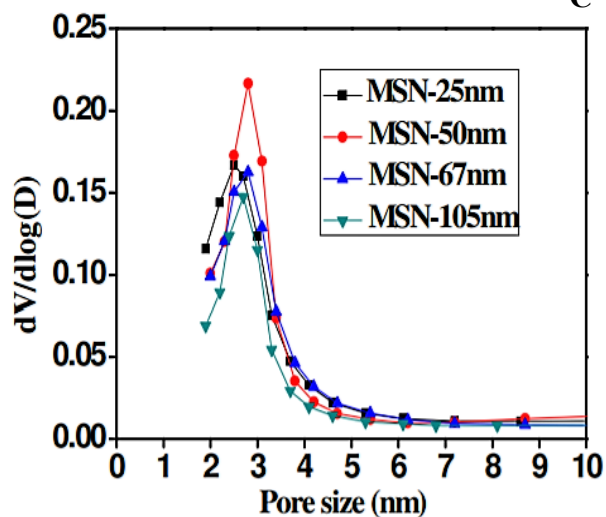


Figure 3.6 A) Properties of four different-sized MSNs. B) TEM images of (i) MSNs, (ii) MSNs-NH₂, in different diameters: (a) 25 nm, (b) 50 nm, (c) 67 nm, (d) 105 nm. C) Pore size distribution of different-sized MSNs. Readapted from the Supplementary Information of Pan et al. (2012).

3.2.2 Multilayer coating of nanoparticles

3.2.2.1 Layer-by-Layer Assembly

Layer-by-Layer (LbL) assembly is a versatile technique involving alternating deposition of compounds with complementary interactions in order to fabricate functional surface coatings, allowing to coat a substrate with a range of physiochemical properties and geometries without damaging the substrate (Saurer et al., 2013; Shukla et al., 2012). Typically, LbL assembly is performed under aqueous conditions with the possibility to incorporate small molecules and biologic agents avoiding the use of solvents, temperatures, pH values, and ionic strengths that can damage these compounds (Alkekha et al., 2020a). Conventional LbL assembly have well-established protocol with generally understood properties of the coating films (Björnmalm et al., 2017). According to the literature, researchers have explored the use of LbL biomaterials for cellular engineering (T. Liu et al., 2019), tissue engineering and regenerative medicine (Fukuda et al., 2018), biosensors (X. Cai et al., 2013), antimicrobial materials (Séon et al., 2015) and drug delivery systems (Costa et al., 2015). In [figure 3.7](#) the main interactions exploited in LbL assembly are reported.

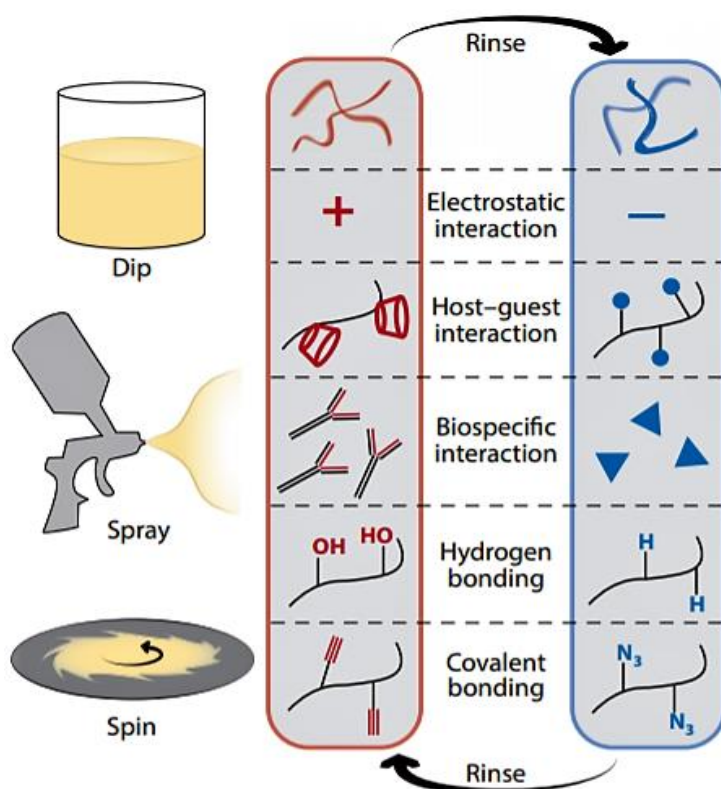


Figure 3.7 Schematic of common LbL approaches and common interactions exploited in LbL assembly. Readapted from Alkekha et al. (2020).

It is possible to perform LbL assembly on different shape substrate such as planar or particulate substrates. Immersive assembly is the standard conventional process for LbL technique on planar substrate ([Figure 3.8 A](#)). It involves sequential immersions of the substrate into polymer solutions for deposition, with washing steps between the deposition steps (Richardson et al., 2016). The process is usually driven by electrostatic interactions between oppositely charged materials, but it has been demonstrated that several variables such as salt concentration, layering materials concentration, immersion time, washing parameters, van der Waals and hydrogen bonding, can all influence the film growth (Bertrand et al., 2000; Dubas & Schlenoff, 1999). Moreover, in the earlier studies, researchers used short adsorption times in the order of 1 minute per layer for material deposition (Iler, 1966). It has been later demonstrated that substrates should be immersed for more than 12 minutes for optimal layer stability and adhesion (Lvov et al., 1993). Unfortunately, time and operator handwork requirements for depositions cause a difficult high throughput of immersive LbL assembly. To overcome these issues, various methodologies have been developed accelerate layering process and reduce manual involvement by changing kinetics adsorption and automating deposition steps (Richardson et al., 2016). For instance, Shim et al., proposed the addition of dimethylformamide into the deposition solutions in order to remove the washing and drying steps, resulting in a de-wetting LbL assembly method (Shim et al., 2007). Fu et al., reported the use of a magnetic stirrer bar to mix the polymer solution during deposition steps in order to speed up the assembly kinetics and reduce time requirement ([Figure 3.8 B](#)) (Fu et al., 2011). On the other hand, LbL assembly on particulate substrates is composed by more steps because of the requirement of a separation step of centrifugation between deposition and washing steps ([Figure 3.9](#)) (Caruso et al., 1998; Sukhorukov et al., 1998). Centrifugation step could lead to aggregation of nanoparticles and it makes LbL for particulate substrates more difficult to automatize. To solve this issue, Nagaraja et al., proposed a novel approach using solvent-exchange steps deposition and centrifugation to reduce the aggregation of nanoparticles during the washing step (Nagaraja et al., 2016).

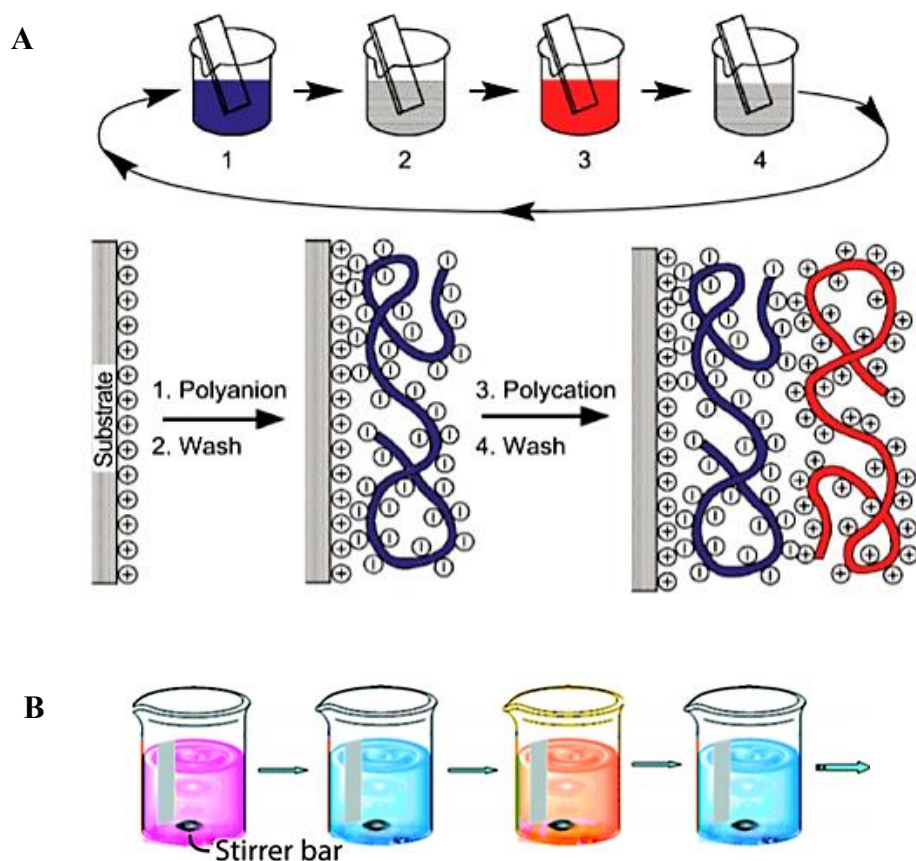


Figure 3.9 A) Schematic illustration of immersive LbL assembly on a planar substrate using oppositely charged polymers and the charge characteristics of the films after each deposition step. B) Schematic illustration of expedited immersive assembly on a planar substrate using a magnetic stirrer bar in the polymer solutions. Readapted from Richardson et al. (2016).

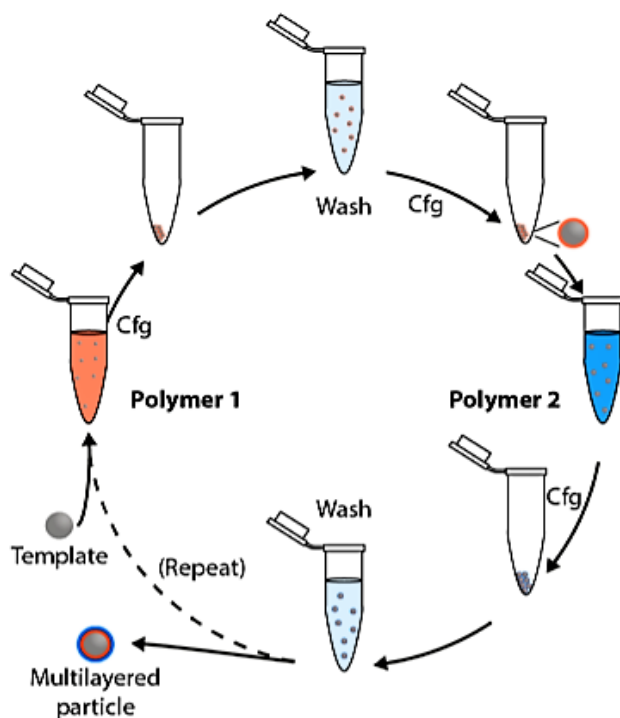


Figure 3.8 Schematic illustration of immersive assembly on particulate substrates using centrifugation in between washing steps. Readapted from Richardson et al. (2016).

According to the literature, among the other methods to perform LbL assembly, the most used are spin coating process and spray assembly technique. Spin LbL assembly is performed casting the solution onto a spinning substrate, resulting in more homogeneous films due to electrostatic interactions, centrifugal and viscous forces, and air shear (Chiarelli et al., 2001; Kharlampieva et al., 2009). This method is easy to automate by using injection system with rotating substrates, as shown in [figure 3.10](#), but it could generate films can be thicker where the solution was cast compared to the edges of the substrate (Richardson et al., 2016). In the last few decades it has been demonstrated that spray assembly, in comparison with immersive method, can provide a similar film quality more quickly (Izquierdo et al., 2005). Spray assembly technique produces films by spraying polymer solutions onto a substrate and spraying water to remove excess material ([Figure 3.11](#)), and the characteristic parameters of the process are polymer concentration, spray duration, flow rate, resting duration, vertical or horizontal spray and washing step time (Kyung & Shiratori, 2011; Merrill & Sun, 2009; Mulhearn et al., 2012). It is possible to combine spray assembly with other techniques to overcome some issue. For instance, spray assembly could lead to inhomogeneity in the films because of the gravity draining and nozzle shape, but this problem can be solved by combining rotation of an horizontal substrate with spray process (spin-spray assembly) (Alongi et al., 2013; Gittleson et al., 2015).

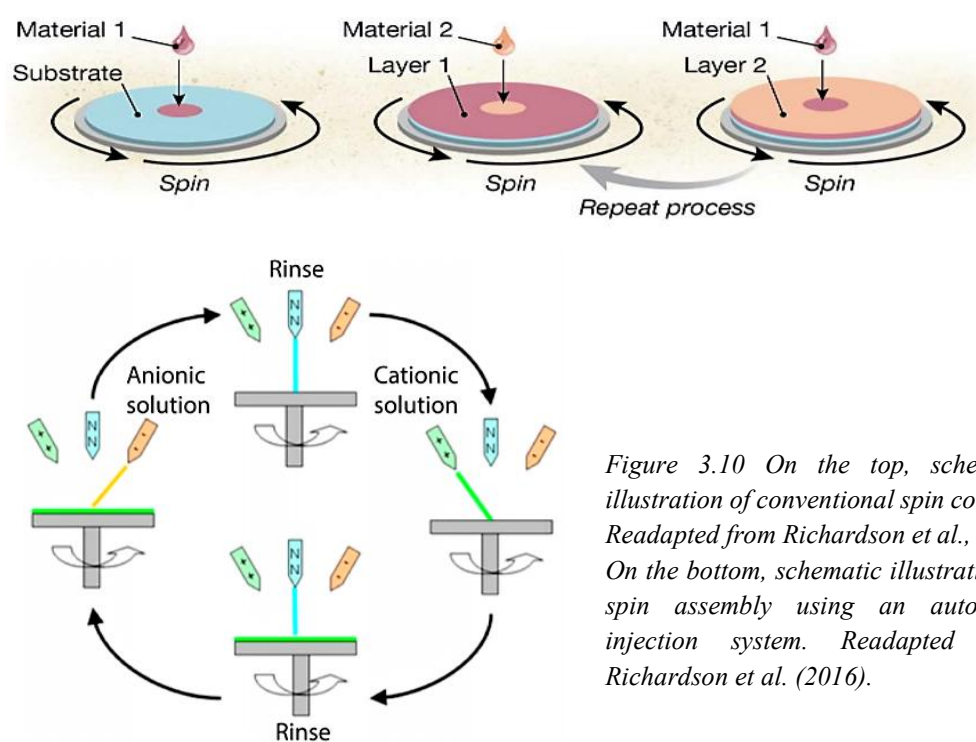


Figure 3.10 On the top, schematic illustration of conventional spin coating. Readapted from Richardson et al., 2015. On the bottom, schematic illustration of spin assembly using an automatic injection system. Readapted from Richardson et al. (2016).

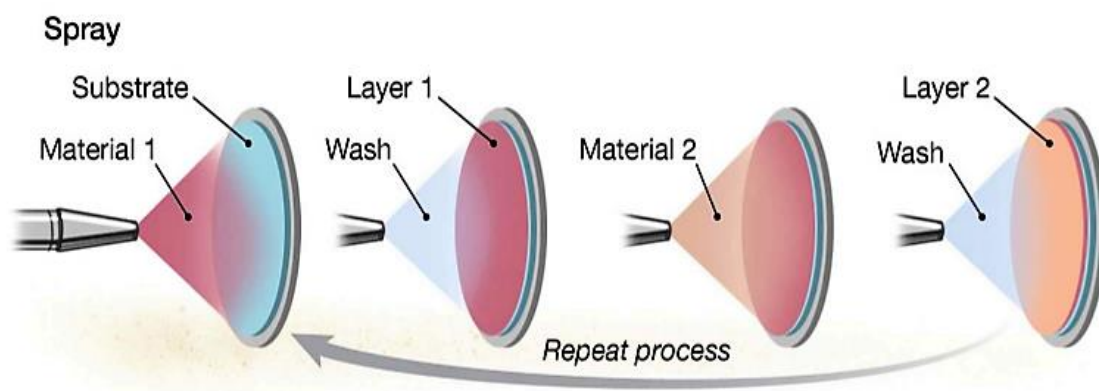


Figure 3.11 Schematic illustration of manual spray assembly using polymer solutions. Readapted from Richardson et al. (2015).

According to the literature, in a LbL process several components could be assembled. The main elements in a multilayer architecture are polyelectrolytes, including synthetic polymers such as polyethylenimine (PEI), poly-L-lysine (PLL), poly(sodium 4-styrenesulfonate) (PSS), poly(acrylic acid) (PAA), poly(diallyldimethylammonium chloride) (PDADMAC), and naturally derived polymers such as alginate (ALG), hyaluronic acid (HA), and chitosan (CHI) (Alkekhia et al., 2020a). Moreover, the versatility of LbL technique allows to incorporate drugs and other biomolecules depending on molecule's physical and chemical properties like charge and hydrophobicity and the desired release profile (Alkekhia et al., 2020a). Controlled release of therapeutic agents can be obtained by incorporating responsive film components in LbL process that cause conformational change to the multilayer structure in response to specific external stimuli (Delcea et al., 2011). The most exploited stimuli in nanotheranostic field for cancer treatment, is pH, thanks to the hypoxic and slightly acidic (pH 6.4-6.8 (R. K. Jain & Stylianopoulos, 2010)) environment of tumours. For instance, Feng et al., created ALG/CHI-coated aminated MSNs loaded with Dox and demonstrated that Dox release after 132 hours upon administration was 48.6% at pH 5.2, in comparison with a value of 7.5% at pH 7.4, due to an increased electrostatic repulsion between Dox and CHI caused by ionization of chitosan amino groups in acidic conditions. It leads to a more gradual and prolonged accumulation of drug in the tumour tissue, resulting in an extending therapeutic efficacy (Feng et al., 2014). Several other external stimuli such as NIR irradiation (Wu et al., 2015), magnetic field (Katagiri et al., 2010), and temperature

(Zhu et al., 2013) have been deeply investigated in the literature in order to validate them for creating stimuli-responsive systems (Alkekhia et al., 2020a).

Another fundamental advantage of LbL assembly in nanotheranostic is the possibility to increase the uptake of nanoplateforms by tumour cells. It has been demonstrated that tumour tissue has leaky tumour vasculature, resulting in the enhanced permeation and retention (EPR) effect that causes passive targeting and allows nanoparticles to penetrate in the tumour tissue (Alkekhia et al., 2020a). To improve the efficacy of targeted therapy, natural polymers with binding properties toward tumour receptor can be used as polyelectrolytes, and LbL coatings can incorporate biomolecules useful for active targeting approaches. For instance, CD44 cell surface receptor has been widely exploited for molecular targeting because of its overexpression on several solid tumour cell types (Yan et al., 2015). It has been proved that HA binds CD44 and is internalized via endocytosis (Mattheolabakis et al., 2015). Nam et al., reported DNA NPs coated with a multilayer structure of HA/PLL polymers, exploiting HA characteristics to achieve an high CD44-mediated selective uptake by ovarian cancer cells (Nam et al., 2019), and Dreaden et al., elaborated PLL/HA LbL-coated polystyrene NPs, ensuring pH-sensitive response thanks to the PLL/HA complex and CD44-mediated uptake by breast cancer cells due to HA presence (Dreaden et al., 2014a). In another LbL platform, a small interfering RNA (siRNA) complex was layered onto PLGA particles using PAR/HA multilayer, and antibodies against a blood cancer marker (CD20) were conjugated on the external HA layer. Reduced leukaemia cell proliferation and lower expression of B cell lymphoma were assessed over 46 days experiment on orthotopic non-Hodgkin lymphoma murine model, demonstrating great success of dual targeting system (CD44/CD20) (Choi et al., 2019).

After LbL assembly process, characterization is a fundamental step to understand properties of resulting multilayer films such as thickness, porosity, morphology, permeability, etc (Richardson et al., 2016). In the [figure 3.12](#) are summarized the most important and used techniques applicable to characterize and analyse films obtained by LbL on particulate substrates. The figure is proposed in order to provide a general overview of the techniques and it is not exhaustive (Richardson et al., 2016).

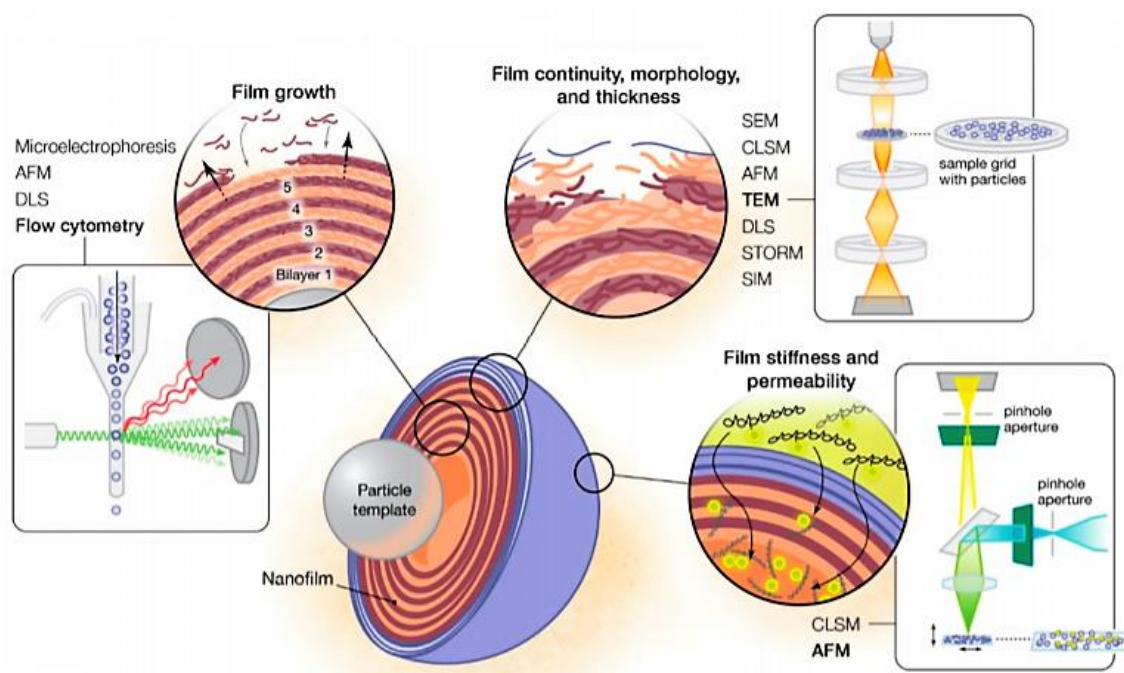


Figure 3.12 Schematic illustration of different characterization techniques applicable to characterize films on particulate substrates. Different techniques can be used on different substrates and can be used for confirming or quantifying various film properties. Readapted from Richardson et al. (2016).

For the design of our nanoplatform, we decided to exploit the properties of hyaluronic acid (HA) ([figure 3.13 A](#)) as anionic polyelectrolyte and poly(L-lysine) ([figure 3.13 B](#)) as cationic polyelectrolyte respectively. We selected them in order to realise both a receptor-targeting structure thanks to the selective affinity of HA with cell-surface CD44 receptor, and a pH stimuli-responsive system thanks to the widely investigated PLL/HA complex (Dreaden et al., 2014a). Moreover, FDA approved nanoformulations, available on the market and applied in clinics, i.e. Onivyde®, Abraxane®, Marqibo® and Nanotherm® show limited monotherapeutic effect as shortcoming in their follow-up (Su & Hu, 2018). According to this, we decided to incorporate a photosensitizer (PS) in the nanoparticle's multilayer coating to promote photodynamic therapy in addition to pharmacologic therapy. Photosensitizers are chemical compounds able to damage tumour cells by producing reactive oxygen species (ROS) (Celli et al., 2010; W. H. Chen et al., 2017). PSs can transfer light energy to surrounding molecular oxygen, generating singlet

² Abbreviations: AFM, atomic force microscopy; CLSM, confocal laser scanning microscopy; DLS, dynamic laser scattering; SEM, scanning electron microscopy; SIM, structured illumination microscopy; STORM, stochastic optical reconstruction microscopy; TEM, transmission electron microscopy.

oxygen ($^1\text{O}_2$), the lowest state of oxygen. It is a reactive oxygen species characterized by a high cytotoxicity and it rapidly attacks any organic compounds it encounters. Then, it is rapidly eliminated from cells, in an average of 3 μs (Skovsen et al., 2005). The most widely used PSs are porphyrins and phthalocyanines, but they have issues in terms of hydrophobic aggregation leading to limited $^1\text{O}_2$ quantum yield and low biocompatibility (Konan et al., 2002; Voskuhl et al., 2013). Recently, according to the literature, researchers have made great efforts in the study of supramolecular PSs (supraPSs), supramolecular complexes commonly constructed via noncovalent host-guest interaction (Bai et al., 2015; Liang et al., 2014). Bonchio et al., found a way to improve stability and efficiency of PSs in biological environment. They studied a porphyrin-based Ps called Tetrakis(4-sulfonatophenyl)-porphyrin (TPPS4) and exploited the strong affinity of the porphyrin core toward a β -cyclodextrin (βCD) guest to form highly stable inclusion complexes (Bonchio et al., 2002). Starting from a detailed structural study for TPPS4, Bonchio et al., demonstrated that two βCD molecules penetrate to cover the centre of the porphyrin ring thanks to the existence of host-guest interactions with high binding constants. As a result, TPPS4 is shielded from the bulk solution (Bonchio et al., 2002; Kano et al., 2002). The chemical composition of βCD and TPPS4 are shown in the [figure 3.14](#) for a better understanding of the host-guest interaction.

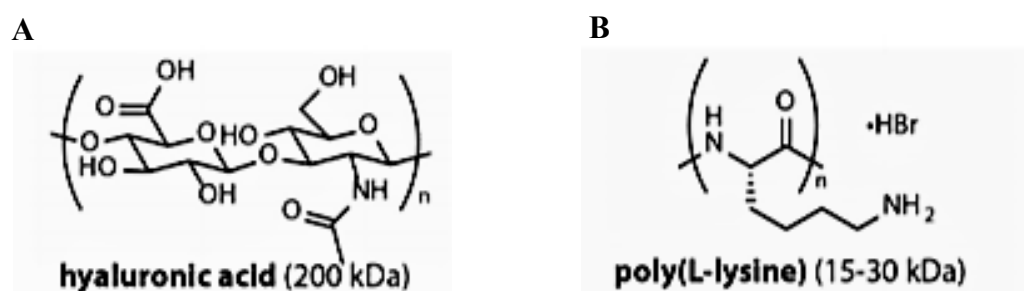


Figure 3.13 A) Polyanion and B) polycation components of the LbL nanoparticle. Readapted from Dreaden et al. (2014).

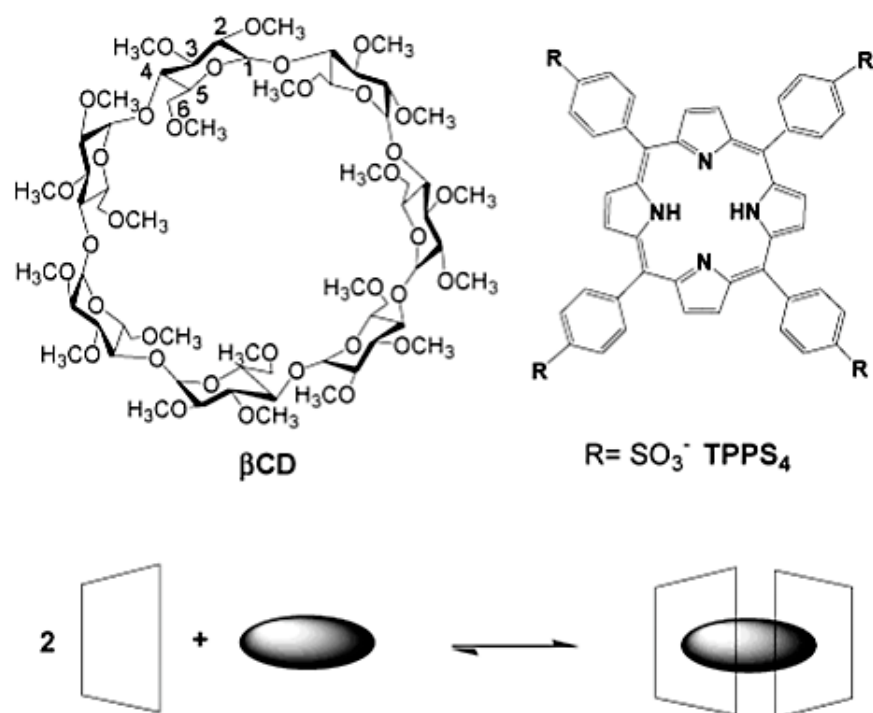


Figure 3.14 Formation of host-guest inclusion complex between the Porphyrin TPPS4 and the β -CD. Readapted from Bonchio et al. (2002).

In this context, at first, we decided to propose a bilayer composed by two layers of HA that present β CDs linked with a “click” chemistry reaction using carbodiimide crosslinker chemistry (NHS, EDC). TPPS4 molecules are incorporated between the two HA- β CD layers ensuring high stability thanks to strength of bonds between TPPS4 and β CD as mentioned above. TPPS4 and HA-CD are deposited onto MSN-NH₂ through an immersive LbL assembly. The surface charge remains negative after the process due to anionic characteristic of both HA and TPPS4 (Bonchio et al., 2002; W. H. Chen et al., 2017; Kano et al., 2002). In [figure 3.15](#) the structure of nanoparticle until HA-CD-TPPS4 coating is presented, with a focus on bilayer composition.

Moreover, TPPS4 is fundamental for our nanoplatform because it allows to an imaging-guided tumour-targeted therapy thanks to NIR fluorescence imaging. In fact, upon an excitation wavelength of 630 nm, TPPS4 molecules generate a fluorescence emission signal with a wavelength of 650-700 nm that could be easily collect (W. H. Chen et al., 2017). W. H. Chen et al., exploited NIR fluorescence of TPPS4 linked onto MSNs in squamous-cell carcinoma (SCC-7) cancer cells of a murine model and in *ex vivo* tissue after 24 hours from administration (W. H. Chen et al., 2017). Analysis demonstrated an

evident major accumulation of nanoparticles in the tumour site, in comparison with free TPPS4 administration ([figure 3.16](#)).

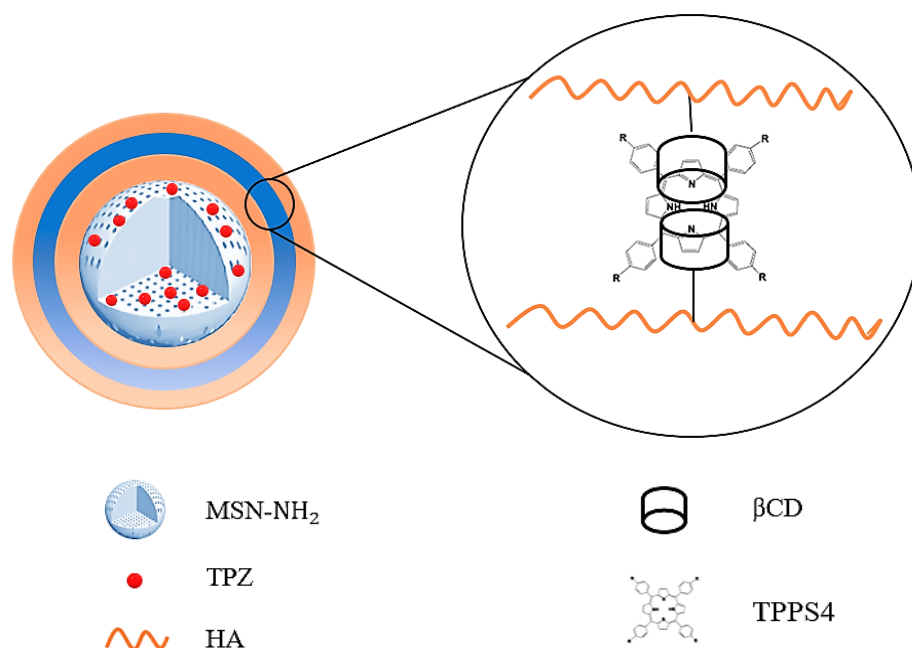


Figure 3.15 Schematic illustration of the first bilayer, with a focus on the HA-CD-TPPS4 complex.

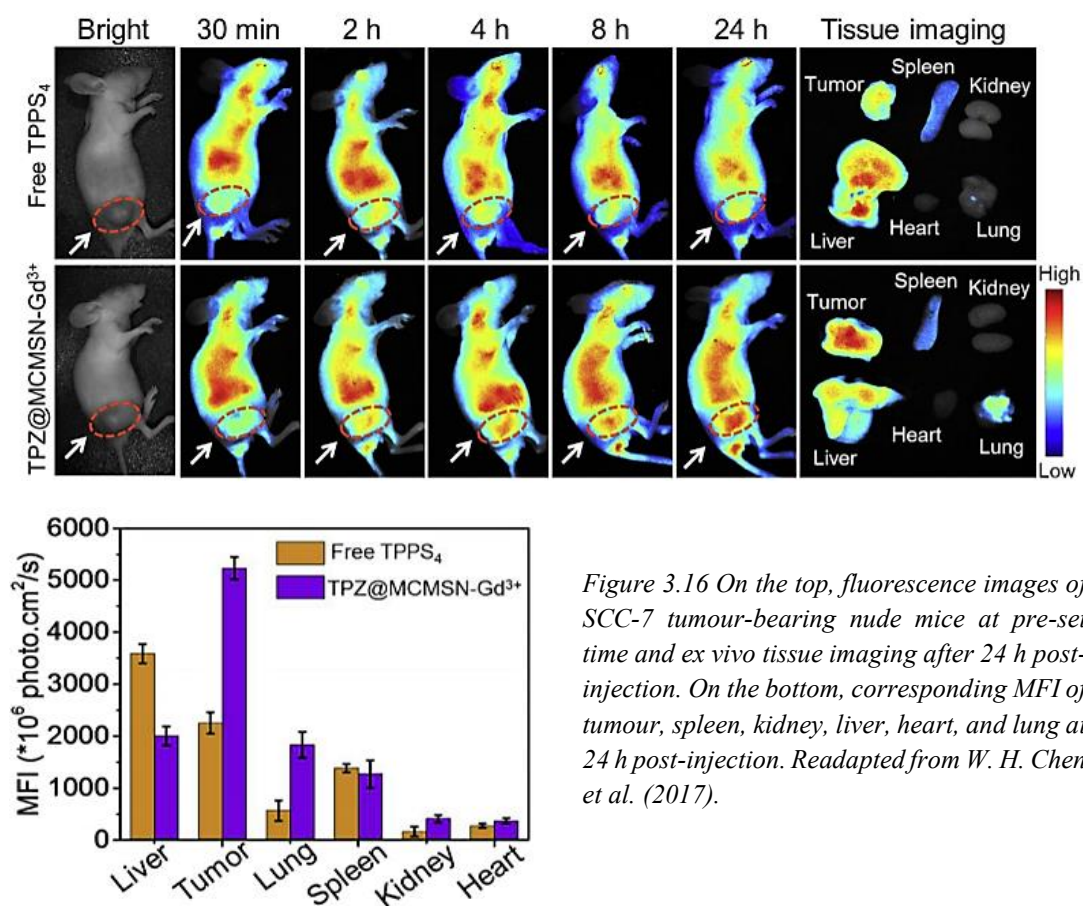


Figure 3.16 On the top, fluorescence images of SCC-7 tumour-bearing nude mice at pre-set time and ex vivo tissue imaging after 24 h post-injection. On the bottom, corresponding MFI of tumour, spleen, kidney, liver, heart, and lung at 24 h post-injection. Readapted from W. H. Chen et al. (2017).

They also conducted a CLSM analysis to investigate ROS generation in CD44 negative normal cells (kidney fibroblast cell line, COS7) and CD44 receptor-enriched tumorigenic cells (human breast adenocarcinoma cells (MCF-7) and squamous-cell carcinoma cells (SCC-7)). As expected, it has been discovered that there was almost no presence of ROS in COS7 cells, indicating a low cellular uptake; on the other hand, there was a gradually increased production of ROS in tumour cells, resulting in a huge disruption of endo/lysosomal organelles by photo-induced intracellular ROS (acridine orange (AO) staining assay), as shown in [figure 3.17](#) (W. H. Chen et al., 2017).

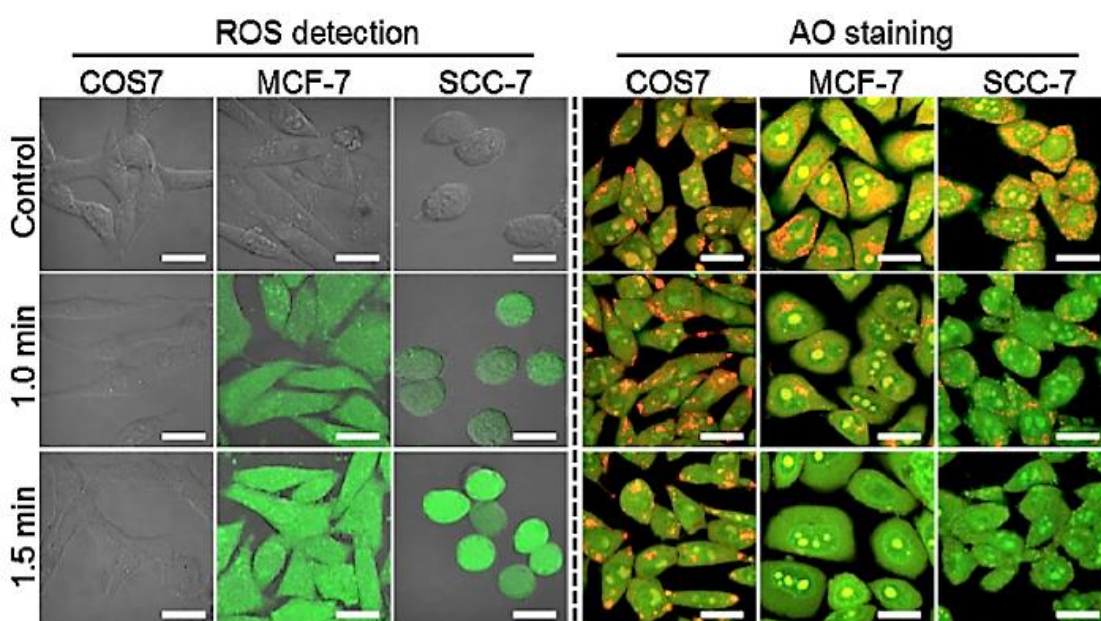


Figure 3.17 Real-time CLSM observation of intracellular photoactivity of MSNs. ROS generation was detected by using DCF-DA as sensor. AO staining assay of detecting acid organelles disruption in COS7, MCF-7, and SCC-7 cells under laser irradiation (660 nm, 1 W cm^{-2}) over time. Scale bar: 20 μm . Readapted from W. H. Chen et al. (2017).

Finally, the last layer of our nanoparticle was made up of PLL in order to obtain a pH stimuli-responsive system and to provide an external surface positive charge able to ensure attractive behaviour towards negative charged membrane of tumour cells. Moreover, anticancer drug Doxorubicin was incorporated in the last PLL layer for multimodal therapy approach, trying to avoid monotherapy resistance of tumours (Su & Hu, 2018). According to literature characterization of HA and PLL multilayer coating, taking into account the number of layers of our nanopatform, hydrodynamic diameter

should be of about 70 nm and zeta potential should settle around $+ 49 \pm 2$ mV (Alkekha et al., 2020b; W. H. Chen et al., 2017; Dreaden et al., 2014a).

3.2.3 External Surface Functionalization

As mentioned above, size is a fundamental property regarding *in vivo* fate of nanoparticles. Renal filtration rapidly removes particles with size smaller than 10-20 nm from the bloodstream (Kievit & Zhang, 2011). It has also been demonstrated in the literature that particles sized between 30 and 200 nm are able to passively target cancer cells. In fact, tumour tissues are characterized by a leaky vasculature and the unorganized endothelial cells allows nanoplateforms to invade the tumour environment. Moreover, the inefficient lymphatic drainage let nanoparticles remain inside the neoplastic tissues (Knop et al., 2010). These factors, known as enhanced permeability and retention (EPR) effect, constitute a form of passive targeting ([figure 3.18](#)) (Fang et al., 2011).

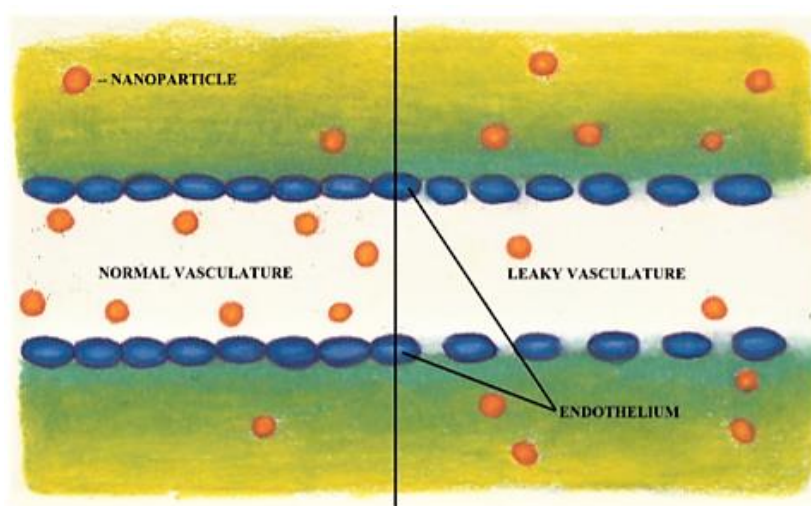


Figure 3.18 Schematic illustration of normal and cancerous vasculature. This latter allows EPR effect. Readapted from Zwicke et al. (2012).

Nevertheless, nanoparticles are extraneous objects in the body, and they immediately begin to interact with biomolecules after the administration. A process called opsonization takes place in the biological environment, in which non-specific adsorption of proteins creates a corona allowing immune cells to recognize and uptake nanoparticles (Dobrovol'skaia et al., 2008). Researchers widely investigated efficient approaches in order to overcome action of blood proteins and immune system, developing polymeric coating for ensuring stability and avoiding opsonization-associated phagocytosis (Hadjesfandiari & Parambath, 2018). PEGylation represents a milestone among the variety of “stealth” approaches, and the use of polyethylene glycol (PEG) for this purpose

has been approved by FDA for several drug formulations ([table 3.4](#)) (Anselmo & Mitragotri, 2016).

Table 3.4 Drug-delivery systems stabilized with PEG that have received regulatory approval in the USA and/or the EU. Readapted from Knop et al. (2010).

PEG DRUG DESCRIPTION	COMPANY	INDICATION	YEAR OF APPROVAL
Adagen (11-17x5 kDa mPEG per adenosine deaminase)	Enzon Inc. (USA & Europe)	Severe combined immunodeficiency	1990 (USA)
Oncospar (5kDa mPEG-L-asparaginase)	Enzon Inc. (USA) / Rhone-Poulenc Rorer (Europe)	Acute lymphoblastic leukemia	1994 (USA)
Doxil/Caelyx (SSL formulation of doxorubicin)	Alza Corp. (USA) / Schering-Plough Corp. (Europe)	Kaposi's sarcoma, ovarian cancer, breast cancer, multiple myeloma	1995 (USA) 1999 (USA) All 1996 (EU)
PEG-Intron (2x20 kDa mPEG-interferon- α -2a)	Schering-Plough Corp. (USA & EU)	Chronic hepatitis C	2000 (EU) 2001 (USA)
Pegasys (12 kDa mPEG-interferon- α -2b)	Hoffmann-La Roche (USA & EU)	Chronic hepatitis C	2002 (USA & EU)
Neulasta (20 kDa mPEG-G-CSF)	Amgen Inc. (USA & EU)	Febrile neutropenia	2002 (USA & EU)
Somavert (4-6x5 kDa mPEG per structurally modified HG receptor antagonist)	Pfizer (USA & EU)	Acromegaly	2002 (EU) 2003 (USA)
Macugen (2x20 kDa mPEG-anti-VEGF-aptamer)	Pfizer (EU)/ OSI Pharm. Inc. and Pfizer (USA)	Age-related macular degeneration	2004 (USA) 2006 (EU)
Cimzia (2x40 kDa mPEG-anti-TNF α)	UCB S. A. (USA & EU)	Crohn's disease, rheumatoid arthritis	2008 (USA) 2009 (USA) 2009 (EU)

It has been demonstrated that PEG molar mass and polydispersity index (PDI) are fundamental for biocompatibility and stealth behaviour. PEG chains allow to create a hydrophilic barrier layer for avoiding adsorption of proteins in the blood serum, hiding particles from phagocytic cells (Owens & Peppas, 2006). The most accepted theory explaining reasons of PEG stealth properties was proposed by Jeon et al.,

in 1991. According to their work, PEG chains have an extended conformation when on nanoparticles surface in solution. Proteins are attracted to the surface by Van der Waals and other forces, and begin to compress PEG chains, resulting in a more condensed and higher energy conformation of PEG. This novel conformation produce repulsive forces that exceed attractive forces between proteins and nanoparticles (Jeon et al., 1991; Owens & Peppas, 2006). PEG with different molar mass is used for different medical and pharmaceutical applications. For instance, PEG with molar mass between 20 kDa and 50 kDa is used for low-molar mass drugs, instead PEG with molar mass of about 5 kDa is used for larger drugs such as antibodies and nanoparticulate systems (Knop et al., 2010). It has been demonstrated that different methods of nanoparticles surface PEGylation are possible, but the most exploited approaches are physical adsorption and covalent grafting (Yoncheva et al., 2005). The versatility and clinical applicability of PEG or PEG-containing polymer has greatly led researchers to investigate and exploit PEG in several nanoformulations for tumour treatment, and many PEGylated cancer nanosystems have undergone clinical investigations and have obtained approval for clinical application (Hussain et al., 2019). Some of them are summarized in [table 3.5](#).

Table 3.5 PEGylated anticancer nanocarriers in preclinical and clinical trials or approved for clinical use. Readapted Hussain et al. (2019).

TYPE OF NANOCARRIERS	DRUG LOADED	INDICATIONS	STATUS	REF.
PEGylated liposomes	PTX	Enhanced plasma half-life of drug in rat and improved antitumor effect	Preclinical trials	(T. Yang et al., 2007)
PEGylated polymeric micelles	PTX	Increased drug uptake into tumor-bearing nude mice with significant decrease in tumor size	Preclinical trials	(Hu et al., 2008)
PEGylated lipid nanoparticles	Docetaxel	Prolonged plasma half-life of drugs with substantial accumulation at the tumor site	Preclinical trials	(Khalid et al., 2006)
PEGylated polymeric nanoparticles	Cisplatin	Tumor growth inhibition	Preclinical trials	(Mattheolabakis et al., 2009)
PEGylated polymer micelles (NK911)	DOX	Accumulation of drug in solid tumor	Phase I clinical trials	(Matsumura et al., 2004)
PEGylated liposomes (SPI-77)	Cisplatin	Reduction in systemic toxicity and increased tumor accumulation	Phase II clinical trials	(Seetharamu et al., 2010)

PEGylated micelles (NC-6004 Nanoplatin™)	Cisplatin derivatives	Drug accumulation in cancer cells with nephrotoxicity and neurotoxicity	Phase III clinical trials	(Vllasaliu et al., 2014)
PEGylated liposomes	Cisplatin	Tumor targeting with decreased adverse events (i.e., renal toxicity, peripheral neuropathy, ototoxicity, and myelotoxicity)	Phase III clinical trials	(Boulikas, 2009)
PEGylated liposomes (Doxil®)	DOX	Alleviated systemic toxicity with increased plasma circulation half-life and tumor accumulation	Approved	(Hofheinz et al., 2005)
PEGylated polymeric micelles (Genexol- PM)	PTX	Alleviated systemic toxicity, prolonged plasma circulation half-life, increased tumor accumulation, and improved anticancer efficacy	Approved in South Korea	(Werner et al., 2013)

According to the literature, in the past few years, researchers have investigated some suitable alternatives to the use of PEG as nanoparticles coating. For instance, important classes of polymers based on poly(glycerols), poly(oxazolines), poly(vinylpyrrolidinones) and poly(zwitterions) showed excellent antifouling and stability properties (Hadjesfandiari & Parambath, 2018).

However, for the design of our nanoplatform, we decide to use PEG as stealth external coating. Moreover, we propose to conjugate a specific biomolecule to the PEG chains in order to exploit active targeting toward cancer cells. In fact, approaches based only on passive targeting depending on EPR effect show in many cases low amounts of nanoparticles which effectively reach the tumour site, in comparison with the injected dose (Diou et al., 2012). Active targeting can solve this problem utilizing external driving force to attract and lead nanoparticles to the tumour tissues and attaching targeting ligands to the surface to bind nanoparticles with receptors expressed by cancer cells. The most investigated ligands in nanotheranostic platforms below to the classes of peptides (Medarova et al., 2009), proteins (Bartlett et al., 2007), aptamers (A. Z. Wang et al., 2008), or small biomolecules (Diou et al., 2012; X. Yang et al., 2010).

For instance, albumin, a critical nutrient for growth of tumours, can be used for improving tumour penetration (Su & Hu, 2018). T. Lin et al., created a self-assembled blood-brain barrier (BBB)-penetrating albumin particle through green synthesis method, and demonstrated that albumin-conjugated particles are able to across BBB and enhance tumour penetration (T. Lin et al., 2016).

Peptide IF7 (IFLLWQR) is well known for binding a biomarker expressed on tumour endothelium, Annexin 1, and D.-H. Yu et al., tried to achieve antitumor and antiangiogenic effect producing an IF7-conjugated nanoparticle loaded with paclitaxel. They proved the enhanced tumour penetration thanks to the application of IF7 (D.-H. Yu et al., 2015).

Arginine-glycine-aspartic acid (RGD) can also use in this contest because of its capacity to bind $\alpha_v\beta_3/\alpha_v\beta_5$ integrins, overexpressed on endothelial cells of tumour vessels, and many researchers investigated its application and showed the promising effect penetration capability of RGD-conjugated drug delivery systems (Gao et al., 2014; Miura et al., 2013; R. Wang et al., 2018).

Transferrin receptor (TfR) has been found to be overexpressed on BBB in the brain and in the glioma, and several experimental works show the efficacy of transferrin (Tf) as a tumour-targeting ligand. For instance, Miao et al., conjugated paclitaxel loaded nanoparticles with a component of transferrin class. Lactoferrin (Lf), demonstrating the enhanced cytotoxic effect of the drug against tumour thanks to the improved tumour penetration (Miao et al., 2014).

However, among various biomolecules for active targeting, we decided to exploit folic acid (FA) ([figure 3.19](#)) for our MSNs. In particular, we proposed to link FA to the aminated PEG chains before the external functionalization, creating NH₂-PEG-FA complexes. Our aim was to obtain a stealth behaviour and to enhance active targeting towards cancer cells, considering and monitoring size of nanoplatform.

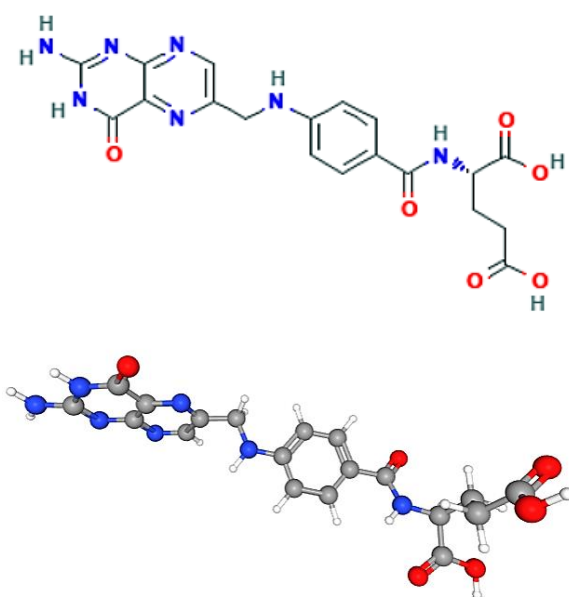


Figure 3.19 Schematic illustration of 2D chemical structure and ball-and-sticks model of folic acid. Readapted from www.pubchem.ncbi.nlm.nih.gov.

Folic acid is a small molecule stable at various temperatures and pH values, and it is able to bind to folate surface receptor. This latter is overexpressed in many tumours such as brain, kidney, epithelial, ovarian, breast, lung and others (Garin-Chesa et al., 1993; Parker et al., 2005). After the bond between folate and its receptor, nanoparticles are internalized through endocytotic pathway, and acidic environment of tumour causes the dissociation of folate from folate receptor and nanoparticles can perform its function. Moreover, folate receptor is recycled and return to the cell membrane (figure 3.20) (Mansoori et al., 2010; Zwicke et al., 2012).

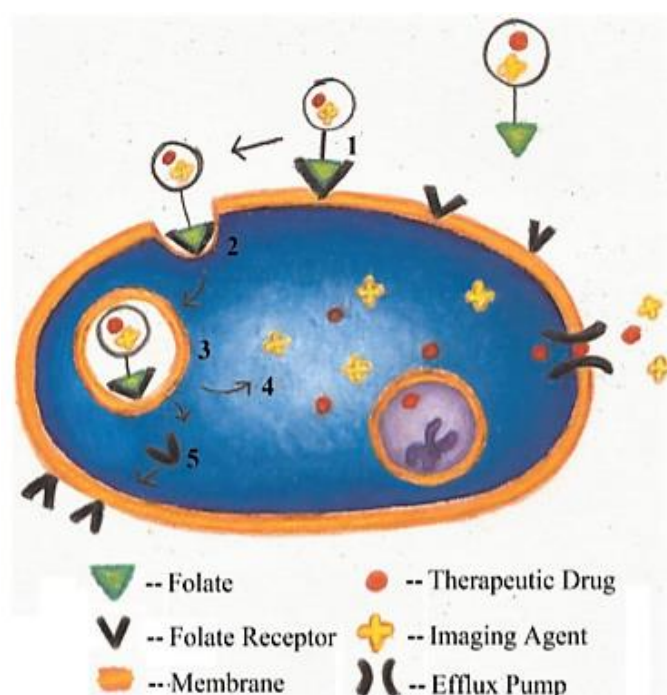


Figure 3.20 Schematic illustration of endocytotic pathway of nanoparticle conjugated to folate. Readapted from Zwicke et al. (2012).

According to the literature, several studies proved the efficacy of nanosystems exhibiting FA on the external surface. Yoo & Park, demonstrated the effect of doxorubicin aggregates of about 200 nm functionalised with PEG-FA chains on *in vivo* murine models. They showed a significant tumour suppression by using DOX-PEG-FA, in comparison with free DOX nanoaggregates (Yoo & Park, 2004). Tabasi et al., proved the enhanced toxicity against cancer cells of mesoporous silicon nanoparticles loaded with doxorubicin and functionalised with FA compared with free doxorubicin (Tabasi et al., 2012).

3.2.4 Drugs for Cancer Treatment

A key role in nanotheranostic systems is represented from anticancer drugs. According to the literature, researchers have investigated several drug formulations to understand chemical structure, stability and side effects in biological environment, and the efficacy against various types of tumour. It has been demonstrated that drugs increase exponentially their stability and efficacy by encapsulating in nanomedicine systems, such as polymeric, lipidic nanoparticles, mesoporous nanoparticles and the others mentioned in the previous sections. As a result, in the last decades, FDA and EMA approved nanoplatfroms using different active drugs in the clinic, and a huge number of them is undergoing clinical trials. Some of them are summarised in [table 3.6](#) (Tran et al., 2017).

Table 3.6 Nanomedicines currently approved and in clinical trials phase. Readapted from Tran et al. (2017).

APPROVED					
NAME	TYPE	ACTIVE DRUG	DIAMETER	TYPE OF CANCER	YEAR APPROVED
Doxil/caelyx	Liposome (PEGylated)	Doxorubicin	80-90 nm	HIV-associated Kaposi's sarcoma, ovarian cancer, metastatic breast cancer, multiple myeloma	FDA (1995) EMA (1996)
DaunoXome	Liposome (non-PEGylated)	Daunorubicin	45 nm	HIV-associated Kaposi's sarcoma	FDA (1996)
Lipo-Dox	Liposome	Doxorubicin	180 nm	Kaposi's sarcoma, breast and ovarian cancer	Taiwan (1998)
Myocet	Liposome	Doxorubicin	190 nm	Breast cancer	EMA (2000)
Abraxane	Nanoparticle albumin bound	Paclitaxel	130 nm	Advanced non-small-cell lung cancer, metastatic pancreatic cancer, metastatic breast cancer	FDA (2005) EMA (2008)
Genexol-PM	PEG-PLA polymeric micelle	Paclitaxel	20-50 nm	Breast cancer, lung cancer, ovarian cancer	South Korea (2007)
MM-398 (Onivyde)	Liposome (PEGylated)	Irinotecan	80-140 nm	Metastatic pancreatic cancer	FDA (2015)
IN CLINICAL TRIALS					
NAME	TYPE	ACTIVE DRUG	DIAMETER	TYPE OF CANCER	PHASE OF TRIAL

CRLX101	Polymer	Camptothecin	30-40 nm	Ovarian, rectal, renal, lung, stomach, gastroesophageal	I/II
Anti-EGFR immune liposome	Liposome	Doxorubicin	130-200 nm	Breast cancer	II
LipoCURC	Liposome	Curcumin	-	Advanced cancer with failed standard of care therapy	I/II
LiPlaCis	Liposome	Cisplatin	-	Advanced or refractory solid tumours, metastatic breast cancer	I/II
PROMITIL	Liposome	Mitomycin-C	~ 90 nm	Solid tumours	I

Among the various drugs validated for anticancer applications, we decided to exploit the combined action of two drugs: Tirapazamine (TPZ) and Doxorubicin (DOX).

Tirapazamine is an aromatic heterocycle di-*N*-oxide that has demonstrated its cytotoxicity against cancer cells only in hypoxic environments. Specifically, an intracellular reductase metabolises TPZ in order to produce a highly reactive radical species. This latter causes chromosomal aberrations and DNA single and double strand breaks, as shown in [figure 3.21](#), and cell death is the natural consequence (S. B. Reddy & Williamson, 2009).

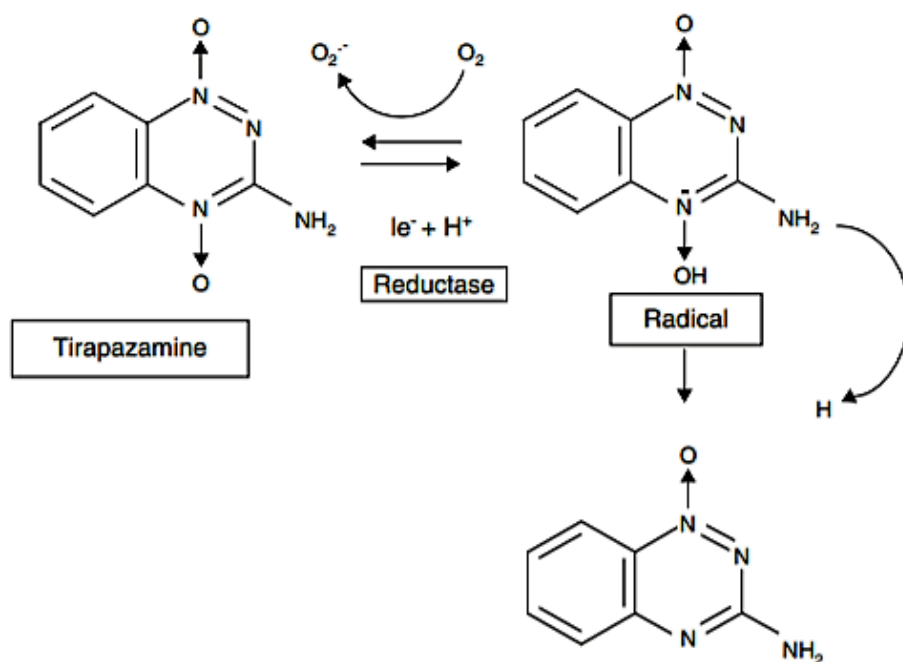


Figure 3.21 Tirapazamine mechanism of action. Readapted from S. B. Reddy & Williamson (2009).

Nevertheless, it has also been proven that Tirapazamine has low anticancer effects on murine models *in vivo* when used as single therapeutic agent, on the other hand, clinical trials showed its effect in killing cells when used in combination with other therapeutic modality such as radiotherapy or another anticancer drug (S. B. Reddy & Williamson, 2009). In this contest, we propose to incorporate TPZ in the mesoporous structure of our nanoparticle core because of the presence of TPPS₄ in the layer of nanoplatfrom. This could represent an interesting combined modality of therapy, in fact, the photosensitizer performs reducing amount of O₂, making the environment more hypoxic. Consequently, TPZ has the possibility to better perform its function.

Additionally, we decided to improve anticancer therapy effects of our nanoparticles introducing Doxorubicin between the last two layers. DOX is the most widely investigated drug in cancer treatment field, and several works are based on its use. DOX has not only been found to have great therapeutic effect, but also it demonstrated an inherent fluorescence, providing an imaging modality and giving the possibility to use DOX as a theranostic agent by itself (Park et al., 2016).

3.2.5 Materials and Methods: manufacturing process proposal

In this section we want to propose a possible manufacturing process based on validated protocols present in the literature. We widely analyse them in order to set the experimental steps for producing our nanoparticle in laboratory.

3.2.5.1 Mesoporous silica core synthesis

Solution of 2 g of CTAC and 0.06 g of TEA must be stirred in 20 mL water for 1 h at 95°. After that, 1.5 mL of TEOS must be added dropwise and stirred for 1 h. Centrifugation and washing of the product with methanol, successively particles are dispersed in 50 mL of HCl/MeOH (1% v/v) to remove CTAC template. Subsequent steps are collection of nanoparticles by centrifugation, washing step with water and then with methanol, drying to obtain MSN.

Reaction of 100 mg of MSNs with 2 mL of APTES in 20 mL of methanol must be conducted at room temperature, overnight, under stirring. Centrifugation and washing with methanol to obtain MSN-NH₂ (W. H. Chen et al., 2017).

3.2.5.2 Loading of Tirapazamine

100 mg of MSN-NH₂ stirred in TPZ solution of 1 mg mL⁻¹ overnight (W. H. Chen et al., 2017).

3.2.5.3 Layer-by-Layer Assembly

First layer of HA-βCD has to be deposited on MSN-NH₂ by LbL immersive method, dispersing 100 mg of nanoparticles in 3 mL of HA-βCD solution (1 mg mL⁻¹) and incubating for 15 min in order to obtain the electrostatic interaction of HA-βCD on the nanoparticles. After that, centrifugation and washing step with water. Successively, dispersion of nanoparticles in 3 mL of TPPS₄ solution (1 mg mL⁻¹) and subsequent washing step. In this step, TPPS₄ can be adsorbed on the HA-βCD layer through host-guest interaction. Another HA-βCD must be deposited through the same LbL process. For deposition of PLL, nanoparticles must be added to a stirring 45 mL solution of PLL (500 μM) at room temperature in dark. After that, NPs must be collected by centrifugation (W. H. Chen et al., 2017; Dreaden et al., 2014b).

3.2.5.4 External Surface Functionalisation

For synthesizing FA-PEG-NH₂, Boc-NH-PEG-NH₂ must be dissolved in DMSO with addition of folic acid, pyridine and dicyclohexylcarbodiimide. Reaction takes place for 24 h at room temperature. Then, evaporation of pyridine must be conducted. After isolation of polymer in diethyl ether, the solid product must be dissolved in water, filtered, dialysed, and freeze-dried. For removing Boc group, TFA need to be used for 2 h. Addition of FA-PEG-NH₂ (300 µg/mL) in solution with nanoparticles allow to obtain the complete structure of our nanoparticle (Ward et al., 2002).

4 BRIEF COMPUTATIONAL APPROACH

For all the nanotheranostic drug delivery platforms, kinetics of drug release is probably the major key factor to understand and control for achieving an appropriate therapeutic efficiency. In the contest of project design of nanosystems, the only validated way to study kinetics release is to conduct *in vitro* and *in vivo* tests to optimize the nanoplatform architecture. Nevertheless, tracking drugs from capsules into external environment such as medium *in vitro* or biological environment *in vivo* is a difficult, time-consuming, and economically costly task. Therefore, these issues can be partially solved by developing and implementing an appropriate *in silico* model to understand release mechanism in advance, and allowing to make right decisions before *in vitro* and *in vivo* tests (Peppas & Narasimhan, 2014; Siepmann & Peppas, 2012).

Moreover, another possible method to optimize design and development of nanoplatforms is to previously understand the strength of interaction between external surface conjugated biomolecules and receptors overexpressed on cancer cells surface, in order to improve active targeting modality and to realise nanotheranostic systems appropriate to treat specific types of cancers.

In this contest, we want to propose the use of a basic MATLAB algorithm as starting point to study drug kinetics release from a layer-by-layer covered nanocapsule, basing our proof of concept on a mathematical mechanistic model presented in a paper of Kaoui et al. Additionally, we demonstrate a way to provide a first step analysis of interaction between biomolecules and receptors by using molecular dynamics simulations through LigandScout computer software (Wolber & Langer, 2005).

4.1 BASIC MATLAB STUDY ON DRUG KINETICS RELEASE FROM MULTILAYER CAPSULES

Among various mechanism acting in drug delivery such as osmosis, drug dissolution, and polymeric swelling, diffusion is the most responsible for defining kinetics release profile (Grassi et al., 2011). Consequently, the model proposed by Kaoui et al., is principally based on diffusion mechanisms analysis. They consider a nanocapsule composed by a core incorporating the initial amount of drug and surrounded by layers of different materials. Different materials properties are considering by using different diffusion constant. The last layer is characterized by a much larger size than the others because it represents the external medium, i.e. fluid or biological environment. As shown in [figure](#)

4.1, in mathematical translation of the system, core is represented by Ω_0 , layers are defined as Ω_i , with $i = 1, 2, \dots, n$. Medium is represented by Ω_s layer. Defining c_0 and c_i as drug concentration respectively in the core and in every layer, drug diffusion in Ω_0 ³ and in the surrounding layers can be described using the second Fick's Law:

$$\frac{\partial c_0}{\partial t} = D_0 \nabla^2 c_0 \text{ in } \Omega_0, \quad (4.1)$$

$$\frac{\partial c_i}{\partial t} = D_i \nabla^2 c_i \text{ in } \Omega_i, i = 1, 2, \dots, n, s \quad (4.2)$$

with D_0 and D_i representing the diffusion coefficient of drug in the core and the layers. The initial condition for concentration is supposed to be given in all layers⁴. About the intralayer boundary conditions, flux continuity at interface between adjacent layers are expressed by:

$$-D_i \nabla_{c_i} \cdot \mathbf{n} = -D_{i+1} \nabla_{c_{i+1}} \cdot \mathbf{n} \text{ at } \partial\Omega_i \cap \partial\Omega_{i+1} \quad (4.3)$$

with \mathbf{n} surface external normal vector (Kaoui et al., 2018).

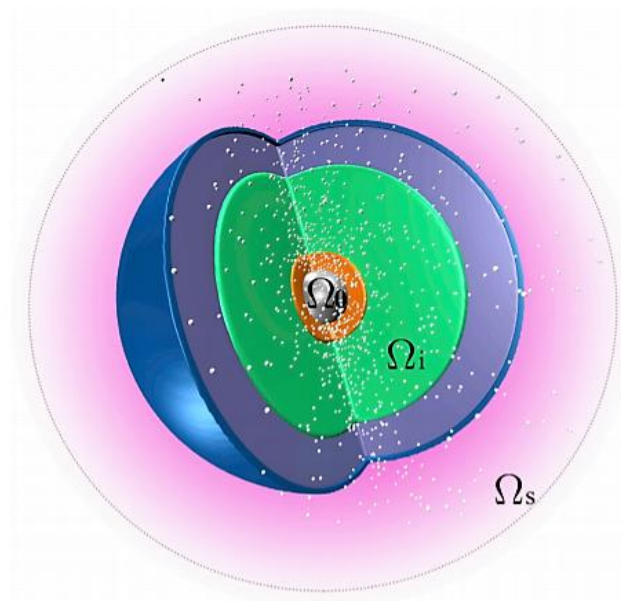


Figure 4.1 Schematic illustration of multilayer model of nanocapsule. Readapted from Kaoui et al. (2018).

³ Assumption that drug dissolution in the core can be considered as instantaneous, in comparison drug diffusion (McGinty & Pontrelli, 2015).

⁴ Widely exploited simplistic assumptions: I) c_0 is constant at core surface $\partial\Omega_0$, as if there is a sustained source of drug; II) c_s is uniform in the release medium Ω_s , as in stirred medium (Arifin et al., 2006; Crank, 1975).

A MATLAB code is proposed to simulate drug diffusion from a multilayer nanocapsule, based on the mathematical model described above. A MATLAB function code provide the analytic form of differential equation system (4.1), (4.2) and (4.3). Then, after manually inserting initial concentration values of drug for the core and for each layer, *ode45* is exploited in order to solve the differential equations system. In [figure 4.2](#) we present the plots⁵ showing profile of drug concentration in the core and in the layers, for a nanocapsule coated by four layers, starting from random values for initial values and diffusion constants. In fact, the most important aspect at this point of computational analysis is to obtain a realistic trend of curves representing drug concentration in time. The fifth layer represent external medium or biological environment. This computational model could be used as starting point for implementing an *in silico* approach to better understand drug release in drug delivery multilayer systems. Obviously, it needs to be more investigated and improved, for example adding differential equation to model others key factors of drug release. Moreover, several experimental data should be collected in order to validate the results of MATLAB analysis.

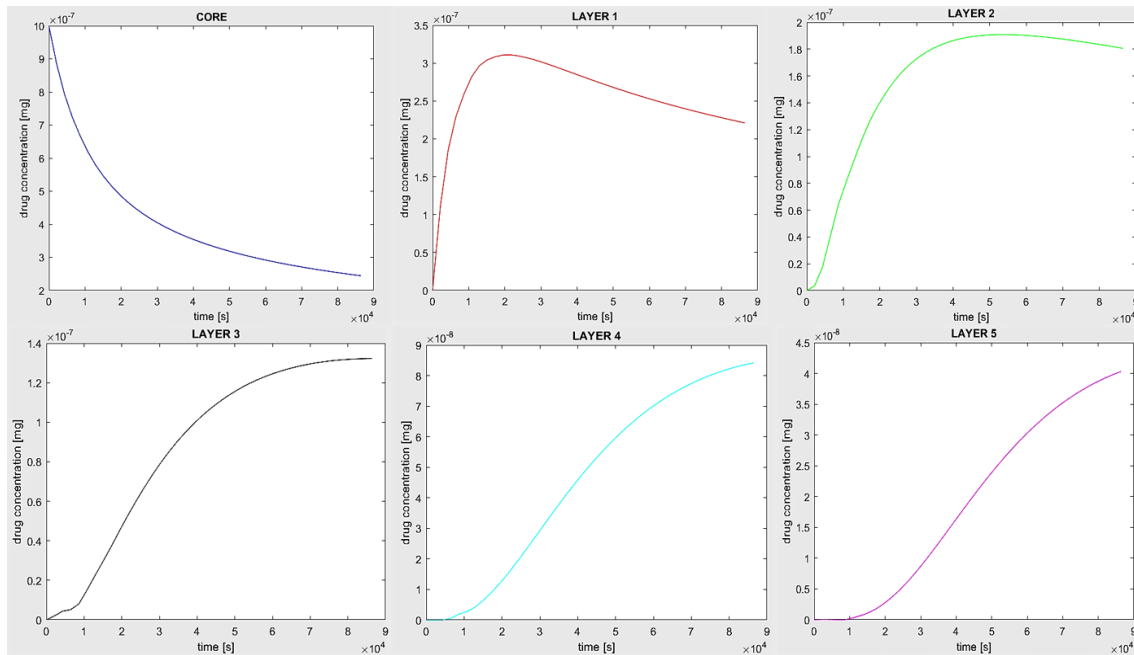


Figure 4.2 Representation of drug concentration variation in time for core and each layer. Values are random. Plots show a trend of curves comparable with expected results in an experimental work in laboratory.

⁵ MATLAB code for conduct the analysis is reported in Appendix.

4.2 LIGANDSCOUT MOLECULAR DYNAMIC SIMULATIONS

Another key in nanotheranostic platforms is the appropriate external functionalisation with biomolecules for active targeting toward receptors overexpressed on cancer cells. We propose the application of the computer software LigandScout as starting point to study biomolecules-receptors interactions. LigandScout is a software that allows to create a 3D pharmacophore⁶ model starting from structural data of molecules-ligand complexes, incorporating the major 3D chemical features such as hydrogen bond donors, acceptors, lipophilic areas, positively and negatively ionizable chemical groups, etc. In fact, these parameters are able to completely describe the interaction between a molecule (ligand) and the surrounding binding site of a macromolecule (Wolber & Kosara, 2006). Specifically, LigandScout allows to download *pdb* format files directly from the protein data bank (RCSB PDB). In each file we can find a crystallography of the protein selected for the analysis, together with validated ligand molecules in the binding sites. In our case, we are interested in analysing proteins acting as receptors expressed on cancer cells, and among various receptors described in the literature, we have decided to investigate CD44 cancer cells receptor, present on cells surface of several types of tumours, and integrin $\alpha\beta3$, expressed on ovarian cancer cells (Akhtar et al., 2014; Dreaden et al., 2014b). After opening *pdb* files on LigandScout, we have created pharmacophore model ([figure 4.3 A, B](#)) of ligand with the strongest interaction and we have conducted virtual screening process using a dataset composed by 10574 approved biomolecules downloaded from go.drugbank.com in *smile* format and converted in *pdb* format using Open Babel GUI application (O'Boyle et al., 2011). Virtual screening process performs fitting every molecule in the dataset on pharmacophore features, providing a value of pharmacophore fit as result. After that, we have selected the molecule characterised by the best pharmacophore fit value and we have conduct molecular dynamic simulation in order to bind it in the binding pocket of the macromolecule (receptor). Consequently, the software provides binding affinity score, useful to understand strength of interaction between selected molecule and receptor. As result, we have found that, among the 10574 tested molecules in virtual screening process, 2-(n-morpholino)-ethanesulfonic acid (MES) and arginylglycylaspartic acid (RGD) presented the best pharmacophore fit score for CD44

⁶ IUPAC definition of pharmacophore: “an ensemble of steric and electronic features that is necessary to ensure the optimal supramolecular interactions with a specific biological target”. It explains how structurally diverse ligands can bind to a common receptor site (Ganellin et al., 1998).

and integrin $\alpha\beta3$ respectively, and we report the molecular dynamic results for MES and RGD in [figure 4.4](#). As we can note, Binding Affinity Score for MES and RGD, respectively -7.97 Kcal/mol and -11.30 Kcal/mol, demonstrate strong interactions with the respective receptors. In fact, it is known from the literature that binding affinity scores lower than -6.1 Kcal/mol are index of strong interaction (Pantsar & Poso, 2018; Shoichet & Kuntz, 1991).

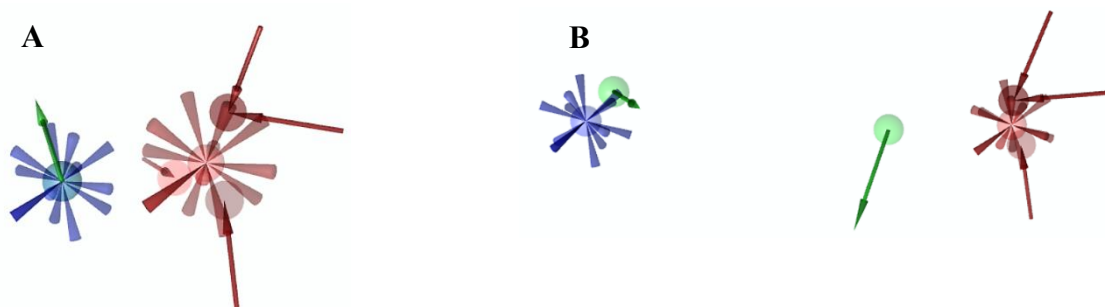


Figure 4.3 Illustration of pharmacophore based on the best ligand for CD44 receptor (A) and $\alpha\beta3$ integrin (B). Blue star represents positive ionizable points, red stars are negative ionizable points, red arrows are H bond acceptor, green arrows are H bond donor.

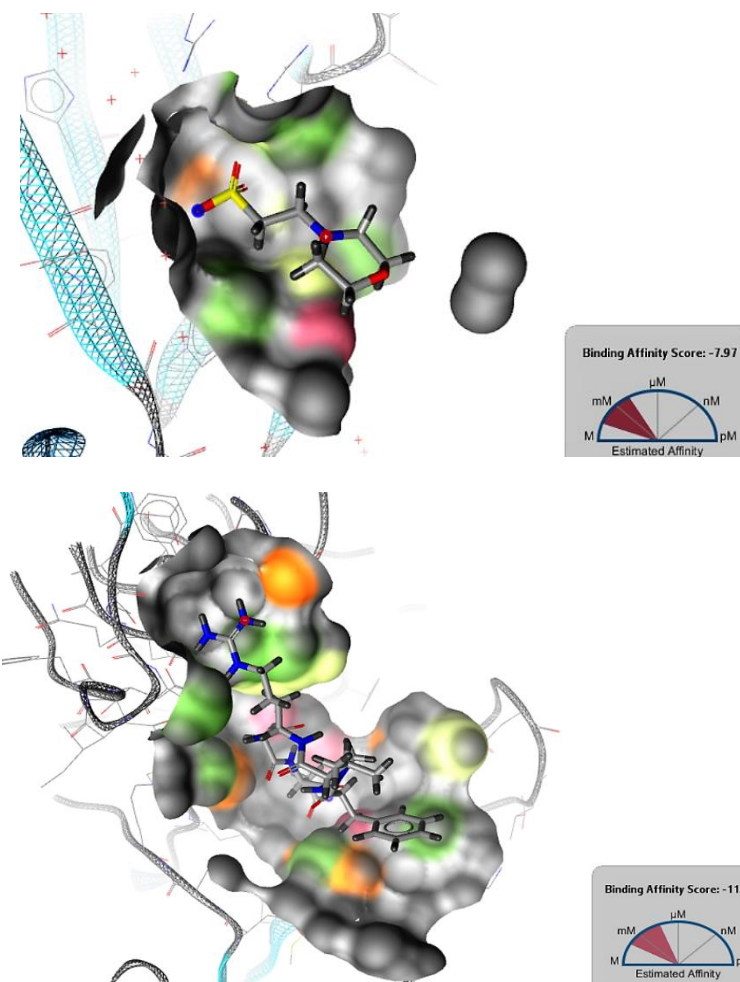


Figure 4.4 Representation of binding affinity in receptor pocket site. On the top, MES illustration. RGD on the bottom. Colours encode by atom binding affinity contribution.

5 CONCLUSION AND FUTURE PERSPECTIVES

Nanotheranostics is a nanomedicine field widely investigated only in the last few decades. Several works have been recently published in literature regarding nanotheranostic platforms proposed in order to enhance tumour treatment. In this field, many researchers are making great efforts in the study of promising interactions between materials, biological molecules and to deeply understand biological process, aiming to provide more suitable and efficient nanosystems, drugs and imaging modality.

In this work, starting from a deep analysis of state-of-art in literature related to recent advances in development of nanotheranostic platforms, we proposed the design of a mesoporous silica-based nanoparticle, loaded with tirapazimine drug, and coated with hyaluronic acid and poly(L-lysine) by using layer-by-layer assembly in order to obtain a pH sensitive system. Moreover, we decided to incorporate a layer made of TPPS₄ photosensitizer to provide photodynamical therapeutic modality and to allow NIR fluorescence imaging for tracking nanoparticles in the tumour site. Doxorubicin was also incorporated between the last two layers to conduct a drug combined therapeutic approach. Finally, we have opted for an external functionalisation composed by FA-PEG chains to ensure a stealth behaviour of nanoparticles and to improve active targeting process for a better cancer tissue uptake. In this bottom-up strategy for NPs design, we focused on size, trying to create nanoparticles with a diameter not much distant from the optimal size of 50 nm, for exploiting efficiently EPR effect in the tumour tissues. Moreover, according to the literature, we focused on the choice of materials that have demonstrated stability in the proposed manufacturing processes and biocompatibility for hypothetical *in vitro* and *in vivo* experimental tests.

Nevertheless, additional challenges need to be considered in order to develop a successful nanotheranostic system. For instance, preclinical *in vivo* tests on animal models seem to be unperfect for predicting realistic efficacy of nanoplatforms, due to some differences between human and animal biological features that can not be overlooked. As example, EPR effect it has been demonstrated to be more pronounced in animal compared with human tumour tissues (Nichols & Bae, 2014).

Overcoming biological barriers is also a fundamental challenge. Many potentially efficient nanotheranostic platforms are unable to reach brain cancer cells because of the presence of blood-brain barrier (BBB) (Kievit & Zhang, 2011). Additionally, in brain

metastases the BBB is disrupted, but blood-tumour barrier (BTB) makes cancer cells uptake still low (Steeg et al., 2011).

In order to be translated in the clinic, designed nanotheranostic systems should ensure the possibility to achieve a mass production. In fact, producing small batches at a time for *in vitro* and *in vivo* tests does not provide information in terms of scalability of the product. Development of efficient protocols and possibility to *in vitro* tests on microfluidic organs-on-chip could give a huge help to achieve reliability of a mass production.

Moreover, in the contest of requirements for government and market approval, cost and quality should be control during the manufacturing process, assays to evaluate pharmacokinetics and biodistribution must be perfectly performed (Ma et al., 2016).

A basic computational approach was proposed in the last section with the aim to provide a starting point for a possible *in silico* way to conduct analysis on properties of materials used in nanoplatfroms. It needs to be necessary more deeply investigated and implemented in terms of realistic parameters, variables and it is essential to collect several experimental data in order to validate computational analysis. After overcoming these latter challenges, this *in silico* approach could be useful in nanoplatfroms design for reducing time consumption and testing costs.

In conclusion, the present work is intended as a preliminary study about the design of an innovative nanotheranostic system, but reliability, feasibility and efficiency should be assessed, and only after that, features of nanoplatfroms can be improved and modified to obtain a successful device.

Appendix

MATLAB Code for studying drug kinetics release from multilayer nanosystems

```
close all
clear all
clc

%{
Operating Conditions
}%

global InitialConc
InitialConc = [1*10^-6; 0; 0; 0; 0; 0]
%This is the initial concentration of drug in each layer,
%can be edited to represent the number of layers

%% INITIALISE SIMULATION

%{
SET Time Interval (in seconds)
}%

EndTime = 3600*24;
ispan = [0 EndTime];
ispan = sort(ispan);
ispan = unique(ispan);

%{
Initialise the dependent variables
In this example, the dependent variables in the differential
equations are the standard units, when needed they can be
defined here
}%

c0 = [InitialConc]; %if other differential equations are
%needed, they should be defined here with initial
conditions

options = odeset('NonNegative', 1:length(c0));
%%

%{
SET Integrator Options
}%

%% SIMULATION LOOP

for j = 2:length(ispan)
```

```

[tSection,      cSection]      =      ode45(@DifEq,[ispan(j-1)
ispan(j)], c0, options);
nt = length (tSection);

if j==2
t = tSection;
c = cSection;
else
t = [t; tSection(2:nt)];
c = [c; cSection(2:nt,:)];
end

c0 = cSection(nt,:);
end

%Generate plots
figure(),

plot(t,c(1:end,1),'b')
title('CORE')
xlabel('time [s]');
ylabel('drug concentration [mg]);

figure(),

plot(t,c(1:end,2),'r')
title('LAYER 1')
xlabel('time [s]');
ylabel('drug concentration [mg]);

figure(),

plot(t,c(1:end,3),'g')
title('LAYER 2')
xlabel('time [s]');
ylabel('drug concentration [mg]);

figure(),

plot(t,c(1:end,4),'k')
title('LAYER 3')
xlabel('time [s]');
ylabel('drug concentration [mg]);

figure(),

plot(t,c(1:end,5),'c')
title('LAYER 4')
xlabel('time [s]');
ylabel('drug concentration [mg]);

```

```
figure(),

plot(t,c(1:end,6),'m')
title('LAYER 5')
xlabel('time [s]');
ylabel('drug concentration [mg]);
```

Function code designed to calculate the rate of change of concentration at each of the defined points

```
function [dc_dt] = DifEq (t, c)

Dab = 0.00006 %cm/s diffusion constant, at the moment, this
is a random number I need to better define from literature

dc_dt(1) = Dab*(c(2)-c(1)); %differential equation for first
%layer

for i=2:length(c)-1 %loop to calculate all layers except
%first and last number of layer

dc_dt(i) = Dab*((c(i+1)-c(i))-(c(i)-c(i-1)));
end

x = length(c)
dc_dt(x) = Dab*(c(x)-c(x-1)); %equation for last layer

%Copy all the derivatives into the output vector in the right
%order

dc_dt = [dc_dt]';

end
```


REFERENCES

- Abulateefeh, S. R., Alkawareek, M. Y., & Alkilany, A. M. (2019). Tunable sustained release drug delivery system based on mononuclear aqueous core-polymer shell microcapsules. *International Journal of Pharmaceutics*, 558, 291–298. <https://doi.org/10.1016/j.ijpharm.2019.01.006>
- Akhtar, M. J., Ahamed, M., Alhadlaq, H. A., Alrokayan, S. A., & Kumar, S. (2014). Targeted anticancer therapy: Overexpressed receptors and nanotechnology. *Clinica Chimica Acta*, 436, 78–92. <https://doi.org/https://doi.org/10.1016/j.cca.2014.05.004>
- Alkekhia, D., Hammond, P. T., & Shukla, A. (2020a). Layer-by-Layer Biomaterials for Drug Delivery. *Annual Review of Biomedical Engineering*, 22, 1–24. <https://doi.org/10.1146/annurev-bioeng-060418-052350>
- Alkekhia, D., Hammond, P. T., & Shukla, A. (2020b). *Layer-by-Layer Biomaterials for Drug Delivery*. 1–24.
- Alongi, J., Carosio, F., Frache, A., & Malucelli, G. (2013). Layer by Layer coatings assembled through dipping, vertical or horizontal spray for cotton flame retardancy. *Carbohydrate Polymers*, 92(1), 114–119. <https://doi.org/https://doi.org/10.1016/j.carbpol.2012.08.086>
- Anselmo, A. C., & Mitragotri, S. (2016). Nanoparticles in the clinic. *Bioengineering & Translational Medicine*, 1(1), 10–29. <https://doi.org/10.1002/btm2.10003>
- Arifin, D. Y., Lee, L. Y., & Wang, C.-H. (2006). Mathematical modeling and simulation of drug release from microspheres: Implications to drug delivery systems. *Advanced Drug Delivery Reviews*, 58(12), 1274–1325. <https://doi.org/https://doi.org/10.1016/j.addr.2006.09.007>
- Bai, H., Yuan, H., Nie, C., Wang, B., Lv, F., Liu, L., & Wang, S. (2015). A Supramolecular Antibiotic Switch for Antibacterial Regulation. *Angewandte Chemie International Edition*, 54(45), 13208–13213. <https://doi.org/10.1002/anie.201504566>
- Banerjee A., Qi J., Gogoi R., Wong J., M. S. (2016). Role of nanoparticle size, shape and surface chemistry in oral drug delivery. *Journal of Controlled Release*, 805, 2–27. <https://doi.org/https://doi.org/10.1016/j.jconrel.2016.07.051>
- Bartlett, D. W., Su, H., Hildebrandt, I. J., Weber, W. A., & Davis, M. E. (2007). Impact of tumor-specific targeting on the biodistribution and efficacy of siRNA nanoparticles measured by multimodality in vivo imaging. *Proceedings of the National Academy of Sciences*, 104(39), 15549 LP – 15554. <https://doi.org/10.1073/pnas.0707461104>
- Belyanina, I., Kolovskaya, O., Zamay, S., Gargaun, A., Zamay, T., & Kichkailo, A. (2017). Targeted magnetic nanotheranostics of cancer. *Molecules*, 22(6), 1–19. <https://doi.org/10.3390/molecules22060975>
- Bertrand, P., Jonas, A., Laschewsky, A., & Legras, R. (2000). Ultrathin polymer coatings by complexation of polyelectrolytes at interfaces: suitable materials, structure and properties. *Macromolecular Rapid Communications*, 21(7), 319–348. [https://doi.org/10.1002/\(SICI\)1521-3927\(20000401\)21:7<319::AID-MARC319>3.0.CO;2-7](https://doi.org/10.1002/(SICI)1521-3927(20000401)21:7<319::AID-MARC319>3.0.CO;2-7)

- Björnmalm, M., Cui, J., Bertleff-Zieschang, N., Song, D., Faria, M., Rahim, M. A., & Caruso, F. (2017). Nanoengineering Particles through Template Assembly. *Chemistry of Materials*, 29(1), 289–306. <https://doi.org/10.1021/acs.chemmater.6b02848>
- Bonchio, M., Carofiglio, T., Carraro, M., Fornasier, R., & Tonellato, U. (2002). Efficient Sensitized Photooxygenation in Water by a Porphyrin - Cyclodextrin Supramolecular Complex. *Organic Letters*, 4(26), 4635–4637. <https://doi.org/10.1021/ol0270069>
- Boulikas, T. (2009). Clinical overview on Lipoplatin™: a successful liposomal formulation of cisplatin. *Expert Opinion on Investigational Drugs*, 18(8), 1197–1218. <https://doi.org/10.1517/13543780903114168>
- Brian F. Zamarron and WanJun Chen. (2011). Dual Roles of Immune Cells and Their Factors in Cancer Development and Progression. *International Journal of Biological Sciences*, 7(5), 651–658. <https://www.ncbi.nlm.nih.gov/pmc/articles/PMC3107473/pdf/ijbsv07p0651.pdf>
- Brown, J. M. (2000). Exploiting the hypoxic cancer cell: mechanisms and therapeutic strategies. *Molecular Medicine Today*, 6(4), 157–162. [https://doi.org/https://doi.org/10.1016/S1357-4310\(00\)01677-4](https://doi.org/https://doi.org/10.1016/S1357-4310(00)01677-4)
- Cai, Q., Luo, Z.-S., Pang, W.-Q., Fan, Y.-W., Chen, X.-H., & Cui, F.-Z. (2001). Dilute Solution Routes to Various Controllable Morphologies of MCM-41 Silica with a Basic Medium. *Chemistry of Materials*, 13(2), 258–263. <https://doi.org/10.1021/cm990661z>
- Cai, X., Gao, X., Wang, L., Wu, Q., & Lin, X. (2013). A layer-by-layer assembled and carbon nanotubes/gold nanoparticles-based bienzyme biosensor for cholesterol detection. *Sensors and Actuators B: Chemical*, 181, 575–583. <https://doi.org/https://doi.org/10.1016/j.snb.2013.02.050>
- Cancer Research UK. (2020). <https://www.cancerresearchuk.org/health-professional/cancer-statistics-for-the-uk#heading-Zero>
- Caruso, F., Lichtenfeld, H., Giersig, M., & Möhwald, H. (1998). Electrostatic Self-Assembly of Silica Nanoparticle–Polyelectrolyte Multilayers on Polystyrene Latex Particles. *Journal of the American Chemical Society*, 120(33), 8523–8524. <https://doi.org/10.1021/ja9815024>
- Celli, J. P., Spring, B. Q., Rizvi, I., Evans, C. L., Samkoe, K. S., Verma, S., Pogue, B. W., & Hasan, T. (2010). Imaging and Photodynamic Therapy: Mechanisms, Monitoring, and Optimization. *Chemical Reviews*, 110(5), 2795–2838. <https://doi.org/10.1021/cr900300p>
- Chen, M., Tang, S., Guo, Z., Wang, X., Mo, S., Huang, X., Liu, G., & Zheng, N. (2014). Core–Shell Pd@Au Nanoplates as Theranostic Agents for In-Vivo Photoacoustic Imaging, CT Imaging, and Photothermal Therapy. *Advanced Materials*, 26(48), 8210–8216. <https://doi.org/10.1002/adma.201404013>
- Chen, N.-T., Cheng, S.-H., Souris, J. S., Chen, C.-T., Mou, C.-Y., & Lo, L.-W. (2013). Theranostic applications of mesoporous silica nanoparticles and their organic/inorganic hybrids. *J. Mater. Chem. B*, 1(25), 3128–3135. <https://doi.org/10.1039/C3TB20249F>

- Chen, W. H., Luo, G. F., Lei, Q., Cao, F. Y., Fan, J. X., Qiu, W. X., Jia, H. Z., Hong, S., Fang, F., Zeng, X., Zhuo, R. X., & Zhang, X. Z. (2016). Rational design of multifunctional magnetic mesoporous silica nanoparticle for tumor-targeted magnetic resonance imaging and precise therapy. *Biomaterials*, 76, 87–101. <https://doi.org/10.1016/j.biomaterials.2015.10.053>
- Chen, W. H., Luo, G. F., Qiu, W. X., Lei, Q., Liu, L. H., Wang, S. B., & Zhang, X. Z. (2017). Mesoporous silica-based versatile theranostic nanoplatfrom constructed by layer-by-layer assembly for excellent photodynamic/chemo therapy. *Biomaterials*, 117, 54–65. <https://doi.org/10.1016/j.biomaterials.2016.11.057>
- Chiarelli, P. A., Johal, M. S., Casson, J. L., Roberts, J. B., Robinson, J. M., & Wang, H.-L. (2001). Controlled Fabrication of Polyelectrolyte Multilayer Thin Films Using Spin-Assembly. *Advanced Materials*, 13(15), 1167–1171. [https://doi.org/10.1002/1521-4095\(200108\)13:15<1167::AID-ADMA1167>3.0.CO;2-A](https://doi.org/10.1002/1521-4095(200108)13:15<1167::AID-ADMA1167>3.0.CO;2-A)
- Chithrani, B. D., Ghazani, A. A., & Chan, W. C. W. (2006). Determining the Size and Shape Dependence of Gold Nanoparticle Uptake into Mammalian Cells. *Nano Letters*, 6(4), 662–668. <https://doi.org/10.1021/nl052396o>
- Choi, K. Y., Correa, S., Min, J., Li, J., Roy, S., Laccetti, K. H., Dreaden, E., Kong, S., Heo, R., Roh, Y. H., Lawson, E. C., Palmer, P. A., & Hammond, P. T. (2019). Binary Targeting of siRNA to Hematologic Cancer Cells In Vivo Using Layer-by-Layer Nanoparticles. *Advanced Functional Materials*, 29(20), 1900018. <https://doi.org/10.1002/adfm.201900018>
- Cobley, C. M., Chen, J., Cho, E. C., Wang, L. V., & Xia, Y. (2011). Gold nanostructures : a class of multifunctional materials for biomedical applications. *Chem Soc Rev*, 44–56. <https://doi.org/10.1039/b821763g>
- Cosco, D., Paolino, D., De Angelis, F., Cilurzo, F., Celia, C., Di Marzio, L., Russo, D., Tsapis, N., Fattal, E., & Fresta, M. (2015). Aqueous-core PEG-coated PLA nanocapsules for an efficient entrapment of water soluble anticancer drugs and a smart therapeutic response. *European Journal of Pharmaceutics and Biopharmaceutics : Official Journal of Arbeitsgemeinschaft Fur Pharmazeutische Verfahrenstechnik e.V.*, 89, 30–39. <https://doi.org/10.1016/j.ejpb.2014.11.012>
- Costa, R. R., Alatorre-Meda, M., & Mano, J. F. (2015). Drug nano-reservoirs synthesized using layer-by-layer technologies. *Biotechnology Advances*, 33(6, Part 3), 1310–1326. <https://doi.org/10.1016/j.biotechadv.2015.04.005>
- Crank, J. (1975). *The mathematics of diffusion*, 414 p. Oxford University Press, New York.
- Croissant, J. G., Fatieiev, Y., & Khashab, N. M. (2017). Degradability and Clearance of Silicon, Organosilica, Silsesquioxane, Silica Mixed Oxide, and Mesoporous Silica Nanoparticles. *Advanced Materials*, 29(9), 1604634. <https://doi.org/10.1002/adma.201604634>
- Dawson, L. A., & Sharpe, M. B. (2006). *Image-guided radiotherapy : rationale , benefits , and limitations*.
- De Frates, K., Markiewicz, T., Gallo, P., Rack, A., Weyhmiller, A., Jarmusik, B., & Hu, X. (2018). Protein polymer-based nanoparticles: Fabrication and medical

- applications. *International Journal of Molecular Sciences*, 19(6), 1–20. <https://doi.org/10.3390/ijms19061717>
- De Matteis, L., Jary, D., Lucía, A., García-Embid, S., Serrano-Sevilla, I., Pérez, D., Ainsa, J. A., Navarro, F. P., & M. de la Fuente, J. (2018). New active formulations against M. tuberculosis: Bedaquiline encapsulation in lipid nanoparticles and chitosan nanocapsules. *Chemical Engineering Journal*, 340(xxxx), 181–191. <https://doi.org/10.1016/j.cej.2017.12.110>
- Delcea, M., Möhwald, H., & Skirtach, A. G. (2011). Stimuli-responsive LbL capsules and nanoshells for drug delivery. *Advanced Drug Delivery Reviews*, 63(9), 730–747. <https://doi.org/https://doi.org/10.1016/j.addr.2011.03.010>
- Deng, S., Gigliobianco, M. R., Censi, R., & Di Martino, P. (2020). Polymeric nanocapsules as nanotechnological alternative for drug delivery system: Current status, challenges and opportunities. *Nanomaterials*, 10(5). <https://doi.org/10.3390/nano10050847>
- Diou, O., Tsapis, N., Giraudeau, C., Valette, J., Gueutin, C., Bourasset, F., Zanna, S., Vauthier, C., & Fattal, E. (2012). Long-circulating perfluorooctyl bromide nanocapsules for tumor imaging by 19FMRI. *Biomaterials*, 33(22), 5593–5602. <https://doi.org/https://doi.org/10.1016/j.biomaterials.2012.04.037>
- Dobrovolskaia, M. A., Aggarwal, P., Hall, J. B., & McNeil, S. E. (2008). Preclinical Studies To Understand Nanoparticle Interaction with the Immune System and Its Potential Effects on Nanoparticle Biodistribution. *Molecular Pharmaceutics*, 5(4), 487–495. <https://doi.org/10.1021/mp800032f>
- Dreaden, E. C., Morton, S. W., Shopsowitz, K. E., Choi, J.-H., Deng, Z. J., Cho, N.-J., & Hammond, P. T. (2014a). Bimodal Tumor-Targeting from Microenvironment Responsive Hyaluronan Layer-by-Layer (LbL) Nanoparticles. *ACS Nano*, 8(8), 8374–8382. <https://doi.org/10.1021/nn502861t>
- Dreaden, E. C., Morton, S. W., Shopsowitz, K. E., Choi, J. H., Deng, Z. J., Cho, N. J., & Hammond, P. T. (2014b). Bimodal tumor-targeting from microenvironment responsive hyaluronan layer-by-layer (LbL) nanoparticles. *ACS Nano*, 8(8), 8374–8382. <https://doi.org/10.1021/nn502861t>
- Dubas, S. T., & Schlenoff, J. B. (1999). Factors Controlling the Growth of Polyelectrolyte Multilayers. *Macromolecules*, 32(24), 8153–8160. <https://doi.org/10.1021/ma981927a>
- Dykman, L. A., & Khlebtsov, N. G. (2016). Multifunctional gold-based nanocomposites for theranostics. *Biomaterials*, 108, 13–34. <https://doi.org/https://doi.org/10.1016/j.biomaterials.2016.08.040>
- Egeblad, M., & Werb, Z. (2002). New functions for the matrix metalloproteinases in cancer progression. *Nature Reviews Cancer*, 2(3), 161–174. <https://doi.org/10.1038/nrc745>
- Elbaz, N. M., Owen, A., Rannard, S., & McDonald, T. O. (2020). Controlled synthesis of calcium carbonate nanoparticles and stimuli-responsive multi-layered nanocapsules for oral drug delivery. *International Journal of Pharmaceutics*, 574, 118866. <https://doi.org/10.1016/j.ijpharm.2019.118866>

- Fang, J., Nakamura, H., & Maeda, H. (2011). The EPR effect: Unique features of tumor blood vessels for drug delivery, factors involved, and limitations and augmentation of the effect. *Advanced Drug Delivery Reviews*, 63(3), 136–151. <https://doi.org/https://doi.org/10.1016/j.addr.2010.04.009>
- Feng, W., Nie, W., He, C., Zhou, X., Chen, L., Qiu, K., Wang, W., & Yin, Z. (2014). Effect of pH-Responsive Alginate/Chitosan Multilayers Coating on Delivery Efficiency, Cellular Uptake and Biodistribution of Mesoporous Silica Nanoparticles Based Nanocarriers. *ACS Applied Materials & Interfaces*, 6(11), 8447–8460. <https://doi.org/10.1021/am501337s>
- Fowler, C. E., Khushalani, D., Lebeau, B., & Mann, S. (2001). Nanoscale Materials with Mesostructured Interiors. *Advanced Materials*, 13(9), 649–652. [https://doi.org/10.1002/1521-4095\(200105\)13:9<649::AID-ADMA649>3.0.CO;2-G](https://doi.org/10.1002/1521-4095(200105)13:9<649::AID-ADMA649>3.0.CO;2-G)
- Fu, Y., Li, S.-J., Xu, J., Yang, M., Zhang, J.-D., Jiao, Y.-H., Zhang, J.-C., Zhang, K., & Jia, Y.-G. (2011). Facile and Efficient Approach to Speed up Layer-by-Layer Assembly: Dipping in Agitated Solutions. *Langmuir*, 27(2), 672–677. <https://doi.org/10.1021/la104524k>
- Fukuda, Y., Akagi, T., Asaoka, T., Eguchi, H., Sasaki, K., Iwagami, Y., Yamada, D., Noda, T., Kawamoto, K., Gotoh, K., Kobayashi, S., Mori, M., Doki, Y., & Akashi, M. (2018). Layer-by-layer cell coating technique using extracellular matrix facilitates rapid fabrication and function of pancreatic β -cell spheroids. *Biomaterials*, 160, 82–91. <https://doi.org/https://doi.org/10.1016/j.biomaterials.2018.01.020>
- Gaber, M., Hany, M., Mokhtar, S., Helmy, M. W., Elkodairy, K. A., & Elzoghby, A. O. (2019). Boronic-targeted albumin-shell oily-core nanocapsules for synergistic aromatase inhibitor/herbal breast cancer therapy. *Materials Science and Engineering C*, 105(May), 110099. <https://doi.org/10.1016/j.msec.2019.110099>
- Ganellin, C., Lindberg, P., & Mitscher, L. (1998). Glossary of terms used in medicinal chemistry. *Pure Appl Chem*, 70, 1129–1143.
- Gao, H., Xiong, Y., Zhang, S., Yang, Z., Cao, S., & Jiang, X. (2014). RGD and Interleukin-13 Peptide Functionalized Nanoparticles for Enhanced Glioblastoma Cells and Neovasculature Dual Targeting Delivery and Elevated Tumor Penetration. *Molecular Pharmaceutics*, 11(3), 1042–1052. <https://doi.org/10.1021/mp400751g>
- Garin-Chesa, P., Campbell, I., Saigo, P. E., Lewis Jr, J. L., Old, L. J., & Rettig, W. J. (1993). Trophoblast and ovarian cancer antigen LK26. Sensitivity and specificity in immunopathology and molecular identification as a folate-binding protein. *The American Journal of Pathology*, 142(2), 557–567. <https://pubmed.ncbi.nlm.nih.gov/8434649>
- Gil, P. R., del Mercato, L. L., del Pino, P., Muñoz-Javier, A., & Parak, W. J. (2008). Nanoparticle-modified polyelectrolyte capsules. *Nano Today*, 3(3–4), 12–21. [https://doi.org/10.1016/S1748-0132\(08\)70040-9](https://doi.org/10.1016/S1748-0132(08)70040-9)
- Gittleston, F. S., Hwang, D., Ryu, W.-H., Hashmi, S. M., Hwang, J., Goh, T., & Taylor, A. D. (2015). Ultrathin Nanotube/Nanowire Electrodes by Spin-Spray Layer-by-Layer Assembly: A Concept for Transparent Energy Storage. *ACS Nano*, 9(10),

- 10005–10017. <https://doi.org/10.1021/acsnano.5b03578>
- Globocan. (2019). All cancers. *Globocan*, 876, 2018–2019. <https://doi.org/10.1051/0004-6361/201016331>
- Grassi, M., Lamberti, G., Cascone, S., & Grassi, G. (2011). Mathematical modeling of simultaneous drug release and in vivo absorption. *International Journal of Pharmaceutics*, 418(1), 130–141. <https://doi.org/10.1016/j.ijpharm.2010.12.044>
- Greish, K. (2007). Enhanced permeability and retention of macromolecular drugs in solid tumors: A royal gate for targeted anticancer nanomedicines. *Journal of Drug Targeting*, 15(7–8), 457–464. <https://doi.org/10.1080/10611860701539584>
- Guo, J., Rahme, K., He, Y., Li, L., Holmes, J. D., & Driscoll, C. M. O. (2017). *Gold nanoparticles enlighten the future of cancer theranostics*. 6131–6152.
- Hadjesfandiari, N., & Parambath, A. (2018). 13. Stealth coatings for nanoparticles: polyethylene glycol alternatives. In *Engineering of Biomaterials for Drug Delivery Systems*. Elsevier Ltd. <https://doi.org/10.1016/B978-0-08-101750-0.00013-1>
- Haley, B., & Frenkel, E. (2008). Nanoparticles for drug delivery in cancer treatment. *Urologic Oncology: Seminars and Original Investigations*, 26(1), 57–64. <https://doi.org/10.1016/j.urolonc.2007.03.015>
- Hanahan, D., & Weinberg, R. A. (2017). Biological Hallmarks of cancer. *Holland-Frei Cancer Medicine*, 01(April), 1–10. <https://doi.org/10.1002/9781119000822.hfcm002>
- Hayashi, K., Nakamura, M., Sakamoto, W., Yogo, T., Miki, H., Ozaki, S., Abe, M., Matsumoto, T., & Ishimura, K. (2013). Superparamagnetic nanoparticle clusters for cancer theranostics combining magnetic resonance imaging and hyperthermia treatment. *Theranostics*, 3(6), 366–376. <https://doi.org/10.7150/thno.5860>
- He, Q., Zhang, Z., Gao, F., Li, Y., & Shi, J. (2011). In vivo Biodistribution and Urinary Excretion of Mesoporous Silica Nanoparticles: Effects of Particle Size and PEGylation. *Small*, 7(2), 271–280. <https://doi.org/10.1002/smll.201001459>
- He, X., Wu, X., Wang, K., Shi, B., & Hai, L. (2009). Methylene blue-encapsulated phosphonate-terminated silica nanoparticles for simultaneous in vivo imaging and photodynamic therapy. *Biomaterials*, 30(29), 5601–5609. <https://doi.org/10.1016/j.biomaterials.2009.06.030>
- Hobbs, S. K., Monsky, W. L., Yuan, F., Roberts, W. G., Griffith, L., Torchilin, V. P., & Jain, R. K. (1998). Regulation of transport pathways in tumor vessels: Role of tumor type and microenvironment. *Proceedings of the National Academy of Sciences*, 95(8), 4607–4612. <https://doi.org/10.1073/pnas.95.8.4607>
- Hofheinz, R.-D., Gnad-Vogt, S. U., Beyer, U., & Hochhaus, A. (2005). Liposomal encapsulated anti-cancer drugs. *Anti-Cancer Drugs*, 16(7). https://journals.lww.com/anti-cancerdrugs/Fulltext/2005/08000/Liposomal_encapsulated_anti_cancer_drugs.2.aspx
- Hu, Z., Luo, F., Pan, Y., Hou, C., Ren, L., Chen, J., Wang, J., & Zhang, Y. (2008). Arg-Gly-Asp (RGD) peptide conjugated poly(lactic acid)–poly(ethylene oxide) micelle

- for targeted drug delivery. *Journal of Biomedical Materials Research Part A*, 85A(3), 797–807. <https://doi.org/10.1002/jbm.a.31615>
- Huang, P., Bao, L., Zhang, C., Lin, J., Luo, T., Yang, D., He, M., Li, Z., Gao, G., Gao, B., Fu, S., & Cui, D. (2011). Biomaterials Folic acid-conjugated Silica-modified gold nanorods for X-ray / CT imaging-guided dual-mode radiation and photothermal therapy. *Biomaterials*, 32(36), 9796–9809. <https://doi.org/10.1016/j.biomaterials.2011.08.086>
- Hussain, Z., Khan, S., Imran, M., Sohail, M., Shah, S. W. A., & de Matas, M. (2019). PEGylation: a promising strategy to overcome challenges to cancer-targeted nanomedicines: a review of challenges to clinical transition and promising resolution. In *Drug Delivery and Translational Research*. Drug Delivery and Translational Research. <https://doi.org/10.1007/s13346-019-00631-4>
- Iler, R. K. (1966). Multilayers of colloidal particles. *Journal of Colloid and Interface Science*, 21(6), 569–594. [https://doi.org/10.1016/0095-8522\(66\)90018-3](https://doi.org/10.1016/0095-8522(66)90018-3)
- Izquierdo, A., Ono, S. S., Voegel, J.-C., Schaaf, P., & Decher, G. (2005). Dipping versus Spraying: Exploring the Deposition Conditions for Speeding Up Layer-by-Layer Assembly. *Langmuir*, 21(16), 7558–7567. <https://doi.org/10.1021/la047407s>
- Jain, P. K., Lee, K. S., El-sayed, I. H., & El-sayed, M. A. (2006). *Calculated Absorption and Scattering Properties of Gold Nanoparticles of Different Size, Shape, and Composition: Applications in Biological Imaging and Biomedicine*. 7238–7248.
- Jain, R. K., & Stylianopoulos, T. (2010). Delivering nanomedicine to solid tumors. *Nature Reviews Clinical Oncology*, 7(11), 653–664. <https://doi.org/10.1038/nrclinonc.2010.139>
- Jeon, S. I., Lee, J. H., Andrade, J. D., & De Gennes, P. G. (1991). Protein—surface interactions in the presence of polyethylene oxide: I. Simplified theory. *Journal of Colloid and Interface Science*, 142(1), 149–158. [https://doi.org/10.1016/0021-9797\(91\)90043-8](https://doi.org/10.1016/0021-9797(91)90043-8)
- Jiang, W., Kim, B. Y. S., Rutka, J. T., & Chan, W. C. W. (2008). Nanoparticle-mediated cellular response is size-dependent. *Nature Nanotechnology*, 3(3), 145–150. <https://doi.org/10.1038/nnano.2008.30>
- Kandasamy, G., & Maity, D. (2015). Recent advances in superparamagnetic iron oxide nanoparticles (SPIONs) for in vitro and in vivo cancer nanotheranostics. *International Journal of Pharmaceutics*, 496(2), 191–218. <https://doi.org/10.1016/j.ijpharm.2015.10.058>
- Kano, K., Nishiyabu, R., Asada, T., & Kuroda, Y. (2002). Static and Dynamic Behavior of 2:1 Inclusion Complexes of Cyclodextrins and Charged Porphyrins in Aqueous Organic Media. *Journal of the American Chemical Society*, 124(33), 9937–9944. <https://doi.org/10.1021/ja020253n>
- Kaoui, B., Lauricella, M., & Pontrelli, G. (2018). Mechanistic modelling of drug release from multi-layer capsules. *Computers in Biology and Medicine*, 93(October 2017), 149–157. <https://doi.org/10.1016/j.compbiomed.2017.12.010>
- Katagiri, K., Nakamura, M., & Koumoto, K. (2010). Magneto-responsive Smart Capsules

- Formed with Polyelectrolytes, Lipid Bilayers and Magnetic Nanoparticles. *ACS Applied Materials & Interfaces*, 2(3), 768–773. <https://doi.org/10.1021/am900784a>
- Kelkar, S. S., & Reineke, T. M. (2011). *Theranostics : Combining Imaging and Therapy*. 1879–1903.
- Khalid, M. N., Simard, P., Hoarau, D., Dragomir, A., & Leroux, J.-C. (2006). Long Circulating Poly(Ethylene Glycol)-Decorated Lipid Nanocapsules Deliver Docetaxel to Solid Tumors. *Pharmaceutical Research*, 23(4), 752–758. <https://doi.org/10.1007/s11095-006-9662-5>
- Kharlampieva, E., Kozlovskaya, V., Chan, J., Ankner, J. F., & Tsukruk, V. V. (2009). Spin-Assisted Layer-by-Layer Assembly: Variation of Stratification as Studied with Neutron Reflectivity. *Langmuir*, 25(24), 14017–14024. <https://doi.org/10.1021/la9014042>
- Kievit, F. M., & Zhang, M. (2011). Cancer Nanotheranostics: Improving Imaging and Therapy by Targeted Delivery Across Biological Barriers. *Advanced Materials*, 23(36), H217–H247. <https://doi.org/10.1002/adma.201102313>
- Knežević, N., & Kaluderović, G. N. (2017). Silicon-based nanotheranostics. *Nanoscale*, 9(35), 12821–12829. <https://doi.org/10.1039/c7nr04445c>
- Knežević, N. Ž., & Durand, J.-O. (2015). Large pore mesoporous silica nanomaterials for application in delivery of biomolecules. *Nanoscale*, 7(6), 2199–2209. <https://doi.org/10.1039/C4NR06114D>
- Knop, K., Hoogenboom, R., Fischer, D., & Schubert, U. S. (2010). *Drug Delivery Poly (ethylene glycol) in Drug Delivery : Pros and Cons as Well as Potential Alternatives Angewandte*. 6288–6308. <https://doi.org/10.1002/anie.200902672>
- Kobayashi, T. (2011). Cancer hyperthermia using magnetic nanoparticles. *Biotechnology Journal*, 6(11), 1342–1347. <https://doi.org/10.1002/biot.201100045>
- Konan, Y. N., Gurny, R., & Allémann, E. (2002). State of the art in the delivery of photosensitizers for photodynamic therapy. *Journal of Photochemistry and Photobiology B: Biology*, 66(2), 89–106. [https://doi.org/https://doi.org/10.1016/S1011-1344\(01\)00267-6](https://doi.org/https://doi.org/10.1016/S1011-1344(01)00267-6)
- Kostevsek, N., Locatelli, E., Garrovo, C., Arena, F., Monaco, I., Nikolov, I. P., Sturm, S., Rozman, K. Z., Lorusso, V., Giustetto, P., Bardini, P., Biffi, S., & Comes Franchini, M. (2016). The one-step synthesis and surface functionalization of dumbbell-like gold-iron oxide nanoparticles: A chitosan-based nanotheranostic system. *Chemical Communications*, 52(2), 378–381. <https://doi.org/10.1039/c5cc08275g>
- Kyung, K.-H., & Shiratori, S. (2011). Nanoscale Texture Control of Polyelectrolyte Multilayer Using Spray Layer-by-Layer Method. *Japanese Journal of Applied Physics*, 50(2), 25602. <https://doi.org/10.1143/jjap.50.025602>
- Lai, C.-Y., Trewyn, B. G., Jeftinija, D. M., Jeftinija, K., Xu, S., Jeftinija, S., & Lin, V. S.-Y. (2003). A Mesoporous Silica Nanosphere-Based Carrier System with Chemically Removable CdS Nanoparticle Caps for Stimuli-Responsive Controlled Release of Neurotransmitters and Drug Molecules. *Journal of the American Chemical Society*, 125(15), 4451–4459. <https://doi.org/10.1021/ja028650l>
- Laurent, S., Elst, L. Vander, Roch, A., & Muller, R. N. (2007). Structure, synthesis and

- characterization of contrast agents for magnetic resonance molecular imaging. *NMR-MRI, USR and Mossbauer Spectroscopies in Molecular Magnets*, 71–87. https://doi.org/10.1007/978-88-470-0532-7_3
- Lee, H., Shin, T. H., Cheon, J., & Weissleder, R. (2015). Recent Developments in Magnetic Diagnostic Systems. *Chemical Reviews*, 115(19), 10690–10724. <https://doi.org/10.1021/cr500698d>
- Li, P., Dai, Y.-N., Zhang, J.-P., Wang, A.-Q., & Wei, Q. (2008). Chitosan-alginate nanoparticles as a novel drug delivery system for nifedipine. *International Journal of Biomedical Science : IJBS*, 4(3), 221–228.
- Liang, R., Tian, R., Ma, L., Zhang, L., Hu, Y., Wang, J., Wei, M., Yan, D., Evans, D. G., & Duan, X. (2014). A Supermolecular Photosensitizer with Excellent Anticancer Performance in Photodynamic Therapy. *Advanced Functional Materials*, 24(21), 3144–3151. <https://doi.org/10.1002/adfm.201303811>
- Lin, T., Zhao, P., Jiang, Y., Tang, Y., Jin, H., Pan, Z., He, H., Yang, V. C., & Huang, Y. (2016). Blood–Brain–Barrier–Penetrating Albumin Nanoparticles for Biomimetic Drug Delivery via Albumin-Binding Protein Pathways for Antiglioma Therapy. *ACS Nano*, 10(11), 9999–10012. <https://doi.org/10.1021/acsnano.6b04268>
- Lin, Y.-S., Abadeer, N., & Haynes, C. L. (2011). Stability of small mesoporous silica nanoparticles in biological media. *Chem. Commun.*, 47(1), 532–534. <https://doi.org/10.1039/C0CC02923H>
- Liu, T., Wang, Y., Zhong, W., Li, B., Mequanint, K., Luo, G., & Xing, M. (2019). Biomedical Applications of Layer-by-Layer Self-Assembly for Cell Encapsulation: Current Status and Future Perspectives. *Advanced Healthcare Materials*, 8(1), 1800939. <https://doi.org/10.1002/adhm.201800939>
- Liu, Y., Liu, Y., Bu, W., Cheng, C., Zuo, C., Xiao, Q., Sun, Y., Ni, D., Zhang, C., Liu, J., & Shi, J. (2015). Hypoxia Induced by Upconversion-Based Photodynamic Therapy: Towards Highly Effective Synergistic Bioreductive Therapy in Tumors. *Angewandte Chemie*, 127(28), 8223–8227. <https://doi.org/10.1002/ange.201500478>
- Loverde, S. M., Klein, M. L., & Discher, D. E. (2011). Nanoparticle Shape Improves Delivery: Rational Coarse Grain Molecular Dynamics (rCG-MD) of Taxol in Worm-Like PEG-PCL Micelles. *Advanced Materials*, 23(1), 1–7. <https://doi.org/10.1038/jid.2014.371>
- Lu, A. H., Salabas, E. L., & Schüth, F. (2007). Magnetic nanoparticles: Synthesis, protection, functionalization, and application. *Angewandte Chemie - International Edition*, 46(8), 1222–1244. <https://doi.org/10.1002/anie.200602866>
- Lu, F., Wu, S. H., Hung, Y., & Mou, C. Y. (2009). Size effect on cell uptake in well-suspended, uniform mesoporous silica nanoparticles. *Small*, 5(12), 1408–1413. <https://doi.org/10.1002/smll.200900005>
- Lvov, Y., Decher, G., & Moehwald, H. (1993). Assembly, structural characterization, and thermal behavior of layer-by-layer deposited ultrathin films of poly(vinyl sulfate) and poly(allylamine). *Langmuir*, 9(2), 481–486. <https://doi.org/10.1021/la00026a020>
- Ma, Y., Huang, J., Song, S., Chen, H., & Zhang, Z. (2016). Cancer-Targeted

- Nanotheranostics: Recent Advances and Perspectives. *Small*, 12(36), 4936–4954. <https://doi.org/10.1002/sml.201600635>
- Mansoori, G. A., Brandenburg, K. S., & Shakeri-Zadeh, A. (2010). A Comparative Study of Two Folate-Conjugated Gold Nanoparticles for Cancer Nanotechnology Applications. In *Cancers* (Vol. 2, Issue 4). <https://doi.org/10.3390/cancers2041911>
- Manzano, M., & Vallet-Regí, M. (2020). Mesoporous Silica Nanoparticles for Drug Delivery. *Advanced Functional Materials*, 30(2), 3–5. <https://doi.org/10.1002/adfm.201902634>
- Matsumura, Y., Hamaguchi, T., Ura, T., Muro, K., Yamada, Y., Shimada, Y., Shirao, K., Okusaka, T., Ueno, H., Ikeda, M., & Watanabe, N. (2004). Phase I clinical trial and pharmacokinetic evaluation of NK911, a micelle-encapsulated doxorubicin. *British Journal of Cancer*, 91(10), 1775–1781. <https://doi.org/10.1038/sj.bjc.6602204>
- Mattheolabakis, G., Milane, L., Singh, A., & Amiji, M. M. (2015). Hyaluronic acid targeting of CD44 for cancer therapy: from receptor biology to nanomedicine. *Journal of Drug Targeting*, 23(7–8), 605–618. <https://doi.org/10.3109/1061186X.2015.1052072>
- Mattheolabakis, G., Taoufik, E., Haralambous, S., Roberts, M. L., & Avgoustakis, K. (2009). In vivo investigation of tolerance and antitumor activity of cisplatin-loaded PLGA-mPEG nanoparticles. *European Journal of Pharmaceutics and Biopharmaceutics*, 71(2), 190–195. <https://doi.org/https://doi.org/10.1016/j.ejpb.2008.09.011>
- Mattu, C., Pabari, R. M., Boffito, M., Sartori, S., Ciardelli, G., & Ramtoola, Z. (2013). Comparative evaluation of novel biodegradable nanoparticles for the drug targeting to breast cancer cells. *European Journal of Pharmaceutics and Biopharmaceutics*, 85(3 PART A), 463–472. <https://doi.org/10.1016/j.ejpb.2013.07.016>
- Maude, S. L., Teachey, D. T., Porter, D. L., & Grupp, S. A. (2015). CD19-targeted chimeric antigen receptor T-cell therapy for acute lymphoblastic leukemia. *Blood*, 125(26), 4017–4023. <https://doi.org/10.1182/blood-2014-12-580068>
- McGinty, S., & Pontrelli, G. (2015). A general model of coupled drug release and tissue absorption for drug delivery devices. *Journal of Controlled Release*, 217, 327–336. <https://doi.org/https://doi.org/10.1016/j.jconrel.2015.09.025>
- Meads, C., Auguste, P., Davenport, C., Małysiak, S., Sundar, S., Kowalska, M., Zapalska, A., Guest, P., Thangaratinam, S., Martin-Hirsch, P., Borowiack, E., Barton, P., Roberts, T., & Khan, K. (2013). Positron emission tomography/computerised tomography imaging in detecting and managing recurrent cervical cancer: Systematic review of evidence, elicitation of subjective probabilities and economic modeling. *Health Technology Assessment*, 17(12), 7–144. <https://doi.org/10.3310/hta17120>
- Medarova, Z., Rashkovetsky, L., Pantazopoulos, P., & Moore, A. (2009). Multiparametric Monitoring of Tumor Response to Chemotherapy by Noninvasive Imaging. *Cancer Research*, 69(3), 1182 LP – 1189. <https://doi.org/10.1158/0008-5472.CAN-08-2001>
- Meijers, W. C., & De Boer, R. A. (2019). Common risk factors for heart failure and cancer. *Cardiovascular Research*, 115(5), 844–853.

<https://doi.org/10.1093/cvr/cvz035>

- Ménard, M., Meyer, F., Parkhomenko, K., Leuvre, C., Francius, G., Bégin-Colin, S., & Mertz, D. (2019). Mesoporous silica templated-albumin nanoparticles with high doxorubicin payload for drug delivery assessed with a 3-D tumor cell model. *Biochimica et Biophysica Acta. General Subjects*, 1863(2), 332–341. <https://doi.org/10.1016/j.bbagen.2018.10.020>
- Meng, H., Leong, W., Leong, K. W., Chen, C., & Zhao, Y. (2018). Walking the line: the fate of nanomaterials at biological barriers. *Biomaterials*, 174, 41–53. <https://doi.org/10.1016/j.biomaterials.2018.04.056>
- Merrill, M. H., & Sun, C. T. (2009). Fast, simple and efficient assembly of nanolayered materials and devices. *Nanotechnology*, 20(7), 75606. <https://doi.org/10.1088/0957-4484/20/7/075606>
- Miao, D., Jiang, M., Liu, Z., Gu, G., Hu, Q., Kang, T., Song, Q., Yao, L., Li, W., Gao, X., Sun, M., & Chen, J. (2014). Co-administration of Dual-Targeting Nanoparticles with Penetration Enhancement Peptide for Antiglioblastoma Therapy. *Molecular Pharmaceutics*, 11(1), 90–101. <https://doi.org/10.1021/mp400189j>
- Miura, Y., Takenaka, T., Toh, K., Wu, S., Nishihara, H., Kano, M. R., Ino, Y., Nomoto, T., Matsumoto, Y., Koyama, H., Cabral, H., Nishiyama, N., & Kataoka, K. (2013). Cyclic RGD-Linked Polymeric Micelles for Targeted Delivery of Platinum Anticancer Drugs to Glioblastoma through the Blood–Brain Tumor Barrier. *ACS Nano*, 7(10), 8583–8592. <https://doi.org/10.1021/nn402662d>
- Moon, H. K., Lee, S. H., & Choi, H. C. (2009). In vivo near-infrared mediated tumor destruction by photothermal effect of carbon nanotubes. *ACS Nano*, 3(11), 3707–3713. <https://doi.org/10.1021/nn900904h>
- Moorthi, C., Manavalan, R., & Kathiresan, K. (2011). Nanotherapeutics to overcome conventional cancer chemotherapy limitations. *Journal of Pharmacy and Pharmaceutical Sciences*, 14(1), 67–77. <https://doi.org/10.18433/j30c7d>
- Mulhearn, W. D., Kim, D. D., Gu, Y., & Lee, D. (2012). Facilitated transport enhances spray layer-by-layer assembly of oppositely charged nanoparticles. *Soft Matter*, 8(40), 10419–10427. <https://doi.org/10.1039/C2SM26456K>
- Nabil, G., Bhise, K., Sau, S., Atef, M., El-Banna, H. A., & Iyer, A. K. (2019). Nano-engineered delivery systems for cancer imaging and therapy: Recent advances, future direction and patent evaluation. *Drug Discovery Today*, 24(2), 462–491. <https://doi.org/10.1016/j.drudis.2018.08.009>. Author
- Nagaraja, A. T., You, Y.-H., Choi, J.-W., Hwang, J.-H., Meissner, K. E., & McShane, M. J. (2016). Layer-by-layer modification of high surface curvature nanoparticles with weak polyelectrolytes using a multiphase solvent precipitation process. *Journal of Colloid and Interface Science*, 466, 432–441. <https://doi.org/https://doi.org/10.1016/j.jcis.2015.12.040>
- Nam, K., Kim, T., Kim, Y. M., Yang, K., Choe, D., Mensah, L. B., Choi, K. Y., & Roh, Y. H. (2019). Size-controlled synthesis of polymerized DNA nanoparticles for targeted anticancer drug delivery. *Chemical Communications*, 55(34), 4905–4908. <https://doi.org/10.1039/C9CC01442J>

- National Cancer Institute. (2020). *www.cancer.gov*. <https://www.cancer.gov/about-cancer/treatment/types>
- Nichols, J. W., & Bae, Y. H. (2014). EPR: Evidence and fallacy. *Journal of Controlled Release*, 190, 451–464. <https://doi.org/https://doi.org/10.1016/j.jconrel.2014.03.057>
- Nooney, R. I., Thirunavukkarasu, D., Chen, Y., Josephs, R., & Ostafin, A. E. (2002). Synthesis of Nanoscale Mesoporous Silica Spheres with Controlled Particle Size. *Chemistry of Materials*, 14(11), 4721–4728. <https://doi.org/10.1021/cm0204371>
- O'Boyle, N. M., Banck, M., James, C. A., Morley, C., Vandermeersch, T., & Hutchison, G. R. (2011). Open Babel: An open chemical toolbox. *Journal of Cheminformatics*, 3(1), 33. <https://doi.org/10.1186/1758-2946-3-33>
- Osaki, F., Kanamori, T., Sando, S., Sera, T., & Aoyama, Y. (2004). A Quantum Dot Conjugated Sugar Ball and Its Cellular Uptake. On the Size Effects of Endocytosis in the Subviral Region. *Journal of the American Chemical Society*, 126(21), 6520–6521. <https://doi.org/10.1021/ja048792a>
- Owens, D. E., & Peppas, N. A. (2006). Opsonization, biodistribution, and pharmacokinetics of polymeric nanoparticles. In *International Journal of Pharmaceutics* (Vol. 307, Issue 1, pp. 93–102). <https://doi.org/10.1016/j.ijpharm.2005.10.010>
- Pan, L., He, Q., Liu, J., Chen, Y., Zhang, L., & Shi, J. (2012). Nuclear targeting via TAT on Mesoporous NPs. *Journal of the American Chemical Society*, 134(13), 5722–5725.
- Pantsar, T., & Poso, A. (2018). Binding Affinity via Docking: Fact and Fiction. *Molecules (Basel, Switzerland)*, 23(8), 1899. <https://doi.org/10.3390/molecules23081899>
- Park, D., Ahn, K.-O., Jeong, K.-C., & Choi, Y. (2016). Polypyrrole-based nanotheranostics for activatable fluorescence imaging and chemo/photothermal dual therapy of triple-negative breast cancer. *Nanotechnology*, 27(18), 185102. <https://doi.org/10.1088/0957-4484/27/18/185102>
- Parker, N., Turk, M. J., Westrick, E., Lewis, J. D., Low, P. S., & Leamon, C. P. (2005). Folate receptor expression in carcinomas and normal tissues determined by a quantitative radioligand binding assay. *Analytical Biochemistry*, 338(2), 284–293. <https://doi.org/https://doi.org/10.1016/j.ab.2004.12.026>
- Peer, D., Karp, J. M., Hong, S., Farokhzad, O. C., Margalit, R., & Langer, R. (2007). Nanocarriers as an emerging platform for cancer therapy. *Nature Nanotechnology*, 2(12), 751–760. <https://doi.org/10.1038/nnano.2007.387>
- Penet, M. F., Krishnamachary, B., Chen, Z., Jin, J., & Bhujwalla, Z. M. (2014). Molecular imaging of the tumor microenvironment for precision medicine and theranostics. *Advances in Cancer Research*, 124, 235–256. <https://doi.org/10.1016/B978-0-12-411638-2.00007-0>
- Peppas, N. A., & Narasimhan, B. (2014). Mathematical models in drug delivery: How modeling has shaped the way we design new drug delivery systems. *Journal of Controlled Release*, 190, 75–81. <https://doi.org/https://doi.org/10.1016/j.jconrel.2014.06.041>
- Prabhakar, U., Jayalakshmi, Y., & Wang, C. K. (2019). Cancer Diagnostics and

- Therapeutics. In S. A. Morris (Ed.), *Nanotheranostics for Cancer Applications* (pp. 33–66).
- Prabhu, R. H., Patravale, V. B., & Joshi, M. D. (2015). Polymeric nanoparticles for targeted treatment in oncology: Current insights. *International Journal of Nanomedicine*, *10*, 1001–1018. <https://doi.org/10.2147/IJN.S56932>
- Rai, M., & Jamil, B. (2019). *Nanotheranostics*.
- Reddy, L. H., Arias, J. L., Nicolas, J., & Couvreur, P. (2012). Magnetic nanoparticles: Design and characterization, toxicity and biocompatibility, pharmaceutical and biomedical applications. *Chemical Reviews*, *112*(11), 5818–5878. <https://doi.org/10.1021/cr300068p>
- Reddy, S. B., & Williamson, S. K. (2009). Tirapazamine: A novel agent targeting hypoxic tumor cells. In *Expert Opinion on Investigational Drugs* (Vol. 18, Issue 1, pp. 77–87). <https://doi.org/10.1517/13543780802567250>
- Richardson, J. J., Cui, J., Björnmalm, M., Braunger, J. A., Ejima, H., & Caruso, F. (2016). Innovation in Layer-by-Layer Assembly. *Chemical Reviews*, *116*(23), 14828–14867. <https://doi.org/10.1021/acs.chemrev.6b00627>
- Robinson, J. T., Welsher, K., Tabakman, S. M., Sherlock, S. P., Wang, H., Luong, R., & Dai, H. (2010). High performance in vivo near-IR (>1 μm) imaging and photothermal cancer therapy with carbon nanotubes. *Nano Research*, *3*(11), 779–793. <https://doi.org/10.1007/s12274-010-0045-1>
- Roy Chowdhury, M., Schumann, C., Bhakta-Guha, D., & Guha, G. (2016). Cancer nanotheranostics: Strategies, promises and impediments. *Biomedicine and Pharmacotherapy*, *84*, 291–304. <https://doi.org/10.1016/j.biopha.2016.09.035>
- Sahoo, A. K., Banerjee, S., & Ghosh, S. S. (2014). *Simultaneous RGB Emitting Au Nanoclusters in Chitosan Nanoparticles for Anticancer Gene Theranostics*. [salute.gov.it](http://www.salute.gov.it/portale/news/p3_2_1_1_1.jsp?lingua=italiano&menu=notizie&p=dalministero&id=3897). (2020). http://www.salute.gov.it/portale/news/p3_2_1_1_1.jsp?lingua=italiano&menu=notizie&p=dalministero&id=3897
- Santra, S., Kaittanis, C., Grimm, J., & Perez, J. M. (2009). Drug/dye-loaded, multifunctional iron oxide nanoparticles for combined targeted cancer therapy and dual optical/magnetic resonance imaging. *Small*, *5*(16), 1862–1868. <https://doi.org/10.1002/sml.200900389>
- Sarmento, B., Ferreira, D., Veiga, F., & Ribeiro, A. (2006). Characterization of insulin-loaded alginate nanoparticles produced by ionotropic pre-gelation through DSC and FTIR studies. *Carbohydrate Polymers*, *66*(1), 1–7. <https://doi.org/10.1016/j.carbpol.2006.02.008>
- Saurer, E. M., Jewell, C. M., Roenneburg, D. A., Bechler, S. L., Torrealba, J. R., & Lynn, D. M. (2013). Polyelectrolyte Multilayers Promote Stent-Mediated Delivery of DNA to Vascular Tissue. *Biomacromolecules*, *14*(5), 1696–1704. <https://doi.org/10.1021/bm4005222>
- Seetharamu, N., Kim, E., Hochster, H., Martin, F., & Muggia, F. (2010). Phase II study of liposomal cisplatin (SPI-77) in platinum-sensitive recurrences of ovarian cancer. *Anticancer Research*, *30*(2), 541–545.

- Séon, L., Lavalle, P., Schaaf, P., & Boulmedais, F. (2015). Polyelectrolyte Multilayers: A Versatile Tool for Preparing Antimicrobial Coatings. *Langmuir*, 31(47), 12856–12872. <https://doi.org/10.1021/acs.langmuir.5b02768>
- Shan, J., Budijono, S. J., Hu, G., Yao, N., Kang, Y., Ju, Y., & Prud'Homme, R. K. (2011). Pegylated composite nanoparticles containing upconverting phosphors and meso-tetraphenyl porphine (TPP) for photodynamic therapy. *Advanced Functional Materials*, 21(13), 2488–2495. <https://doi.org/10.1002/adfm.201002516>
- Shang, L., Nienhaus, K., & Nienhaus, G. U. (2014). Engineered nanoparticles interacting with cells: size matters. *Journal of Nanobiotechnology*, 12(1), 5. <https://doi.org/10.1186/1477-3155-12-5>
- Shim, B. S., Podsiadlo, P., Lilly, D. G., Agarwal, A., Lee, J., Tang, Z., Ho, S., Ingle, P., Paterson, D., Lu, W., & Kotov, N. A. (2007). Nanostructured Thin Films Made by Dewetting Method of Layer-By-Layer Assembly. *Nano Letters*, 7(11), 3266–3273. <https://doi.org/10.1021/nl071245d>
- Shoichet, B. K., & Kuntz, I. D. (1991). Protein docking and complementarity. *Journal of Molecular Biology*, 221(1), 327–346. [https://doi.org/https://doi.org/10.1016/0022-2836\(91\)80222-G](https://doi.org/https://doi.org/10.1016/0022-2836(91)80222-G)
- Shukla, A., Fang, J. C., Puranam, S., & Hammond, P. T. (2012). Release of vancomycin from multilayer coated absorbent gelatin sponges. *Journal of Controlled Release*, 157(1), 64–71. <https://doi.org/https://doi.org/10.1016/j.jconrel.2011.09.062>
- Siepmann, J., & Peppas, N. A. (2012). Modeling of drug release from delivery systems based on hydroxypropyl methylcellulose (HPMC). *Advanced Drug Delivery Reviews*, 64, 163–174. <https://doi.org/https://doi.org/10.1016/j.addr.2012.09.028>
- Silica, F. M., Kobler, J., Möller, K., & Bein, T. (2008). *ACS Nano Bein colloidal suspension.pdf*. 2(4), 791–799.
- Silva, C. O., Pinho, J. O., Lopes, J. M., Almeida, A. J., Gaspar, M. M., & Reis, C. (2019). Current trends in cancer nanotheranostics: Metallic, polymeric, and lipid-based systems. *Pharmaceutics*, 11(1). <https://doi.org/10.3390/pharmaceutics11010022>
- Singh, Rajendra K., Patel, K. D., Leong, K. W., & Kim, H. W. (2017). Progress in Nanotheranostics Based on Mesoporous Silica Nanomaterial Platforms. *ACS Applied Materials and Interfaces*, 9(12), 10309–10337. <https://doi.org/10.1021/acsami.6b16505>
- Singh, Rajendra Kumar, Kim, T.-H., Mahapatra, C., Patel, K. D., & Kim, H.-W. (2015). Preparation of Self-Activated Fluorescence Mesoporous Silica Hollow Nanoellipsoids for Theranostics. *Langmuir*, 31(41), 11344–11352. <https://doi.org/10.1021/acs.langmuir.5b03436>
- Skovsen, E., Snyder, J. W., Lambert, J. D. C., & Ogilby, P. R. (2005). Lifetime and Diffusion of Singlet Oxygen in a Cell. *The Journal of Physical Chemistry B*, 109(18), 8570–8573. <https://doi.org/10.1021/jp051163i>
- Slowing, I., Trewyn, B. G., & Lin, V. S.-Y. (2006). Effect of Surface Functionalization of MCM-41-Type Mesoporous Silica Nanoparticles on the Endocytosis by Human Cancer Cells. *Journal of the American Chemical Society*, 128(46), 14792–14793. <https://doi.org/10.1021/ja0645943>

- Smith, A. M., Duan, H., Mohs, A. M., & Nie, S. (2008). Bioconjugated quantum dots for in vivo molecular and cellular imaging. *Advanced Drug Delivery Reviews*, 60(11), 1226–1240. <https://doi.org/https://doi.org/10.1016/j.addr.2008.03.015>
- Sonali, Viswanadh, M. K., Singh, R. P., Agrawal, P., Mehata, A. K., Pawde, D. M., Narendra, Sonkar, R., & Muthu, M. S. (2018). Nanotheranostics: Emerging strategies for early diagnosis and therapy of brain cancer. *Nanotheranostics*, 2(1), 70–86. <https://doi.org/10.7150/ntno.21638>
- Steeg, P. S., Camphausen, K. A., & Smith, Q. R. (2011). Brain metastases as preventive and therapeutic targets. *Nature Reviews. Cancer*, 11(5), 352–363. <https://doi.org/10.1038/nrc3053>
- Stöber, W., Fink, A., & Bohn, E. (1968). Controlled growth of monodisperse silica spheres in the micron size range. *Journal of Colloid and Interface Science*, 26(1), 62–69. [https://doi.org/https://doi.org/10.1016/0021-9797\(68\)90272-5](https://doi.org/https://doi.org/10.1016/0021-9797(68)90272-5)
- Su, Y. L., & Hu, S. H. (2018). Functional nanoparticles for tumor penetration of therapeutics. *Pharmaceutics*, 10(4), 1–21. <https://doi.org/10.3390/pharmaceutics10040193>
- Sukhorukov, G. B., Donath, E., Davis, S., Lichtenfeld, H., Caruso, F., Popov, V. I., & Möhwald, H. (1998). Stepwise polyelectrolyte assembly on particle surfaces: a novel approach to colloid design. *Polymers for Advanced Technologies*, 9(10-11), 759–767. [https://doi.org/10.1002/\(SICI\)1099-1581\(1998100\)9:10/11<759::AID-PAT846>3.0.CO;2-Q](https://doi.org/10.1002/(SICI)1099-1581(1998100)9:10/11<759::AID-PAT846>3.0.CO;2-Q)
- Tabasi, O., Falamaki, C., & Khalaj, Z. (2012). Functionalized mesoporous silicon for targeted-drug-delivery. *Colloids and Surfaces B: Biointerfaces*, 98, 18–25. <https://doi.org/https://doi.org/10.1016/j.colsurfb.2012.04.018>
- Tallury, P., Payton, K., & Santra, S. (2008). Silica-based multimodal/multifunctional nanoparticles for bioimaging and biosensing applications. *Nanomedicine*, 3(4), 579–592. <https://doi.org/10.2217/17435889.3.4.579>
- Tang, F., Li, L., & Chen, D. (2012). Mesoporous silica nanoparticles: Synthesis, biocompatibility and drug delivery. *Advanced Materials*, 24(12), 1504–1534. <https://doi.org/10.1002/adma.201104763>
- Tang, L., Yang, X., Yin, Q., Cai, K., Wang, H., Chaudhury, I., Yao, C., Zhou, Q., Kwon, M., Hartman, J. A., Dobrucki, I. T., Dobrucki, L. W., Borst, L. B., Lezmi, S., Helferich, W. G., Ferguson, A. L., Fan, T. M., & Cheng, J. (2014). Investigating the optimal size of anticancer nanomedicine. *Proceedings of the National Academy of Sciences of the United States of America*, 111(43), 15344–15349. <https://doi.org/10.1073/pnas.1411499111>
- Toita, R., Murata, M., Abe, K., Narahara, S., Piao, J. S., Kang, J.-H., Ohuchida, K., & Hashizume, M. (2013). Biological evaluation of protein nanocapsules containing doxorubicin. *International Journal of Nanomedicine*, 8, 1989–1999. <https://doi.org/10.2147/IJN.S40239>
- Tran, S., Degiovanni, P. J., Piel, B., & Rai, P. (2017). Cancer nanomedicine : a review of recent success in drug delivery. *Clinical and Translational Medicine*. <https://doi.org/10.1186/s40169-017-0175-0>

- Trewyn, B. G., Nieweg, J. A., Zhao, Y., & Lin, V. S.-Y. (2008). Biocompatible mesoporous silica nanoparticles with different morphologies for animal cell membrane penetration. *Chemical Engineering Journal*, 137(1), 23–29. <https://doi.org/https://doi.org/10.1016/j.cej.2007.09.045>
- Trushina, D. B., Bukreeva, T. V., & Antipina, M. N. (2016). Size-Controlled Synthesis of Vaterite Calcium Carbonate by the Mixing Method: Aiming for Nanosized Particles. *Crystal Growth and Design*, 16(3), 1311–1319. <https://doi.org/10.1021/acs.cgd.5b01422>
- Venturini, C. G., Bruinsmann, F. A., Contri, R. V, Fonseca, F. N., Frank, L. A., D'Amore, C. M., Raffin, R. P., Buffon, A., Pohlmann, A. R., & Guterres, S. S. (2015). Co-encapsulation of imiquimod and copaiba oil in novel nanostructured systems: promising formulations against skin carcinoma. *European Journal of Pharmaceutical Sciences: Official Journal of the European Federation for Pharmaceutical Sciences*, 79, 36–43. <https://doi.org/10.1016/j.ejps.2015.08.016>
- Vivero-Escoto, J. L., Slowing, I. I., Lin, V. S. Y., & Trewyn, B. G. (2010). Mesoporous silica nanoparticles for intracellular controlled drug delivery. *Small*, 6(18), 1952–1967. <https://doi.org/10.1002/sml.200901789>
- Vllasaliu, D., Fowler, R., & Stolnik, S. (2014). PEGylated nanomedicines: recent progress and remaining concerns. *Expert Opinion on Drug Delivery*, 11(1), 139–154. <https://doi.org/10.1517/17425247.2014.866651>
- Volodkin, D. V., Petrov, A. I., Prevot, M., & Sukhorukov, G. B. (2004). Matrix Polyelectrolyte Microcapsules: New System for Macromolecule Encapsulation. *Langmuir*, 20(8), 3398–3406. <https://doi.org/10.1021/la036177z>
- Voskuhl, J., Kauscher, U., Gruener, M., Frisch, H., Wibbeling, B., Strassert, C. A., & Ravoo, B. J. (2013). A soft supramolecular carrier with enhanced singlet oxygen photosensitizing properties. *Soft Matter*, 9(8), 2453–2457. <https://doi.org/10.1039/C2SM27353E>
- Vrignaud, S., Anton, N., Passirani, C., Benoit, J.-P., & Saulnier, P. (2013). Aqueous core nanocapsules: a new solution for encapsulating doxorubicin hydrochloride. *Drug Development and Industrial Pharmacy*, 39(11), 1706–1711. <https://doi.org/10.3109/03639045.2012.730526>
- Wang, A. Z., Bagalkot, V., Vasilliou, C. C., Gu, F., Alexis, F., Zhang, L., Shaikh, M., Yuet, K., Cima, M. J., Langer, R., Kantoff, P. W., Bander, N. H., Jon, S., & Farokhzad, O. C. (2008). Superparamagnetic Iron Oxide Nanoparticle–Aptamer Bioconjugates for Combined Prostate Cancer Imaging and Therapy. *ChemMedChem*, 3(9), 1311–1315. <https://doi.org/10.1002/cmdc.200800091>
- Wang, C., Tao, H., Cheng, L., & Liu, Z. (2011). Near-infrared light induced in vivo photodynamic therapy of cancer based on upconversion nanoparticles. *Biomaterials*, 32(26), 6145–6154. <https://doi.org/10.1016/j.biomaterials.2011.05.007>
- Wang, L. S., Chuang, M. C., & Ho, J. an A. (2012). Nanotheranostics - A review of recent publications. *International Journal of Nanomedicine*, 7, 4679–4695. <https://doi.org/10.2147/IJN.S33065>
- Wang, R., Han, Y., Sun, B., Zhao, Z., Opoku-Damoah, Y., Cheng, H., Zhang, H., Zhou,

- J., & Ding, Y. (2018). Deep Tumor Penetrating Bioparticulates Inspired Burst Intracellular Drug Release for Precision Chemo-Phototherapy. *Small*, 14(12), 1703110. <https://doi.org/10.1002/sml.201703110>
- Wang, T., Feng, Z., He, N., Wang, Z., Li, S., Guo, Y., & Xu, L. (2007). A novel preparation of nanocapsules from alginate-oligochitosan. *Journal of Nanoscience and Nanotechnology*, 7(12), 4571–4574. <https://doi.org/10.1166/jnn.2007.882>
- Ward, C. M., Pechar, M., Oupicky, D., Ulbrich, K., & Seymour, L. W. (2002). *Modification of pLL / DNA complexes with a multivalent hydrophilic polymer permits folate-mediated targeting in vitro and prolonged plasma circulation in vivo.* April, 536–547.
- Werner, M. E., Cummings, N. D., Sethi, M., Wang, E. C., Sukumar, R., Moore, D. T., & Wang, A. Z. (2013). Preclinical Evaluation of Genexol-PM, a Nanoparticle Formulation of Paclitaxel, as a Novel Radiosensitizer for the Treatment of Non-Small Cell Lung Cancer. *International Journal of Radiation Oncology*Biophysics*, 86(3), 463–468. <https://doi.org/https://doi.org/10.1016/j.ijrobp.2013.02.009>
- Wiesing, U. (2019). Theranostics: is it really a revolution? Evaluating a new term in medicine. *Medicine, Health Care and Philosophy*, 22(4), 593–597. <https://doi.org/10.1007/s11019-019-09898-3>
- Wolber, G., & Kosara, R. (2006). Pharmacophores from macromolecular complexes with LigandScout. *Methods and Principles in Medicinal Chemistry*, 32, 131.
- Wolber, G., & Langer, T. (2005). LigandScout: 3-D pharmacophores derived from protein-bound ligands and their use as virtual screening filters. *Journal of Chemical Information and Modeling*, 45(1), 160–169. <https://doi.org/10.1021/ci049885e>
- Wu, Z., Lin, X., Zou, X., Sun, J., & He, Q. (2015). Biodegradable Protein-Based Rockets for Drug Transportation and Light-Triggered Release. *ACS Applied Materials & Interfaces*, 7(1), 250–255. <https://doi.org/10.1021/am507680u>
- Xing, J., Cai, Y., Wang, Y., Zheng, H., & Liu, Y. (2020). Synthesis of Polymer Assembled Mesoporous CaCO₃ Nanoparticles for Molecular Targeting and pH-Responsive Controlled Drug Release. *Advances in Polymer Technology*, 2020, 1–8. <https://doi.org/10.1155/2020/8749238>
- Yan, Y., Zuo, X., & Wei, D. (2015). Concise Review: Emerging Role of CD44 in Cancer Stem Cells: A Promising Biomarker and Therapeutic Target. *STEM CELLS Translational Medicine*, 4(9), 1033–1043. <https://doi.org/10.5966/sctm.2015-0048>
- Yang, J., Chen, J., Pan, D., Wan, Y., & Wang, Z. (2013). PH-sensitive interpenetrating network hydrogels based on chitosan derivatives and alginate for oral drug delivery. *Carbohydrate Polymers*, 92(1), 719–725. <https://doi.org/10.1016/j.carbpol.2012.09.036>
- Yang, K., Zhang, S., Zhang, G., Sun, X., Lee, S. T., & Liu, Z. (2010). Graphene in mice: Ultrahigh in vivo tumor uptake and efficient photothermal therapy. *Nano Letters*, 10(9), 3318–3323. <https://doi.org/10.1021/nl100996u>
- Yang, T., Cui, F.-D., Choi, M.-K., Cho, J.-W., Chung, S.-J., Shim, C.-K., & Kim, D.-D. (2007). Enhanced solubility and stability of PEGylated liposomal paclitaxel: In vitro

- and in vivo evaluation. *International Journal of Pharmaceutics*, 338(1), 317–326. <https://doi.org/https://doi.org/10.1016/j.ijpharm.2007.02.011>
- Yang, W., Guo, W., Le, W., Lv, G., Zhang, F., Shi, L., Wang, X., Wang, J., Wang, S., Chang, J., & Zhang, B. (2016). Albumin-Bioinspired Gd:CuS Nanotheranostic Agent for In Vivo Photoacoustic/Magnetic Resonance Imaging-Guided Tumor-Targeted Photothermal Therapy. *ACS Nano*, 10(11), 10245–10257. <https://doi.org/10.1021/acsnano.6b05760>
- Yang, X., Grailer, J. J., Rowland, I. J., Javadi, A., Hurley, S. A., Steeber, D. A., & Gong, S. (2010). Multifunctional SPIO/DOX-loaded wormlike polymer vesicles for cancer therapy and MR imaging. *Biomaterials*, 31(34), 9065–9073. <https://doi.org/https://doi.org/10.1016/j.biomaterials.2010.08.039>
- Yi, D. K., Sun, I. C., Ryu, J. H., Koo, H., Park, C. W., Youn, I. C., Choi, K., Kwon, I. C., Kim, K., & Ahn, C. H. (2010). Matrix metalloproteinase sensitive gold nanorod for simultaneous bioimaging and photothermal therapy of cancer. *Bioconjugate Chemistry*, 21(12), 2173–2177. <https://doi.org/10.1021/bc100308p>
- Yokota, J. (2000). Tumor progression and metastasis. *Carcinogenesis*, 21(3), 497–503. <https://doi.org/10.1093/carcin/21.3.497>
- Yoncheva, K., Gómez, S., Campanero, M. A., Gamazo, C., & Irache, J. M. (2005). Bioadhesive properties of pegylated nanoparticles. *Expert Opinion on Drug Delivery*, 2(2), 205–218. <https://doi.org/10.1517/17425247.2.2.205>
- Yoo, H. S., & Park, T. G. (2004). Folate-receptor-targeted delivery of doxorubicin nano-aggregates stabilized by doxorubicin–PEG–folate conjugate. *Journal of Controlled Release*, 100(2), 247–256. <https://doi.org/https://doi.org/10.1016/j.jconrel.2004.08.017>
- Yu, D.-H., Liu, Y.-R., Luan, X., Liu, H.-J., Gao, Y.-G., Wu, H., Fang, C., & Chen, H.-Z. (2015). IF7-Conjugated Nanoparticles Target Annexin 1 of Tumor Vasculature against P-gp Mediated Multidrug Resistance. *Bioconjugate Chemistry*, 26(8), 1702–1712. <https://doi.org/10.1021/acs.bioconjchem.5b00283>
- Yu, M. K., Jeong, Y. Y., Park, J., Park, S., Kim, J. W., Min, J. J., Kim, K., & Jon, S. (2008). Drug-loaded superparamagnetic iron oxide nanoparticles for combined cancer imaging and therapy in vivo. *Angewandte Chemie - International Edition*, 47(29), 5362–5365. <https://doi.org/10.1002/anie.200800857>
- Yunessnia lehi, A., Shagholani, H., Ghorbani, M., Nikpay, A., Soleimani lashkenari, M., & Soltani, M. (2019). Chitosan nanocapsule-mounted cellulose nanofibrils as nanoships for smart drug delivery systems and treatment of avian trichomoniasis. *Journal of the Taiwan Institute of Chemical Engineers*, 95, 290–299. <https://doi.org/10.1016/j.jtice.2018.07.014>
- Zha, J., & Roggendorf, H. (1991). Sol–gel science, the physics and chemistry of sol–gel processing, Ed. by C. J. Brinker and G. W. Scherer, Academic Press, Boston 1990, xiv, 908 pp., bound—ISBN 0-12-134970-5. *Advanced Materials*, 3(10), 522. <https://doi.org/10.1002/adma.19910031025>
- Zhang, R., Wu, C., Tong, L., Tang, B., & Xu, Q.-H. (2009). Multifunctional core-shell nanoparticles as highly efficient imaging and photosensitizing agents. *Langmuir: The ACS Journal of Surfaces and Colloids*, 25(17), 10153–10158.

<https://doi.org/10.1021/la902235d>

- Zhang Sulin, Li Ju, Lykotrafitis George, Bao Gang, S. S. (2009). Size-Dependent Endocytosis of Nanoparticles. *Advanced Materials*. <https://doi.org/https://doi.org/10.1002/adma.200801393>
- Zhao, S., Zhang, S., Ma, J., Fan, L., Yin, C., Lin, G., & Li, Q. (2015). Double loaded self-decomposable SiO₂ nanoparticles for sustained drug release. *Nanoscale*, 7(39), 16389–16398. <https://doi.org/10.1039/C5NR03029C>
- Zhou, X., Chen, L., Wang, W., Jia, Y., Chang, A., Mo, X., Wang, H., & He, C. (2015). Electrospun nanofibers incorporating self-decomposable silica nanoparticles as carriers for controlled delivery of anticancer drug. *RSC Adv.*, 5(81), 65897–65904. <https://doi.org/10.1039/C5RA11830A>
- Zhu, Z., Gao, N., Wang, H., & Sukhishvili, S. A. (2013). Temperature-triggered on-demand drug release enabled by hydrogen-bonded multilayers of block copolymer micelles. *Journal of Controlled Release*, 171(1), 73–80. <https://doi.org/https://doi.org/10.1016/j.jconrel.2013.06.031>
- Zwicke, G. L., Ali Mansoori, G., & Jeffery, C. J. (2012). Utilizing the folate receptor for active targeting of cancer nanotherapeutics. *Nano Reviews*, 3(1), 18496. <https://doi.org/10.3402/nano.v3i0.18496>